Chapter 1

Introduction

Since the recent decades, progress of communication technology has gained humankind a lot of convenience in daily life. From wired to wireless communication, the related technologies are advancing rapidly, due to increasing demand of high-transmission applications in real time, such as the high-quality audio and video transmission. To meet the high demand, new high-bit rate transmission schemes are adopted in new standards.

Among those new high-performance communication technologies, Orthogonal Frequency Division Multiplexing (OFDM) has recently received particular interest due to its high data-rate transmission capability with high bandwidth efficiency and its robustness to multi-path interference. This modulation scheme has been used in a lot of wireless standards such as the WLAN IEEE802.11a, the WMAN IEEE802.16a, European Digital Audio Broadcasting (DAB) and Digital Video Broadcasting Terrestrial (DVB-T), as well as the wireline VDSL and ADSL standards.

1.1 Motivation of the Thesis.

In January 2003, WMAN IEEE802.16a in support of broadband wireless access at frequency band of 2-11 GHz was launched for fixed locations in outdoor environments. The resulting standard specifies the air interface of fixed (stationary) broadband wireless access systems providing multiple services. For baseband physical layer of IEEE 802.16a, key technical challenges and ingredients include channel estimation, channel coding and timing/frequency synchronization for correct data reception. In the first part of this thesis, we focus on the designs of channel estimation function block for the IEEE 802.16a standard. We will investigate current channel estimation schemes and designs effective channel estimation techniques for IEEE 802.16a. In addition, channel estimations for DVB-T system (launched in September 1993) will also be investigated for the purpose of software defined radio (SDR).

In the second part, it is frequently assumed that channel response is stationary within a symbol period. With such assumption, the received signal in frequency domain is equal to the multiplication of the transmitted subcarrier data and the channel frequency response. Then the typical channel compensation solution is to use one-tap channel equalizer in frequency domain. The purpose of channel equalizer is to compensate the channel distortion at each subcarrier by dividing each received subcarrier data by its corresponding estimated channel frequency response [1], [2]. However, the assumption of symbol wise time-invariance may not be valid with high Doppler frequency shift or long symbol length. The effect of time-variant channel destroys the orthogonality property between subcarriers and results in inter-channel interference (ICI) [3]. In [4] [5], ICI terms are taken into consideration. Beside time-variant channels, carrier frequency offset also causes inter-channel interference (ICI). The ICI leads to an error floor in signal detection performance so that channel

estimation and equalization must be designed to combat the ICI effect for better transmission efficiency. Channel estimation schemes can be roughly divided into two types: blind approaches [6] and pilot-assisted approaches [7]. Our estimation scheme is based on general pilot-assisted channel estimation schemes. The proposed scheme considers the ICI term due to Doppler spread and carrier frequency offsets. The proposed estimation scheme show that it's robust to ICI effect due to fast-fading channel and carrier frequency offsets. In the second part, our aim is to propose an estimation scheme that is robust in combating fast-fading channel and carrier frequency offsets.

1.2 Organization of the Thesis

This thesis is organized as follows. In Chapter 2, we will introduce the basic principle of OFDM systems and the characteristics of wireless multipath fading channels. In Chapter 3, the physical layers of 802.16a and DVB-T systems are specified. After that, in Chapter 4, we investigate current channel estimation algorithms and design effective channel estimation techniques for IEEE 802.16a and DVB-T systems. In Chapter 5, first we will detail the effect of time-varying channels and carrier frequency offsets for OFDM systems. Then, we propose an effective channel estimation method that improves the method from [8]. The proposed method can combat ICI effectively. Finally, in Chapter 6, a brief conclusion is given.

Chapter2

Fundamentals of OFDM Systems

Techniques of multicarrier transmission has been used for over 30 years. The principle of multicarrier system is to divide the data stream into several parallel ones, each modulated by a specific subcarrier, which was first used in the KinPlex system in 1960s [9]. In 1966, a new idea was proposed by Chang [10] which used parallel data and FDM with overlapping subchannels without inter-channel interference (ICI) and inter-symbol interference (ISI) under band-limited channel condition. There was a crucial evolution in 1971 when Weinstein and Ebert proposed to use discrete Fourier Transform (DFT) in the baseband modulation and demodulation of an OFDM system [11]. Through this approach, only a pair of oscillator (for I-part and Q-part) is needed instead of multiple oscillators to modulate different signals at different carriers.

When signals pass through a time-dispersive channel, ISI and ICI usually occur in the receiver. For combating ISI and ICI problems, cyclic prefix (CP) was introduced by Peled and Ruiz in 1980 [12]. Cyclic prefix, shown in Figure 2.1 is a copy of the tail part of a symbol, which is inserted in between the symbol and its preceding symbol. As long as the cyclic prefix length is longer than its corresponding

time-dispersive channel, inter-symbol interferences can be avoided. At the same time, the cyclic prefix makes the signal periodic and maintains the property of subcarrier orthogonality that prevents the inter-channel interference (ICI).
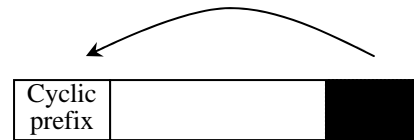

Figure 2.1 Cyclic prefix of an OFDM symbol

# 2.1 OFDM System Model

2.1.1 Continuous-Time Model

In this section, a continuous-time model is used to introduce the whole ODFM baseband system inclusive of the modulator and demodulator. In the modulator, the transmitted data is split into multiple subchannels with overlapping frequency bands and in the demodulator, the transmitted data is extracted from the received data at each subcarrier.

Figure 2.2 (a) shows a typical continuous-time OFDM baseband modulator, in which the transmitted data is split into multiple parallel streams which are modulated by different subcarriers and then transmitted simultaneously. At the receiver, the received signal is demodulated simultaneously by multiple matched filters and then the data at each subcarrier is obtained by sampling the outputs of matched filters. A continuous-time OFDM baseband demodulator is shown in Figure 2.2 (b).

The spectrum of $s(t)$ is shown in Figure 2.3. It is clear that the spectrum of each subchannel is spreading to all the others, but is zero at all other subcarrier frequencies, as a result of the sinc function property. This is the key feature of the orthogonal signal.
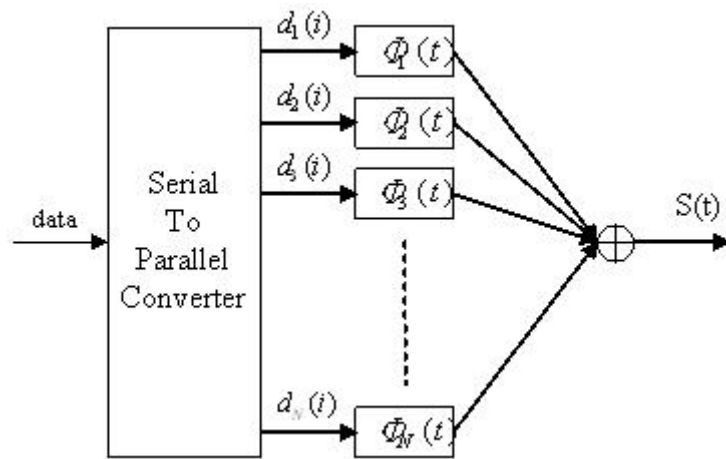
Figure 2.2(a) Continuous-time OFDM baseband modulator
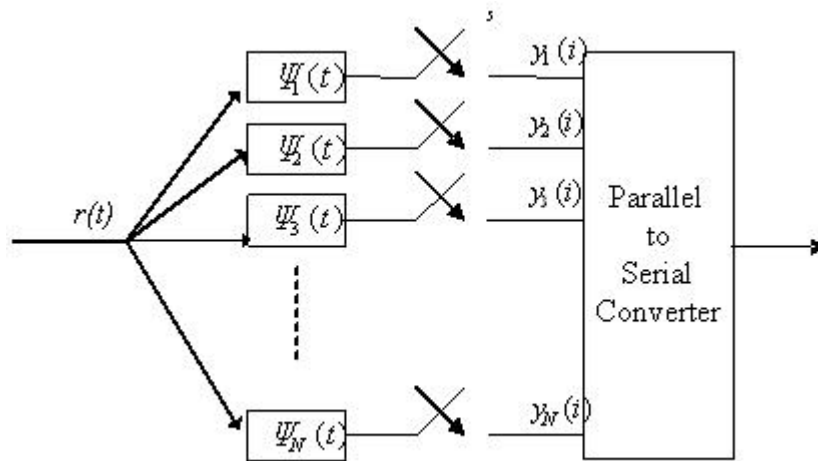
Figure 2.2 (b) Continuous-time OFDM baseband demodulator
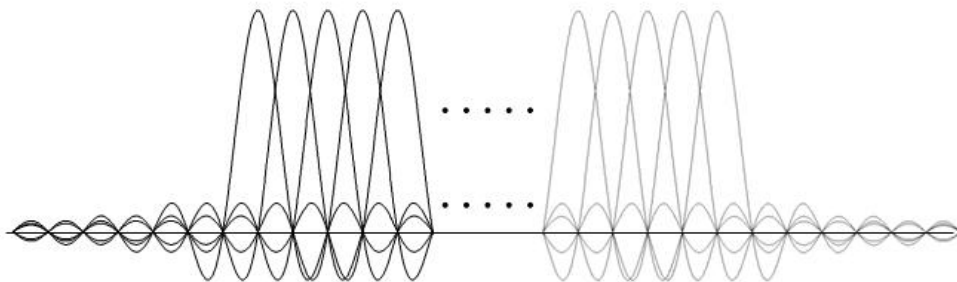
**Figure 2.3** Spectrum of OFDM signal

2.1.2 Discrete-Time Model

In the previous section, in order to simultaneously deal with multiple data, the transmitter must modulate data with multiple subcarriers and the receiver must demodulate with multiple matched filters. In fact, the modulation and demodulation of multiple subcarriers can be implemented efficiently by digital IDFT/DFT, because they can be respectively represented as

$$s(i) = \sum_{k=0}^{N-1} d(k) e^{j\frac{2\pi}{N}ki} \tag{2.1}$$

$$y(i) = \sum_{k=0}^{N-1} r(k) e^{-j\frac{2\pi}{N}ki} \tag{2.2}$$

which are the same as IDFT operation of the transmitted data $d(k)$ and DFT operation of the received data $r(k)$.

Figure 2.4 shows the discrete-time baseband OFDM model. The IDFT transforms the frequency-domain data into the corresponding time-domain data which is delivered over the air. At the receiver, to recover the signal in frequency domain, DFT is adopted in the demodulator as a matched filter. Figure 2.5 shows the discrete – time baseband demodulator. Then the frequency domain signal of each subchannel is obtained from its DFT output.
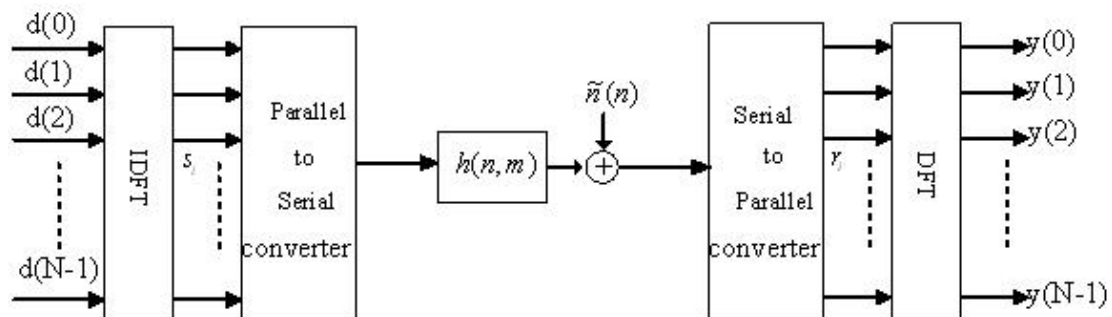
Figure 2.4 Discrete-time OFDM system model

2.1.3 Effect of Cyclic Prefix

Assume the given channel is quasi-static, i.e., constant during the transmission of an OFDM symbol and variable symbol wise, where the quasi-static impulse response is $h(t, \tau)$, t is the time index and τ is the channel path number. The received signal $r(t)$ can be expressed as

$$r(t) = s(t) * h(t, \tau) + \tilde{n}(t) \tag{2.3}$$

where $s(t)$ is the transmitted data and $\tilde{n}(t)$ is the white Gaussian noise sequence. Because of multipath channels, orthogonality as shown in Figure 2.3 will be destroyed by inter-symbol interference (ISI) and inter-channel interference (ICI). However, as long as the length of cyclic prefix is longer than the length of $h(n, m)$, ISI effect can be avoided. At the same time, linear convolution of $s(n)$ and $h(n, m)$ turns out to be circular convolution. It is well known that circular convolution in time domain results in multiplication in frequency domain when the channel is stationary so that the received subcarrier signal $y(i)$ in frequency domain is the multiplication of transmitted subcarrier signal $d(i)$ and subcarrier channel response $H(i)$. Thus, the orthogonality is maintained (if $h(n, m)$ is fixed within the symbol length) and data can be easily recovered by one-tap channel equalizer, i.e., dividing $y(i)$ by the corresponding $H(i)$. Besides, cyclic prefix can be used for frame synchronization and frequency offset estimation [11].

2.2 Channel Characteristics in Wireless Environments [12]

In wireless communications, the transmission path between a transmitter and a receiver can vary from simple line-of-sight to one that is severely obstructed by

buildings, mountains, and foliage. Each path contains the reflection of the transmitted signal. The path amplitude and arrival time are dominated by transmission conditions. Such environment is considered as a multipath channel, whose impulse response can be expressed as

$$h(t, \tau) = \sum_{l=0}^{L-1} a_l(t)\delta(\tau - \varepsilon_l) \tag{2.4}$$

where L is the number of paths, $a_l(t)$ and ε_l are the complex amplitude and delay time of the $l-th$ path, respectively. Usually $a_l(t)'s$ are modeled as complex Gaussian processes with Jake's power spectrum [13], and those paths are uncorrelated with each other. This is so called multipath Rayleigh fading channels. The mean square value of each path gain $a_l(t)$ is usually described by an exponentially-decayed function of the path delay, ε_l, which has the form of

$$E\left[\left|a_l(t)\right|^2\right] = e^{-\frac{\varepsilon_l}{\sigma}} \tag{2.5}$$

where σ is power delay time constant. Another important issue about path gain is the variation along time direction. Alternatively, Doppler frequency is commonly used as an indicator of the variation rate and is defined as

$$f_d = f_C \frac{V}{C} \tag{2.6}$$

where f_c is the carrier frequency, V is the vehicle speed and C is velocity of light. The larger Doppler frequency is the faster channel variation is. Hence, of course in the mobile environment the channel variation is faster than in a fixed case.

If channel impulse response is assumed fixed over a symbol time duration, channel frequency response at each subcarrier for the i-th symbol is given by

$$H_i(k) = \sum_{l=0}^{v-1} \alpha_l(iT_s)e^{-j2\pi k\frac{\varepsilon_l}{NT_c}} = \sum_{l=0}^{v-1} \alpha_l(iT_s)e^{-j\frac{2\pi k\tau_l}{N}} \qquad k = 0, 1, 2\cdots, N-1 \tag{2.7}$$

where $\tau_l = \varepsilon_l/T_c$ and T_c is the sampling period equal to T_s/N.

To obtain the equivalent discrete-time impulse response, IDFT is operated on $H_i(k)$.

$$h_i(n) = IDFT\{H_i(k)\}$$

$$= \frac{1}{N}\sum_{l=0}^{\nu-1}\alpha_l(iT_s)e^{-j\frac{\pi(n+(N-1)\tau_l)}{N}}\frac{\sin(\pi\tau_l)}{\sin(\pi(\tau_l-n)/N)} \quad n = 0,1,2\cdots N-1$$

(2.8)

If the multipath delay times are all sample-spaced, i.e., $\{\tau_l\}$ are all integers, $h_i(n)$ can be simplified to

$$h_i(n) = \frac{1}{N}\sum_{l=0}^{\nu-1}\alpha_l(iT_s)\delta(n-\tau_l) \quad n = 0,1,2\cdots N-1$$

(2.9)

This implies that in sample-spaced cases, the power of discrete-time impulse response will concentrate at some taps. Figure 2.5 shows two equivalent discrete-time channel impulse responses with sample-spaced and non-sampled space multipath time delays, respectively.

In non-sample-spaced cases, it is obvious that the power disperses to all taps. We also show the corresponding frequency responses of these two cases in Figure 2.6. The main difference between these two cases is that in the sample-spaced case, the frequency response is periodically continuous, i.e., transition from tail to head between the periods is quite smooth. However, in non-sampled-spaced case, it is not periodically continuous.

Besides, there are two important quantities that decide the channel conditions, which are coherent bandwidth and coherent time decided by multipath delay spread and Doppler frequency, respectively.
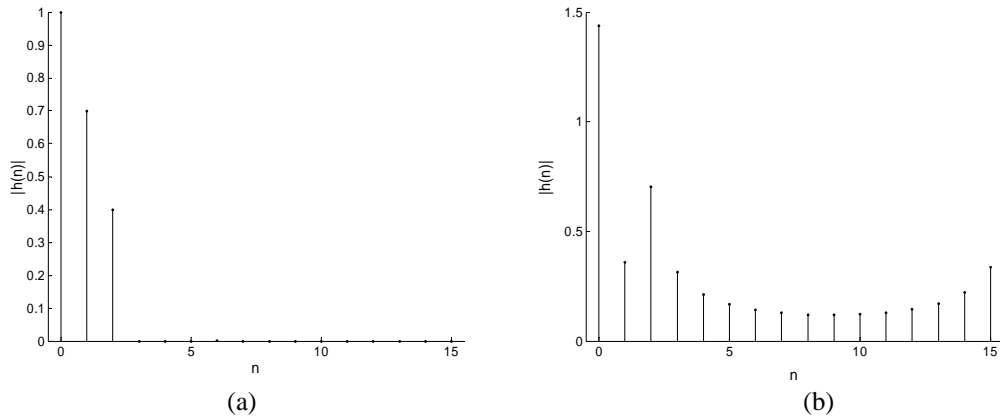
Figure 2.5 The equivalent discrete impulse responses: (a) sampled-spaced $h(t) = \delta(t) + 0.7\delta(t - T_c) + 0.4\delta(t - 2T_c)$; (b) nonsampled- spaced $h(t) = \delta(t) + 0.7\delta(t - 0.5T_c) + 0.2\delta(t - 1.4T_c)$
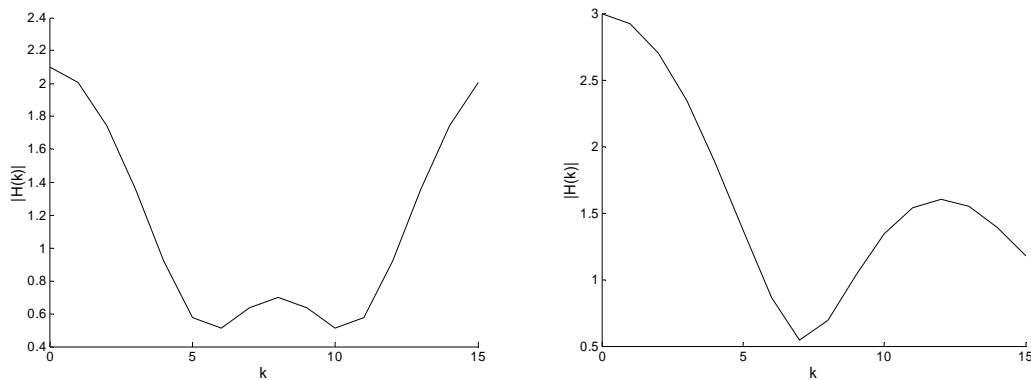
Figure 2.6 The frequency responses for two channels: (a) sampled-spaced $h(t) = \delta(t) + 0.7\delta(t - T_c) + 0.4\delta(t - 2T_c)$; (b) nonsampled- spaced $h(t) = \delta(t) + 0.7\delta(t - 0.5T_c) + 0.2\delta(t - 1.4T_c)$

2.2.1 Flat Fading and Frequency Selective Fading

Flat fading or frequency selective fading is determined by coherent bandwidth which is proportional to the reciprocal of channel *rms* delay. If coherent bandwidth is greater than the bandwidth of transmitted signals, received signals will undergo flat fading, otherwise will undergo frequency selective fading. In flat fading, the multipath structure of channels is such that the spectral characteristics of transmitted signals are preserved at the receiver. Therefore, a signal undergoes flat fading if

$$B_S << B_C \qquad (2.10)$$

11

and

$$T_S \gg \sigma_\tau \tag{2.11}$$

where T_S is the reciprocal bandwidth and B_S is the bandwidth, respectively, of transmitted modulation data, σ_τ and B_C are *rms* delay spread and coherent bandwidth, respectively, of channels.

In contrast, the spectrum of received signals is quite different from that of the transmitted signals under the condition of frequency-selective fading channels. Frequency-selective fading channels are due to multipath delay spread, and received signals include multiple versions of the transmitted waveform which are attenuated and delayed in time. Hence, the received signals are distorted. In summary, a signal undergoes flat-fading channels if

$$B_S > B_C \tag{2.12}$$

and

$$T_S < \sigma_\tau \tag{2.13}$$
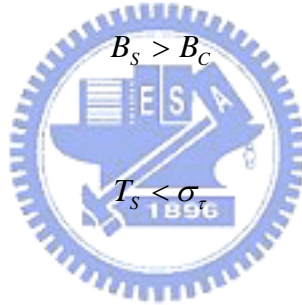
2.2.2 Slow Fading and Fast Fading

A channel is slow fading or fast fading depending on how rapidly transmitted signals change as compared to the variation rate of channels. In a fast fading channel, channel impulse response changes rapidly within a symbol duration. In contrast, channel impulse response changes much slowly in slow fading channels. The variation rate is determined by the coherent time which is proportional to the reciprocal of Doppler frequency defined in (2.6). The larger Doppler frequency is the faster channel variation is. Hence, it is obvious that in mobile environments the channel variation is faster than in the fixed one.

The relationship between various multipath parameters and the types of fading

experienced by signals are summarized in Figure 2.7, where the B_d means the

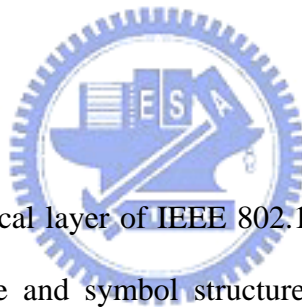bandwidth caused by Doppler frequency which is the inverse of the coherence time.
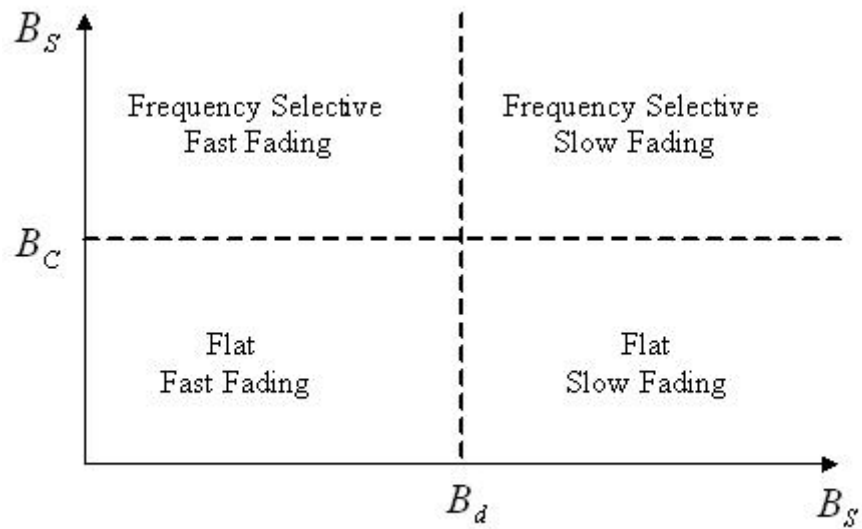
Figure 2.7 Fading type as a function of basedband signal bandwidth

Chapter 3

Physical Layer to IEEE 802.16a and DVB-T Standards

In this chapter, the physical layer of IEEE 802.16a and DVB-T systems will be introduced inclusive of frame and symbol structures, carriers allocation, and data modulation…and etc.

3.1 IEEE 802.16a System [14]

IEEE 802.16 which was published on 8 April 2002 by the Institute of Electrical and Electronics Engineers Standards Association (IEEE-SA) addresses the "first-mile/last-mile" connection in wireless metropolitan area networks. It focuses on the efficient use of bandwidth between 10 and 66 GHz (the 2 to 11 GHz region with PMP and optional Mesh topologies by the end of 2002) and defines a medium access control (MAC) layer that supports multiple physical layer (PHY) specifications. The

10 to 66 GHz standard supports continuously varying traffic levels at many licensed frequencies (e.g., 10.5, 25, 26…, 38 and 39 GHz) for TDD and FDD communications.

IEEE Standard 802.16a published in April 2003 amends IEEE Standard 802.16-2001 by enhancing the MAC layer and providing additional physical layer specifications in support of broadband wireless access at frequencies from 2 to 11 GHz. The 802.16a standard specifies the air interface of fixed broadband wireless access systems providing multiple services. In the document of IEEE 802.16a WMAN standard, there are three system modes: single carrier (SC), OFDM, OFDMA. Here only OFDMA PHY is considered. The WMAN-OFDMA PHY, based on OFDM modulation, is designed in the 2 to 11 GHz frequency bands. For licensed bands, channel bandwidths allowed shall be limited to the regulatory provisioned bandwidth divided by any power of 2 no less than 1.25 MHz.

Before a more detailed technical description of the IEEE 802.16a OFDMA PHY, we list some common abbreviations and the expressions:

(1)   SS (subscriber station): known as the user or the mobile stations

(2)   BS (base station): generalized equipment set providing connectivity, management, and control of subscriber station.

(3)   MAC (media access control): used to control the system access and provide ~~to~~ links of data from the upper layer to the lower layer.

(4)   PHY (physical layer): handles the data transmission and may include use of multiple transmission technologies, each appropriate to a particular frequency range and application.

(5)   DL (downlink): the direction from BS to SS.

(6)   UL (uplink): the direction from SS to BS.

(7)   TDD (time division duplexing): a single channel is used for both upstream and

downstream transmissions.

(8)   FDD (frequency division duplexing): requires two channel pairs, one for upstream and one for downstream.

# 3.1.1 OFDMA Frame Structure [14]

3.1.1.1 OFDMA Symbol Structure

OFMDA symbol structure can be viewed both by time domain and frequency domain as following.

(1) Time-domain description

Inverse Fourier transforming creates the OFDMA time-domain waveform; this time duration is referred to as the useful symbol time T_b. A copy of the last T_g of the useful symbol period, termed Cyclic Prefix (CP), is used to prevent the inter symbol interference due to multipath channels, while maintains the orthogonality of subcarriers. The two together are referred as the symbol time T_s. Figure 3.1 illustrates this structure.

Using a cyclic extension, the samples required for performing the FFT at the receiver can be taken anywhere over the length of the extended symbol. This provides multipath immunity as well as a tolerance for symbol time synchronization errors. On initialization of 802.16a system, a SS should search all possible values of CP until it finds the CP being used by the BS. The SSs shall use the same CP length in the UL. Once a specific CP duration has been selected by the BS for operation on the DL, it should not be changed. Changing the CP would force all the SSs to resynchronize to the BS.
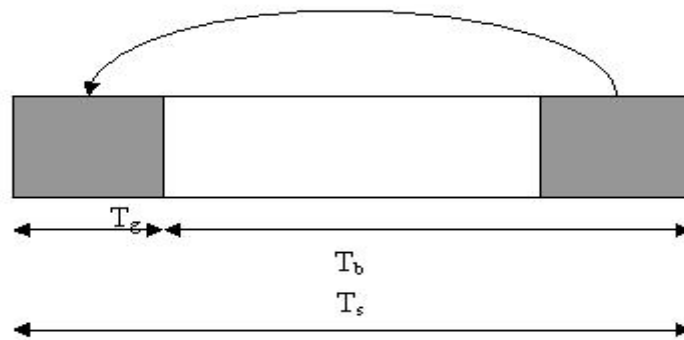
Figure 3.1 802.16a OFDMA symbol time structure
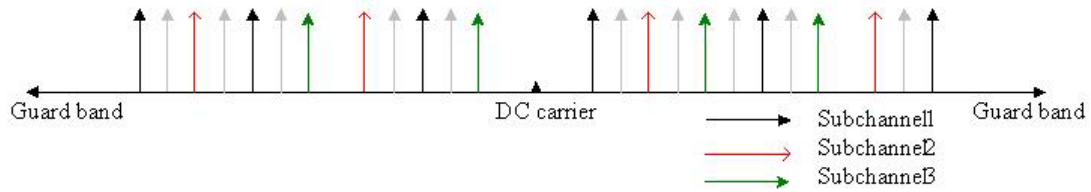
(2) Frequency-domain description

The frequency-domain description includes the basic structure of an OFDMA symbol. An OFDMA symbol is made up of carriers, the number of which determines the FFT size used. There are three types of carriers: data carriers used for data transmission, pilot carriers for various estimation purposes, and null carriers for guard bands and DC carrier which transmit nothing at all.

The purpose of guard bands is to enable the signal to naturally decay and create the FFT 'brick Wall' shaping. In the OFDMA mode, active carriers are divided into subsets of carriers, each subset is termed a subchannel. In the DL, a subchannel may be intended for different (groups of) receivers; in the UL, a transmitter may be assigned one or more subchannels, several transmitters may transmit in parallel. The carriers forming one subchannel may, but need not be adjacent. The concept is shown in Figure 3.2.

3.1.1.2 OFDMA Frame Structure

In licensed bands, the duplexing method shall be either FDD or TDD. FDD SSs may be Half Duplex FDD (H-FDD). In license-exempt bands, the duplexing method shall be TDD as introduced below.

When implementing a TDD system, the frame structure is built from BS and SS

Figure 3.2 802.16a OFDMA frequency description

transmissions. Each burst transmission consists of multiples of three (or six, if STC used) OFDMA symbols. In each frame, the Tx/Rx transition gap (TTG) and Rx/Tx transition gap (RTG) shall be inserted between the downlink and uplink and at the end of each frame respectively to allow the BS to turn around. TTG and RTG shall be at least 5 µs and an integer multiple of the physical slot (PS) in duration, and start on a PS boundary. After the TTG, the BS receiver shall look for the first symbol of a UL burst. After the RTG, the SS receivers shall look for the first symbols of QPSK modulated data in the DL burst.

Figure 3.3 introduce the OFDMA frame structure of TDD mode, and there is no need for TTG and RTG as the downlink and uplink transmit on independent frequencies in FDD systems.

3.1.2 OFDMA Carrier Allocations

For OFDMA, excluding the DC carrier and the guard tones from the OFDMA symbol, one obtains the set of used carriers. For both uplink and downlink these used carriers are allocated to pilot carriers and data carriers. However, there is a subtle difference between uplink and downlink. This difference is that, in the downlink, the pilot carriers are allocated first and then the data carriers are divided exclusively into 32 subchannels. In the uplink, however, the set of used carriers is first partitioned into 32 subchannels, and then the pilot carriers are allocated from within each subchannel.
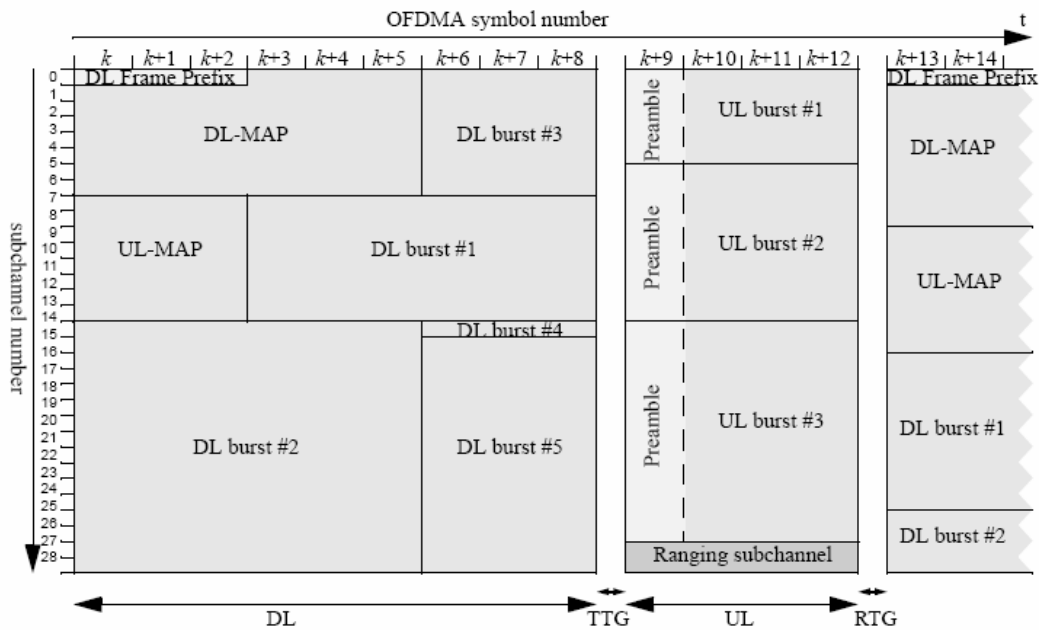
Figure 3.3 802.16a OFDMA TDD time frame [14]

Thus, in the downlink, there is one set of common pilot carriers, but in the uplink, each subchannel contains its own set of pilot carriers. This is necessary since, in OFDMA, the BS downlink broadcasts to all SS, but in the uplink, each subchannel may be transmitted from a different SS.

3.1.2.1 Downlink Carrier Allocations

The used carriers are partitioned into fixed-location pilots, variable location pilots, and data subchannels. The carrier indices of the fixed-location pilots never change and these indices are the members of the set BasicFixedLocationPilots listed in Table 3.1. The variable-location pilots shift their location every symbol and repeat every four symbols, according to the formula $varLocPilot_k = 3L + 12P_{k\,k}$, where $varLocPilot_k$ is the carrier index of a variable-location pilot , and L cycles through the values 0, 2, 1, 3, periodically, and $P_k \in \{0\,1\,2\ldots 141\}$. In some cases a variable-location pilot will coincide with a fixed-location pilot. The sets of BasicFixedLocationPilots are designed so that the number of coinciding pilots is the

same for every symbol and there is no all-pilot preamble in the DL. The allocation of

pilot carriers is illustrated in Figure 3.4
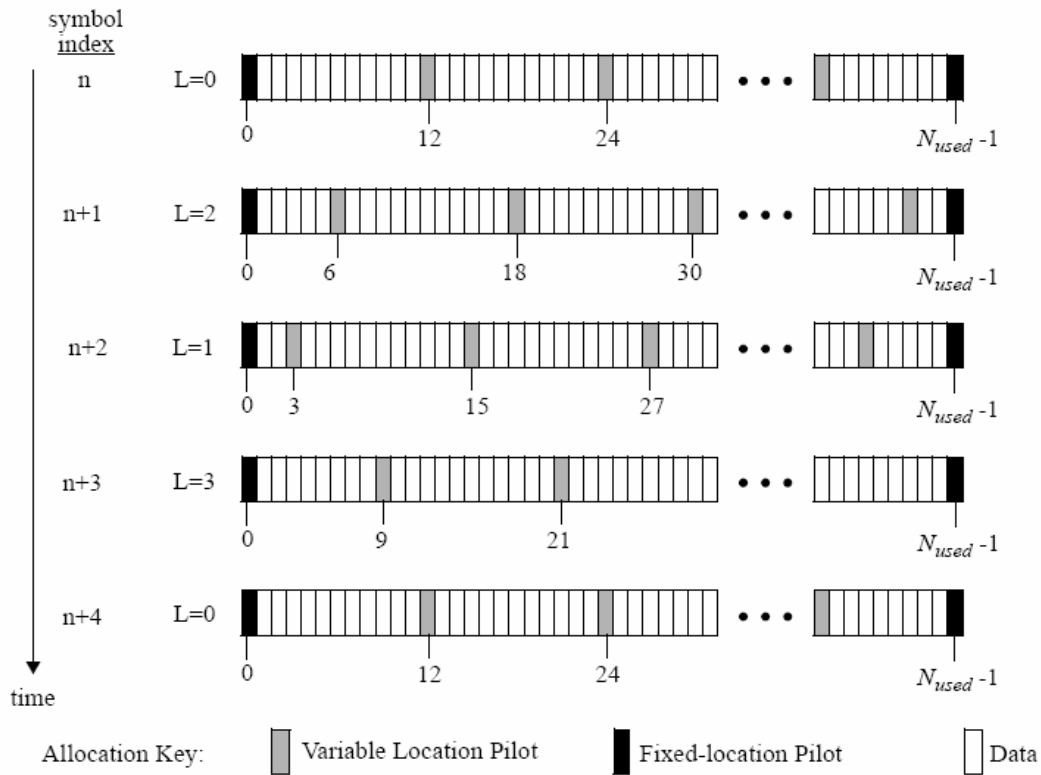
Figure 3.4 Carrier allocation of 802.16a OFDMA DL

After mapping the pilots, the remaining carriers belong to data subchannels. Note

that since the variable-location pilots change location in each symbol and repeat every

fourth symbol, the locations of the carriers in the data subchannels shall change also.

To allocate the data subchannels, the remaining carriers are partitioned into groups of

contiguous carriers. Each subchannel consists of one carrier from each of these groups.

The number of groups is therefore equal to the number of carriers per subchannel, and

it is denoted as *Nsubcarriers*. The number of the carriers in a group is equal to the

number of subchannels, and it is denoted as *Nsubchannels*. The number of data

carriers is thus equal to *Nsubcarriers* × *Nsubchannels*. The OFMDA DL carrier

allocation is listed in Table 3.1.

Table 3.1 802.16a OFDMA DL carrier allocation

Parameter	Value
Number of dc carriers	1
Number of guard carriers, left	173
Number of guard carriers, right	172
N_{used}, Number of used carriers	1702
Total number of carriers	2048
$N_{varLocPilots}$	142
Number of fixed-location pilots	32
Number of variable-location pilots which coincide with fixed-location pilots	8
Total number of pilots[a]	166
Number of data carriers	1536
$N_{subchannels}$	32
$N_{subcarriers}$	48
Number of data carriers per subchannel	48
BasicFixedLocationPilots	{0,39, 261, 330, 342, 351, 522, 636, 645, 651, 708, 726, 756, 792, 849, 855, 918, 1017, 1143, 1155, 1158, 1185, 1206, 1260, 1407, 1419,1428, 1461, 1530,1545, 1572, 1701}
$\{PermutationBase_0\}$	{3, 18, 2, 8, 16, 10, 11, 15, 26, 22, 6, 9, 27, 20, 25, 1, 29, 7, 21, 5, 28, 31, 23, 17, 4, 24, 0, 13, 12, 19, 14, 30}

[a]Variable Location Pilots which coincide with Fixed-location Pilots are counted only once in this value.

### 3.1.2.2 Uplink Carrier Allocations

The carriers are first partitioned into subchannels as in the downlink, except that, for the uplink, the parameters are given in Table 3.2. Note that *Nsubcarriers* of each subchannel in the uplink is 53 containing 48 data carriers, 1 fixed location pilot carrier, and 4 variable-location pilot carriers, instead of 48 as in the downlink.

The fixed-location pilots are always at subcarrier-in-subchannel 26. The variable-location pilots change in each symbol and repeat every 13 symbols, according to L_k, where k = 0 to 12. The sequence L_k is given by L_k = {0,2,4,6,8,10,12,1,3,5,7,9,11}. The first symbol (in k = 0) is produced after the all-pilot symbols (preamble), which consists of permuted carriers. For k = 0, variable-

Table 3.2 802.16a OFDMA UL carrier allocation

Parameter	Value	
Number of dc carriers	1	
N_{used}	1696	
Guard carriers: left, right	176	175
$N_{subchannels}$	32	
$N_{subcarriers}$	53	
Number of data carriers per subchannel	48	
$\{PermutationBase_0\}$	{3, 18, 2, 8, 16, 10, 11, 15, 26, 22, 6, 9, 27, 20, 25, 1, 29, 7, 21, 5, 28, 31, 23, 17, 4, 24, 0, 13, 12, 19, 14, 30}	

location pilots are positioned at indices: 0, 13, 27, 40 for the first cubchannel. For other k values, these locations change by adding L_k to each index. The variable-location pilot locations will never coincide with fixed-location pilot. The remaining 48 carriers are data carriers. The partitioning of each UL subchannel is illustrated in Figure 3.5.
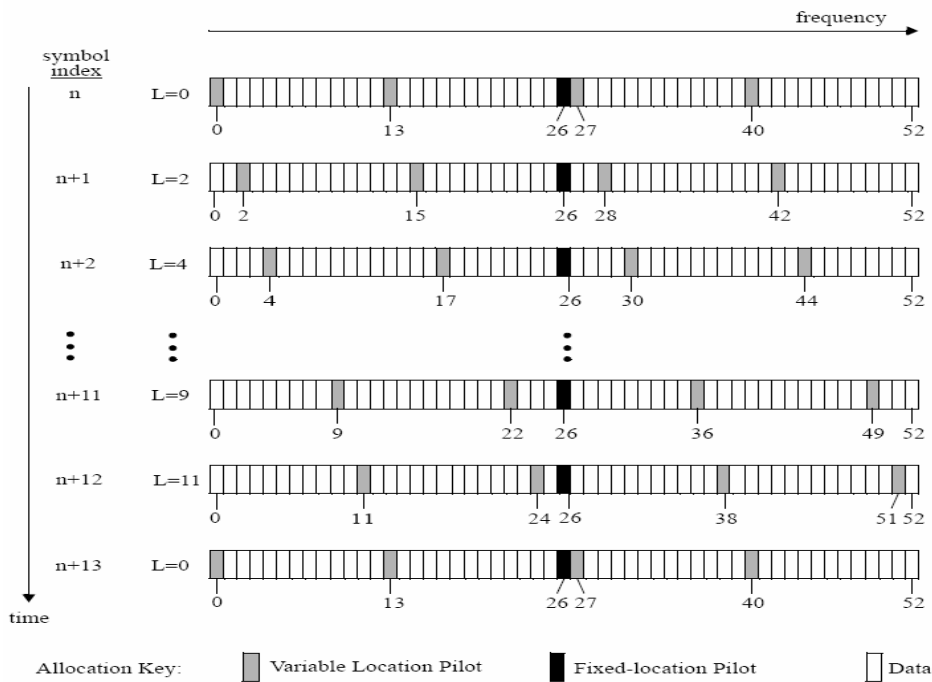
Figure 3.5 Carrier allocation of 802.16a OFDMA UL

3.1.3 Carrier Modulation

3.1.3.1 Data Modulation

For 802.16a system, after bit interleaving, the data bits are entered serially to the constellation mapping unit. Gray-mapped QPSK and 16-QAM as shown in Figure 3.6 shall be supported, whereas the support of 64-QAM is optional. The constellations as shown in Figure 3.6 shall be normalized by multiplying the constellation point with the normalized factor to achieve equal average power.
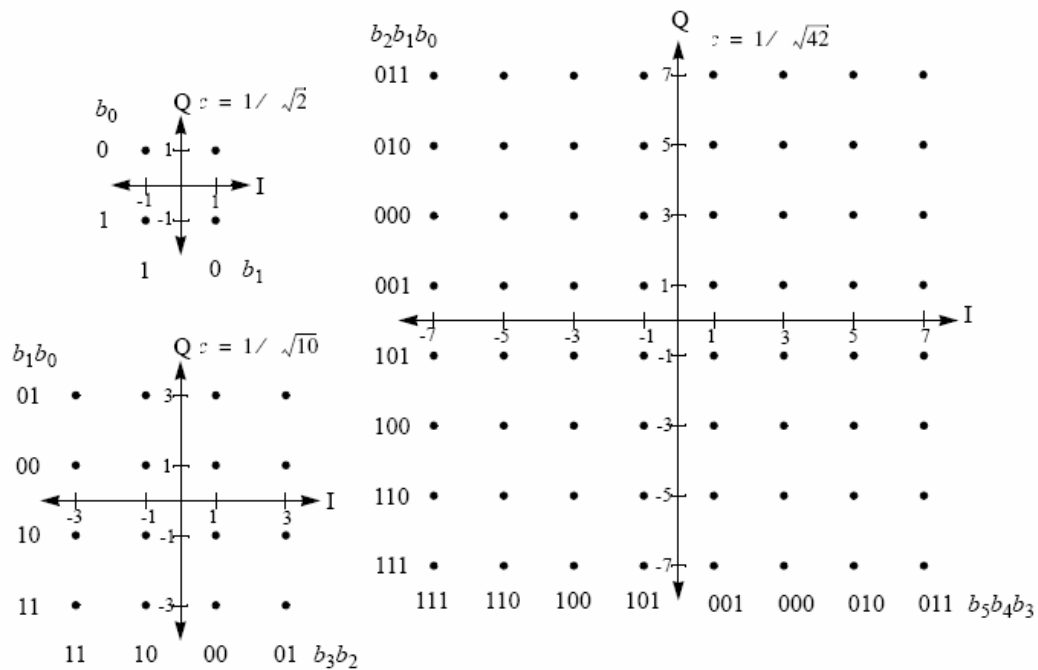

Figure 3.6 QPSK, 16-QAM, 64-QAM constellations of 802.16a

3.1.3.2 Pilot Modulation

Pilot carriers shall be inserted into each data burst in order to constitute a symbol and they shall be modulated according to their carrier location within an OFDMA symbol. The PRBS generator shall be used to produce a sequence, w_k. The polynomial sequence for the PRBS generator is $X^{11} + X^9 + 1$ as depicted in Figure 3.7.
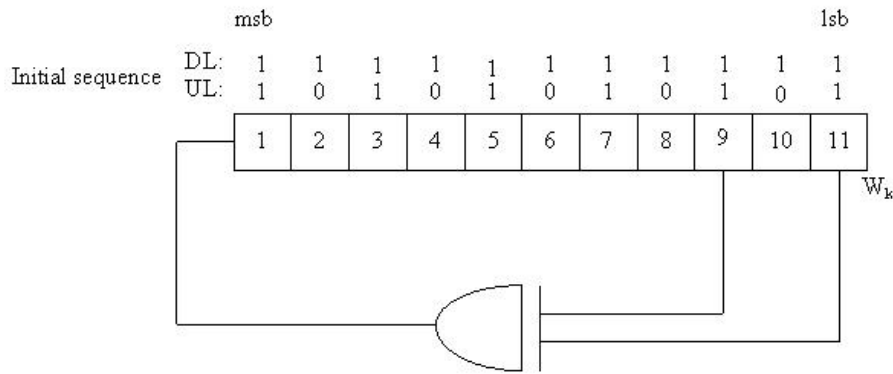
Figure 3.7 PRBS for pilot modulation of 802.16a

The value of the pilot modulation, on carrier k, shall be derived from w_k. When using data transmission on the DL, the initialization vector of the PRBS is: [11111111111] except for the OFDMA DL PHY preamble. When using data transmission on the UL the initialization vector of the PRBS is: [10101010101]. These initializations result in the sequence w_k=11111111111000000001..... in the DL and the sequence w_k=10101010101000000000.... in the UL. The PRBS shall be initialized so that its first output bit coincides with the first usable carrier (as defined in Table 3.2). A new value shall be generated by the PRBS on every usable carrier. For the PRBS allocation, the DC carrier and the side-band carriers are not considered as usable carriers. Each pilot shall be transmitted with a boosting of 2.5 dB over the average power of each data tone, (including the UL preamble).
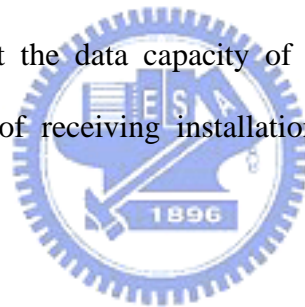
3.2 DVB-T System [15]

Founded in September 1993, the DVB Project is a market-led consortium of public and private sector organizations in the television industry. Its aim is to establish the framework for the introduction of MPEG-2 based digital TV services. Now comprising over 200 organizations from more than 25 countries around the world, DVB fosters market-led systems, which meet the real needs and economic circumstances, of the consumer electronics and the broadcast industry.

Here we describe the DVB-T specification and the choice of operation modes a broadcaster has to make in implementations. The operation mode decision depends on foreseen applications and the introduced varying scenarios expected in different countries. The parameters that can be chosen for a given application are:

(1) Fast Fourier Transform (FFT) length, which specifies the number of carriers (2k: 1 705 carriers; 8k: 6817 carriers)

(2) Carrier modulation (QPSK: 2 bits per carrier; 16-QAM: 4 bits per carrier; 64-QAM: 6 bits per carrier)

(3) Code rate of inner error protection (1/2; 2/3; 3/4; 5/6; 7/8)

(4) Guard interval length (1/4; 1/8; 1/16; 1/32)

(5) Non-hierarchical or hierarchical modulation and modulation parameter α

The choice of mode will set the data capacity of the system and will affect the coverage of different kinds of receiving installation - fixed roof-top antennas or portable receivers.

3.2.1 DVB-T System Overview

The system is defined by the functional blocks of an DVB equipment, which performs the adaptation of a baseband TV signal from the output of a MPEG-2 transport multiplexer, to the terrestrial channel characteristic. The following processes shall be applied to the data stream as depicted in Figure 3.8.

(1) Transport multiplex adaptation and randomization for energy dispersal

(2) Outer coding

(3) Outer interleaving

(4) Inner coding

(5) Inner interleaving

(6) Mapping and modulation

(7) OFDM transmission

First, a splitter is used to split the data stream into high-priority part and low-priority part. These two parts of data could have individual channel coding and modulation method. The method to split the data into two parts is so called Hierarchical transmission. For example, a TV program can be transmitted in both high -quality mode and low-quality mode by high-priority part and low-priority part at the same time. The high-priority part is demodulated by the received signal's quadrant in constellation, and the low priority-part is demodulated by the position of the signal in constellation.
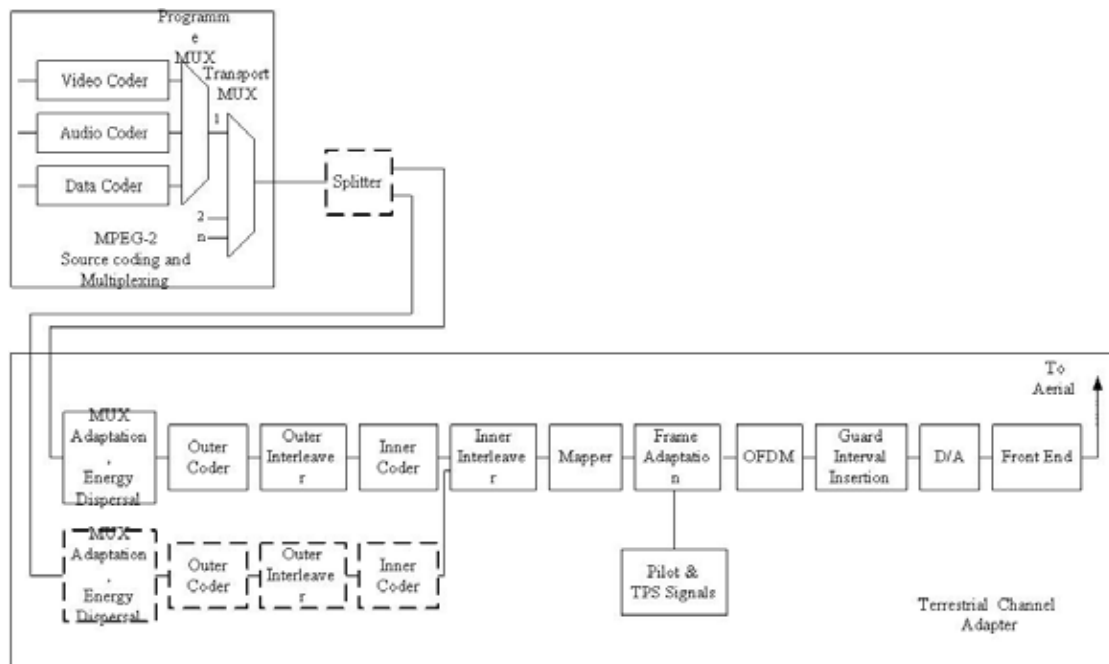

Figure 3.8 Function block diagram of DVB-T system [15]

Transport Multiplexing Adaptation will adapt the energy distribution and increase the randomization of the signal. Every 8 packets (188 bytes per packet: 1 bytes of synchronization word and 187 bytes of data words) of the signal will be multiplied by a pseudo random binary sequence derived by $X^{15} + X^{14} + 1$. Finally, the synchronization word of first packet will be modified from 47_{HEX} to $B8_{HEX}$.

There are two layers of channel coding and interleaver in the DVB-T system. The outer channel coding uses Reed-Solomon Code: RS (204, 188, t = 8). The outer interleaver is a convolutional interleaver working byte-by-byte which may have a smaller delay than that of a block interleaver. The inner channel coding is a convolutional code with code rate = 1/2, 2/3, 3/4, 5/6, or 7/8. The inner interleaver is a block interleaver.

The output data of inner interleaver will be modulated to complex signal by different modulation method. The modulation methods specified in DVB-T systems are QPSK, 16-QAM, 64-QAM, non-uniform 16-QAM, and non-uniform 64-QAM (as illustrated in Figure 3.9), where the non-uniform modulation is used in hierarchical transmission mode.
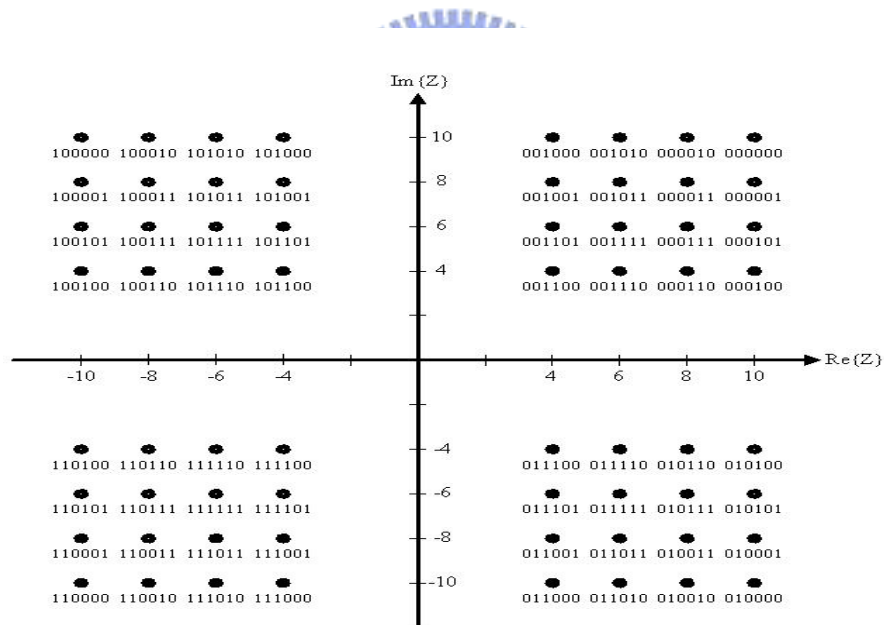
Figure 3.9 Hierarchical transmissions with non-uniform 64-QAM modulation of

DVB-T system

After pilot and TPS (Transmission Parameter Signaling) adaptation, the signal will be handled by IFFT. There are two transmission modes in DVB-T: 2K-mode and 8K-mode. In 2K-mode, 2048-point IFFT will be used, and in 8K-mode 8192-point IFFT will be used. The transmission parameter such as transmission mode,

hierarchical transmission or not, code rates of inner channel coding, and the modulation methods will be recorded in the Transmission Parameter Signaling.

The system is supposed to use the traditional analog broadcasting UHF band with 8MHz bandwidth. The central frequency of the transmitter carrier is defined as:

$$470MHz + 4MHz + i \times 8Hz, \qquad i = 0,1,2,3... \qquad (3.1)$$

By the way, some countries define the transmission bandwidth as 7MHz or 6 MHz. We can only change the sample period (or elementary period) to fit these unique bandwidth regulations. The elementary period T is $7/64\,\mu s$ for 8MHz channels, $1/8\,\mu s$ for 7MHz channels and $7/48\,\mu s$ for 6 MHz channels.

3.2.2 Frame Structure

The transmitted signal is organized in frames. Each frame consists of 68 OFDM symbols. Four frames constitute one super-frame. Each symbol is constituted by a set of 6817 carriers in 8K mode and 1705 carriers in 2K mode. In addition to the transmitted data, an OFDM frame contains:

(1)   Scattered pilot carriers

(2)   Continual pilot carriers

(3)   TPS carriers

The pilots can be used for frame synchronization, frequency synchronization, time synchronization, channel estimation, transmission mode identification. The emitted signal at time *t* can be expressed as:

$$S(t) = \text{Re}\{e^{j2\pi f_c t} \sum_{m=0}^{\infty} \sum_{l=0}^{67} \sum_{k=K\min}^{K\max} C_{m,l,k} \times \psi_{m,l,k}(t)\} \qquad (3.2)$$

where

$$\psi_{m,l,k}(t) = e^{j2\pi\frac{k'}{T_u}(t-\Delta-l\times T_{total}-68\times m\times T_{total})} \qquad if \ (l+68\times m)\times T_{total} \le t \le (l+68\times m+1)\times T_{total}$$

$$\psi_{m,l,k}(t) = 0 \qquad\qquad\qquad\qquad else$$

and k denotes the subcarrier number, $k' = k - (K_{max} + K_{min})/2$ is carrier index relative to the centre frequency, l denotes the OFDM symbol number, m denotes the transmission frame number, $C_{m,l,k}$ is the complex data on each subcarrier, and T_{total} is an OFDM symbol duration composed of two parts: a useful part with duration T_u and a guard interval with duration Δ.

The numerical values for OFDM parameter for the 8K and 2K modes for 8MHz channels are attached in Table 3.3. Each mode can choose four kinds of guard interval duration, (i.e., 1/4, 1/8, 1/16 or 1/32 of a useful symbol duration).

Table 3.3 DVB-T OFDM parameters for 8K & 2K modes, with 8MHz channel

Parameter	8K mode	2K mode
Number of carriers $\quad$ K	6817	1705
Vaule of carrier number $\quad$ K_{min}	0	0
Value of carrier number	6816	1704
Duration $\quad$ T_U	896 us	224 us
Carrier spacing $\quad$ $1/T_U$	1116 Hz	4464 Hz
Space between K_{min} to K_{max}	7.61 MHz	7.61 MHz

3.2.3 Carrier Allocations

DVB-T has three kinds of reference signals: continual pilots, scattered pilots and transmission parameter signaling (TPS). Each of them is derived from a PRBS (Pseudo Random Binary Sequence), $w_k = X^{11} + X^2 + 1$. We can use these reference signals to find correct symbol and frame timing, estimate the frequency offset, and do channel estimation.

3.2.3.1 Continual Pilots

There are 177 continual pilots in 8K mode and 45 in the 2K mode. The continual pilots are inserted into fixed subcarriers at each symbol as shown in Figure 3.10. The value of continual pilot on subcarrier k is given by:

$$\text{Re}\{C_{m,l,k}\} = 4/3 \times 2(1/2 - w_k); \quad \text{Im}\{C_{m,l,k}\} = 0 \qquad (3.3)$$

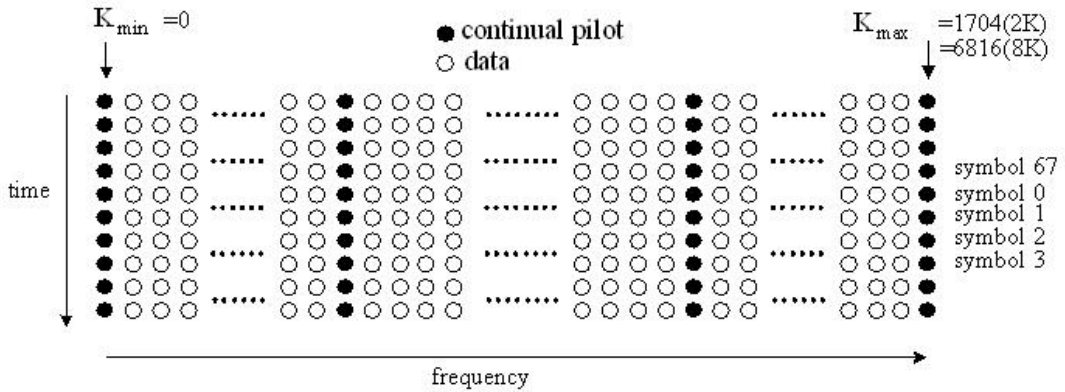The integral frequency offset can be estimated by matching the continual pilot of each symbol.

Figure 3.10 Continual pilot locations of DVB-T system [15]

3.2.3.2 Scattered Pilots

The scattered pilots are applied to do the channel estimation by interpolation. Unlike the continual pilots, scattered pilots are varying symbol by symbol. The positions of scattered pilots are specified by:

$$k = K_{\min} + 3 \times (l \bmod 4) + 12p \mid p \in \text{integer}, \quad p \geq 0, \quad k \in [K_{\min}, K_{\max}] \qquad (3.4)$$

where $K_{\min} = 0$ for both 2K and 8K modes, $K_{\max} = 1704$ for 2K mode and $K_{\max} = 6816$ for 8K mode. Since $(l \bmod 4)$ is used, the scattered pilot location will repeat every four symbols as shown in Figure 3.11.
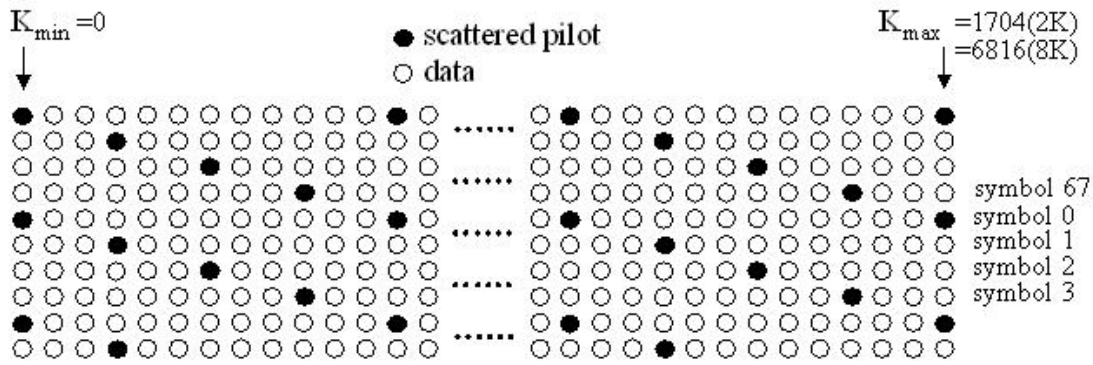
Figure 3.11 Scattered pilot locations of DVB-T system [15]

3.2.3.3 Transmission Parameter Signaling (TPS)

The TPS carriers are used for the purpose of signaling parameters related to the transmission scheme, coding and modulation. The TPS is transmitted in parallel on 17 TPS carriers for the 2K mode and on 68 carriers for the 8K mode. Every TPS carrier in the same symbol conveys the same differentially encoded information bit. The sub-carriers carrying the TPS information are the same in every symbol just like the continual pilots.

The TPS is defined over 68 consecutive OFDM symbols, referred to as one OFDM frame. The reference sequence corresponding to the TPS carriers of the first symbol of each OFDM frame are used to initialize the TPS modulation on each TPS carrier. Each OFDM symbol conveys one TPS bit. Each TPS block (corresponding to one OFDM frame) contains 68 bits, defined as: 1 initialization bit; 16 synchronization bits; 37 information bits and 14 redundancy bits for error protection. We can find the start of a frame by matching 16 synchronization bits. The transmission parameter information shall be transmitted as shown in Table 3.4.

Every TPS carrier is DBPSK modulated, which conveys the same message. The DBPSK is initialized at the beginning of each TPS block. The following rule applies to the differential modulation of carrier k of symbol l $(l > 0)$ in frame m:

Table 3.4 TPS signaling and format of DVB-T system

Bit number	Purpose/Content
s_0	Initialization
$s_1 - s_{16}$	Synchronization word
$s_{17} - s_{22}$	Length indicator
s_{23}, s_{24}	Frame number
s_{25}, s_{26}	Constellation
s_{27}, s_{28}, s_{29}	Hierarchy information
s_{30}, s_{31}, s_{32}	Code rate, HP stream
s_{33}, s_{34}, s_{35}	Code rate, LP stream
s_{36}, s_{37}	Guard interval
s_{38}, s_{39}	transmission mode
$s_{40} - s_{53}$	Reserved for future use
$s_{54} - s_{67}$	Error protection

$$\mathrm{Re}\{C_{m,l,k}\} = (-1)^{S_l} \times \mathrm{Re}\{C_{m,l,k-1}\}, \quad \mathrm{Im}\{C_{m,l,k}\} = 0 \tag{3.4}$$
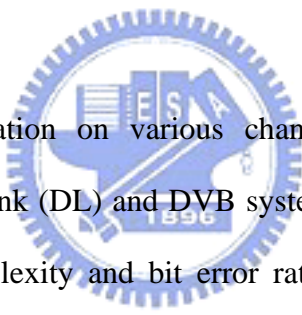
The absolute modulation of the TPS carriers in the first symbol in a frame is derived

from the PRBS $w_k = X^{11} + X^2 + 1$ as follows:

$$\mathrm{Re}\{C_{m,l,k}\} = 2(1/2 - w_k), \quad \mathrm{Im}\{C_{m,l,k}\} = 0; \tag{3.5}$$

Chapter 4

Channel Estimations for 802.16a and DVB-T systems

A comparative investigation on various channel estimation algorithms for 802.16a uplink (UL), Downlink (DL) and DVB system is presented and analyzed in terms of computational complexity and bit error rate in this chapter. The channel estimation schemes based on the comb-type like pilots specified in the standard of 802.16a and DVB system are first utilized to estimate channel frequency responses in the pilot positions. Then the channel frequency response in all subcarriers positions can be estimated by interpolation operations. Six channel interpolation schemes are adopted in this chapter inclusive of piece-wise linear interpolation, Lagrange interpolation, cubic spline interpolation, cubic Bspline interpolation, DFT based interpolation, and DCT based interpolation algorithms.

4.1 Fundamentals of Channel Estimations for OFDM Systems

There are two types of data modulation schemes in wireless digital communication systems. One is the differential modulation schemes, such as differential phase-shift keying (DPSK), while the other is the multi-amplitude modulation scheme, such as quadrature amplitude modulation (QAM). When using the differential modulation scheme, the receiver doesn't need a channel equalizer [16] for the recovery of original data such as DPSK in the European digital-audio broadcast (DAB) system [17]. However, DPSK is appropriate for relatively low data rate. For more efficient data transmission systems, coherent modulation is more appropriate that requires estimation and tracking of fading channels.

OFDM channel estimation techniques are mostly based on two types of approach, one is called "Blind Estimation" based on signalling scheme, and the other is called "Pilot Symbol Aided Modulation" (PSAM), which is based on the transmission of known symbols or pilot symbols inserted in the data sequence. Since PSAM scheme is adopted in the most current OFDM system standards, this chapter takes aim at the channel estimation schemes based on pilot symbols. For PSAM, there are two fundamental types of pilot arrangement in an OFDM system. One is the "Comb-type" and the other is the "Block-type" as illustrated in Figure 4.1 (a) and (b).

4.1.1 Pilot Arrangement

For Block-type arrangement, a symbol whose subcarrier data are all known pilots is normally called a preamble symbol. During a preamble symbol, channel frequency responses can be easily determined by decision-directed methods. However,
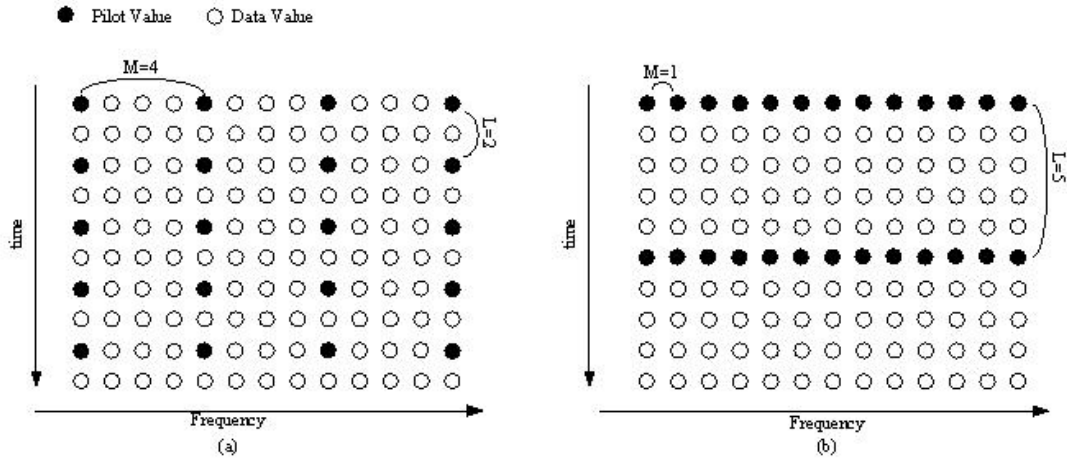
Figure 4.1 (a) Comb-type pilot arrangement (b) Block-type pilot arrangement of an

OFDM system

in fading environments, channel conditions may be different between two consecutive symbols so that Block-type channel estimation methods are hard to track the change of channel conditions. In contrast, Comb-type pilot arrangement doesn't have all pilot-subcarriers, but scatters pilots subcarriers in both symbol and subcarrier directions. In Figure 4.1, pilot density of Comb-type arrangement in symbol index direction is higher than that of Block-type arrangement. Thus it is easier to track channel fading conditions with Comb-type arrangement. Still, interpolation is needed to acquire the channel frequency responses at all data subcarriers.

In general, channel estimation schemes for Block-type arrangement can be easily determined by the least-square (LS) or linear minimum mean square error (LMMSE) optimization techniques. For Comb-type arrangement, channel frequency responses at pilot positions are first determined by the same methods as in Block-type arrangement, and then channel interpolation is done for channel frequency responses in data subcarriers based on the pilot channel estimation results. In the next section, we will introduce the LS and LMMSE estimation methods and some interpolation schemes.

4.1.2 The LS Channel Estimation

LS method is a quite common method in general signal processing. LS method is done based on the *a prioi* data. Assume that there are M pilot subcarriers in an OFDM symbol, which are defined as $X_p(m)$, then
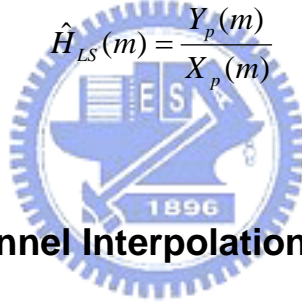
$$Y_p(m) = H_p(m)X_p(m) + Z_p(m) \qquad m = 0,1,2\cdots,M-1 \qquad (4.1)$$

Applying the LS method for the channel frequency response in pilot position is to minimize the following cost function:

$$Min\{(Y_p(m) - \hat{H}_p(m)X_p(m))^2\} \qquad (4.2)$$

To get the optimal least-square-error solution, $\hat{H}_p(m)$ is determined by

$$\hat{H}_{LS}(m) = \frac{Y_p(m)}{X_p(m)} \qquad (4.3)$$

4.1.3 The LMMSE Channel Interpolation

LMMSE optimization is also a quite common technique in general signal processing. They are widely used in wireless communication. LMMSE interpolator and filter have been proposed to do the channel estimations for OFDM systems [18], [19]. Actually, it is just one of the many variations of general MMSE methods. Here, we just introduce the most common form.

Based on LS channel estimation, channel frequency responses at pilot positions can be determined by

$$\hat{H}_p(m) = \frac{Y_p(m)}{X_p(m)} = H_p(m) + \frac{N_p(m)}{X_p(m)} = H_p(m) + \tilde{N}_p(m) \qquad (4.4)$$

Then, one can use a linear interpolator to estimate complete channel frequency responses based on $\hat{H}_p(m)$ as

$$\hat{\mathbf{H}} = \mathbf{A}\hat{\mathbf{H}}_p$$

$$\hat{\mathbf{H}} = \left[\hat{H}(0)\ \hat{H}(1)\ \cdots\ \hat{H}(N-1)\right]^T \quad \hat{\mathbf{H}}_p = \left[\hat{H}_p(0)\ \hat{H}_p(1)\cdots\ \hat{H}_p(M-1)\right]^T \tag{4.5}$$

where $\mathbf{A}$ is an $N \times M$ matrix. To get the optimal solution in minimum mean square error sense, matrix $\mathbf{A}$ can be determined by

$$\min\left\{E\left[\left\|\mathbf{H} - \hat{\mathbf{H}}\right\|^2\right]\right\}$$

$$\Rightarrow E\left[(\mathbf{H} - \mathbf{A}\hat{\mathbf{H}}_p)\hat{\mathbf{H}}_p^H\right] = 0$$

$$\Rightarrow \mathbf{A}_{MMSE} = \mathbf{R}_{\mathbf{H}\hat{\mathbf{H}}_p}\mathbf{R}_{\hat{\mathbf{H}}_p}^{-1} \tag{4.6}$$

$$where\ \ \mathbf{R}_{\mathbf{H}\hat{\mathbf{H}}_p} = E\left[\mathbf{H}\hat{\mathbf{H}}_p^H\right] \quad \mathbf{R}_{\hat{\mathbf{H}}_p} = E\left[\hat{\mathbf{H}}_p\hat{\mathbf{H}}_p^H\right]$$

Since the noise is white Gaussian distributed, the two correlation matrices can be further decomposed as

$$\mathbf{R}_{\mathbf{H}\hat{\mathbf{H}}_p} = E\left[\mathbf{H}(\hat{\mathbf{H}}_p + \tilde{\mathbf{N}}_p)^H\right] = E\left[\mathbf{H}\mathbf{H}_p^H\right] = \mathbf{R}_{\mathbf{H}\mathbf{H}_p}$$

$$\mathbf{R}_{\hat{\mathbf{H}}_p} = E\left[\mathbf{H}_p\mathbf{H}_p^H\right] + E\left[\tilde{\mathbf{N}}_p\tilde{\mathbf{N}}_p^H\right] \tag{4.7}$$

$$\tilde{\mathbf{N}}_p = \left[\tilde{N}_p(0)\ \tilde{N}_p(1)\cdots\tilde{N}_p(M-1)\right]$$

If all $X_p(k)$'s have the same power, then

$$\mathbf{R}_{\hat{\mathbf{H}}_p} = \mathbf{R}_{\mathbf{H}_p} + \frac{\sigma_N^2}{\left|X_p(k)\right|^2}\mathbf{I} = \mathbf{R}_{\mathbf{H}_p} + \frac{\beta}{SNR}\mathbf{I} \tag{4.8}$$

where σ_N^2 is the noise variance, $\beta = E[|d(k)|^2]\big/|X_p(k)|^2$ and $SNR = E[|d(k)|^2]/\sigma_N^2$

Finally, the estimated channel frequency responses in the MMSE sense can be expressed as

$$\hat{\mathbf{H}}_{MMSE} = \mathbf{A}_{MMSE}\hat{\mathbf{H}}_p \tag{4.9}$$

4.1.4 Some Popular Channel Interpolation Techniques

Generally, channel interpolation starts with LS estimations of channel frequency responses at the reference subcarriers. Then the channel frequency response at all

subcarrier positions can be estimated by interpolation. By the concept of convolution theorem, data of each subcarrier can be easily recovered by equalizing the received subcarrier signal. This is the purpose of channel interpolation and estimation.

4.1.4.1 Piecewise Linear Interpolation

Complete channel frequency response can be obtained by linear interpolation between adjacent pilot signals in this scheme. Let the channel frequency responses of pilot subcarriers be $H_p(0), H_p(1),\ldots,H_p(m),\ldots,H_p(N/d)$, then channel estimate of k-th subcarrier can be determined by

$$\hat{H}(k) = (1 - \frac{l}{d})H_p(m) + \frac{l}{d}H_p(m+1) \tag{4.10}$$

where d is the pilot subcarrier spacing, m denotes the location of pilot subcarrier and l is the distance between the m-th pilot subcarrier and the k-th subcarrier.

4.1.4.2 Lagrange Interpolation [20]

An L-th order Lagrange estimation is described by an L-th order polynomial with respect to l/d (as specified in linear interpolation) by using ($L+1$) pilot subcarrier channel samples. Figure 4.2 shows a polynomial of degree L, which passes through the known $L+1$ pilot samples. Then the unknown data between the L known points can be acquired from the polynomial. The coefficients of a fractional delay filter are obtained by the Lagrange interpolation formula, as shown in Eq. (4.11) and Eq. (4.12)

$$\tilde{H}(n) = \sum_{m=0}^{M-1} H_p(m) \prod_{\substack{k=0 \\ k \neq m}}^{M-1} \frac{n-k}{m-k} \tag{4.11}$$

$$Q_l(k,m) \equiv \prod_{\substack{k=0 \\ k \neq m}}^{L-1} \frac{n-k}{m-k}, \ m = 0, 1, 2, ..., M-1 \tag{4.12}$$

A low-order estimation is generally used to save computational burden. For example, the 2-th order Lagrange interpolation is quite popular as shown below

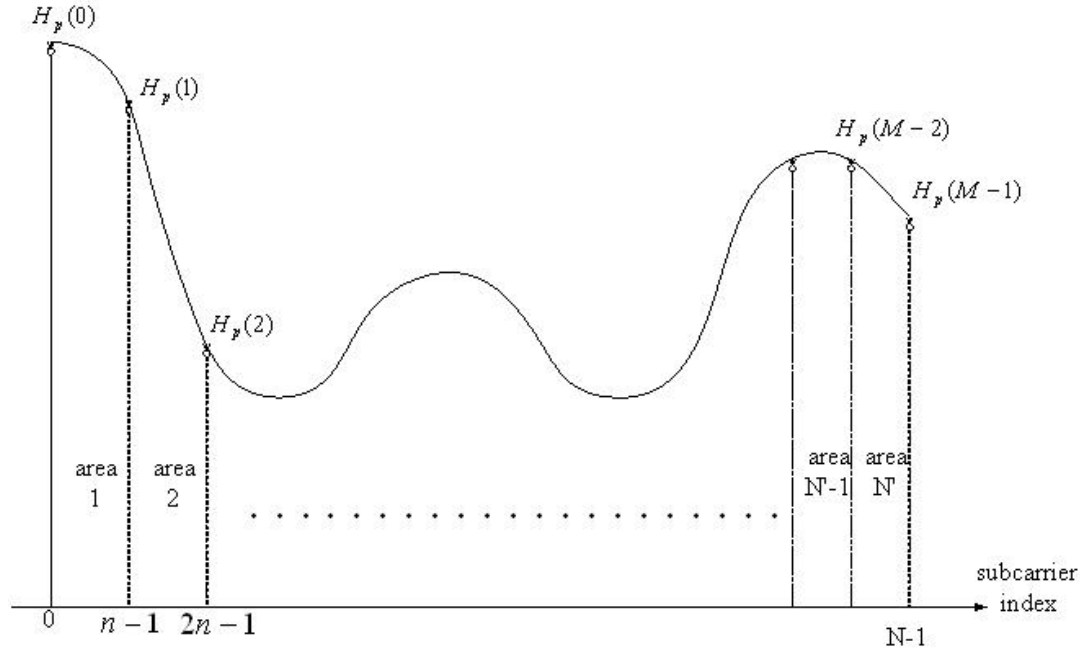$$\hat{H}(k) = Q_{-1}(k,m)H_p(m-1) + Q_0(k,m)H_p(m) + Q_1(k,m)H_p(m+1) \qquad (4.13)$$

where

$$Q_{-1}(k,m) = \frac{(k-m)(k-(m+1))}{(m-1-m)(m-(m+1))}$$

$$Q_0(k,m) = \frac{(k-(m-1))(k-(m+1))}{(m-(m-1))(m-(m+1))}$$

$$Q_1(k,m) = \frac{(k-(m-1))(k-m)}{(m+1-(m-1))(m+1-m)}$$

are determined by the distance between the locations of the subcarrier to be estimated and the reference samples.

Figure 4.2 Lagrange interpolation

4.1.4.3 Spline Interpolation [21]

The linear interpolation in 4.1.4.1 and Lagrange interpolation in 4.1.4.2 are examples of piecewise polynomial interpolators. Spline interpolation is also a polynomial interpolation which is developed under the consideration of signal

continuity in nature including derivative continuity. A popular spline interpolation method is "Cubic Spline". It is a kind of third-order polynomial interpolation technique that preserves slope continuity at the boundary point between two adjacent interpolation intervals. The approach is to fit a cubic polynomial to a pair of adjacent points with the condition that both slopes and curvatures of the two endpoints agree with one another as shown in Figure 4.3.
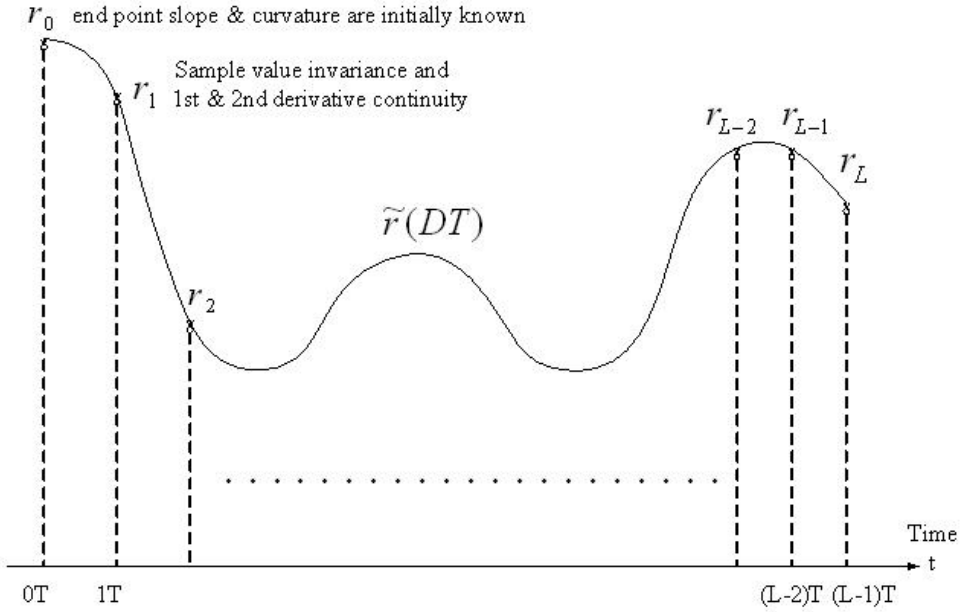
Figure 4.3 Cubic spline interpolation

Based on pervious description, channel estimates based on the cubic polynomials are

$$\hat{H}(k) = c_{0,k} + c_{1,K}(k-m) + c_{2,K}(k-m)^2 + c_{3,K}(k-m)^3 \tag{4.14}$$

where the $c_{0,k}, c_{1,k}, c_{2,k}, c_{3,k}$ are determined by the values of $H_p(m)$, $H_p(m-1)$ and the continuity condition of the first and second derivatives at the boundary points between adjacent cubic interpolation polynomials. But unlike other algorithm, the second derivatives at both band edge points of an OFDM symbol should be specified in Cubic Spline estimation for solving the equation (4.14), which is known as boundary conditions. There are some common choices [21] for boundary conditions

include:

(1) Make zero curvatures at the endpoints. This is equivalent to assuming that $H_p(0)$ and $H_p(M)$ approach linearity at their outer extremities. The result is sometimes referred as *nature spline*.

(2) Make the slope of either or both boundaries a specified value computed *a priori*.

(3) Make $k_0 = k_1$ and $k_{M-1} = k_M$, where k_i is the slope of $H_p(i)$. This is assuming that $H_p(0)$ and $H_p(M)$ approach parabolas at their extremities.

Due to large amount of matrix operations for solving the linear equations, this method is impractical to be applied to channel interpolation. Luckily, there is another type of low-complexity spline polynomials, called "B-spline" polynomial, which also preserves derivative continuity. Details are described in section 4.1.4.4.

4.1.4.4 B-Spline Interpolation [22]

General B-Spline interpolations provide a highly versatile approach to describe curves in computer graphics. B-Spline interpolations consist of sections of polynomial-fitted curves connected by boundary points. The simplest way to construct a B-spline interpolation polynomial is to convolve a square function $h_1(t)$ with itself as many times as desired in accordance with the desired derivative continuity, as shown in Figure 4.4.

In the figure, $h_2(t)$, $h_3(t)$ and $h_4(t)$ are so-called "linear B-spline", "quadratic B-spline", and "cubic B-spline", respectively, as described by Eq. (4.15), Eq. (4.16) and Eq. (4.17). Coefficients of the desired causal interpolation FIR can be easily obtained by time-shifting and substituting t with corresponding values.

41
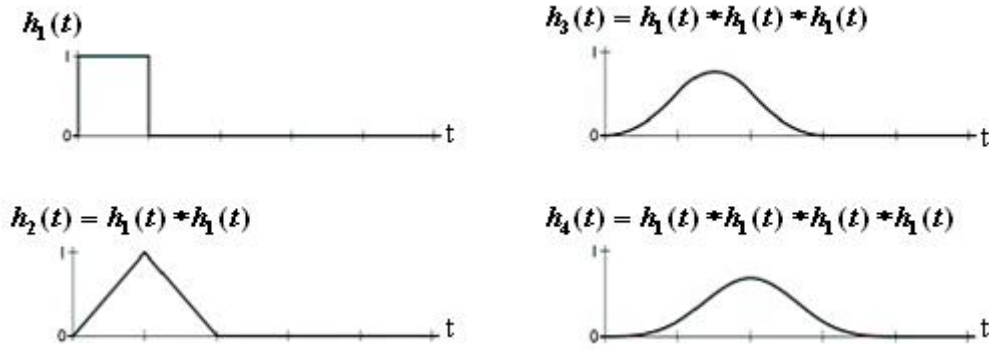
Figure 4.4 Construction of B-Splines

$$\text{Linear B-spline}: h_2(t) = \begin{cases} t+1, & -1 \le t \le 0 \\ 1-t, & 0 \le t \le 1 \end{cases} \tag{4.15}$$

$$\text{Quadratic B-spline}: h_3(t) = \begin{cases} \dfrac{1}{2}(t+\dfrac{3}{2})^2, & -\dfrac{3}{2} \le t \le -\dfrac{1}{2} \\ \dfrac{3}{4}-t^2, & -\dfrac{1}{2} \le t \le \dfrac{1}{2} \\ \dfrac{1}{2}(t-\dfrac{3}{2})^2, & \dfrac{1}{2} \le t \le \dfrac{3}{2} \end{cases} \tag{4.16}$$

$$\text{Cubic B-spline}: h_4(t) = \begin{cases} \dfrac{2}{3}+\dfrac{1}{2}|t|^3-t^2, & 0 \le |t| \le 1 \\ \dfrac{1}{6}(2-|t|)^3, & 1 \le |t| \le 2 \end{cases} \tag{4.17}$$

The most commonly used B-Spline function consist of cubic segments is the "cubic B-Spline". Cubic B-Spline interpolation also provides first and second derivative continuity at the reference boundary samples between adjacent segments, but generates different samples values from original ones at the reference sample locations.

4.1.4.5 DFT-Based Interpolation

DFT-based channel estimator has been proposed in [23], [24]. The estimator is quite different from the interpolation schemes mentioned above, because it is based on the transform-domain interpolation instead of in the time domain. It can utilize fast DFT algorithms to reduce transform complexity. The DFT-based channel estimator

has a restriction on placement of pilot subcarriers. The pilot subcarriers must be equi-spaced along frequency direction, as shown in Figure 4.5.
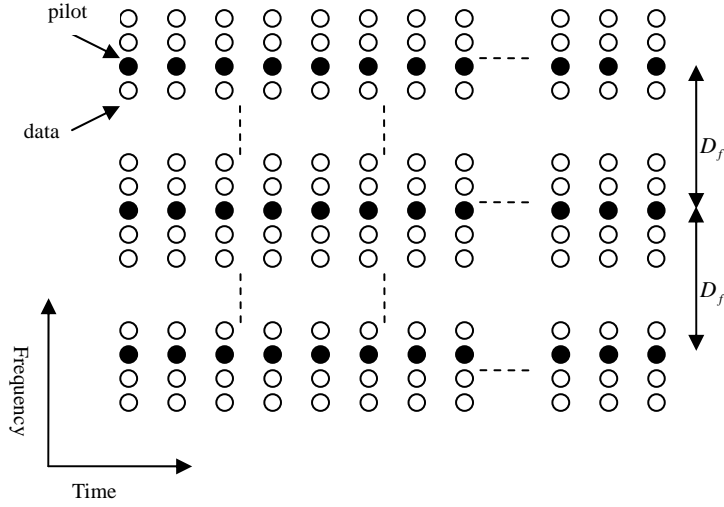

Figure 4.5 Regular equal-spaced pilot placement

Since pilot subcarriers are equi-spaced, channel frequency responses at pilot subcarriers can be viewed as the down samples of complete frequency responses. According to sampling theory, the inverse discrete Fourier transform of $H_p(m)$ would be the aliased version of the channel impulse response as shown in Figure 4.6 (which two-times downsampling as an example). Higher downsampling rates result in more severe aliasing effect than the lower rate cases. With this property, it is obvious that if no aliasing occur, the channel impulse response can be perfectly reconstructed by $IDFT\{H_p(k)\}$. This is the basic concept of DFT-based interpolation.

The DFT-based estimator starts with LS estimates of channel frequency response at pilot subcarriers as described by Eq. (4.3).

$$\hat{H}_p(m) = \frac{Y_p(m)}{X_p(m)} \tag{4.18}$$

Next, M-point IDFT is operated on the $\hat{H}_p(m)$
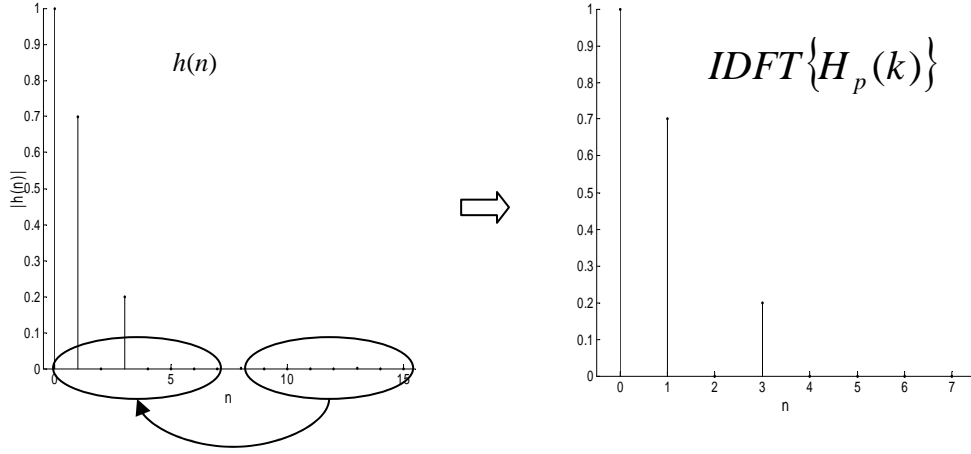
Figure 4.6 Aliasing effect of channel impulse response due to
down-sampling in frequency domain

$$\hat{h}_p(n) = IDFT_k\left\{\hat{H}_p(k)\right\} = \frac{1}{M}\sum_{k=0}^{M-1}\hat{H}_p(k)e^{-j\frac{2\pi nk}{M}} \quad n = 0,1,2,\cdots M-1 \quad (4.19)$$

where M is the pilot number. By the concept of interpolation, the estimated channel

impulse response is obtained by padding $\left\{\hat{h}_p(n)\right\}_{n=0}^{M-1}$ in the middle of $\left\{\hat{h}_p(n)\right\}_{n=0}^{M-1}$.

$$\hat{h}(n) = \begin{cases} \hat{h}_p(n) & 0 \le n \le M/2-1 \\ 0 & otherwise \\ \hat{h}_p(M+n-N) & N\text{-}M/2 \le n \le N-1 \end{cases} \quad (4.20)$$

Where N is the total subcarriers number. After that, N-point DFT is operated on

$\hat{h}(n)$, which is equivalent to do the interpolation in frequency domain.

$$\hat{H}(k) = \sum_{n=0}^{N-1}\hat{h}(n)e^{-j\frac{2\pi nk}{N}} \quad k = 0,1,2\cdots,N-1 \quad (4.21)$$

The whole estimation process of DFT-based estimator is shown in Figure 4.7.
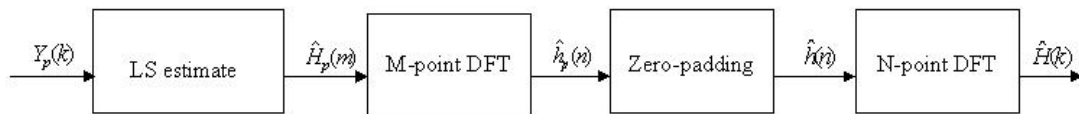
Figure 4.7 DFT-based channel estimator

4.1.4.6 DCT-Based Interpolation

The DCT-based channel interpolation is proposed in [24]. When performing DFT on a set of N-point data, it is equivalent to periodically extend the N-point data to infinite length and then transform it by Discrete-Time Fourier Transform (DTFT). Therefore, if it is discontinuous between two ends of the N-point data, there will be abrupt variation in between consecutive periods after extension and high frequency component will occur in the transform domain. By the interpolation concept, high frequency component is usually the source of aliasing and must be prevented as much as possible. As it turns out, the effect of channel impulse response aliasing due to down-sampled data of channel frequency responses will degrade the performance of DFT-based channel estimator.

Discrete Cosine Transform (DCT) is a well-known technique widely used in the image processing. Compared with DFT, DCT can reduce high frequency components in the transform domain by eliminating the edge effect as mentioned above. The reason is that operation of N-point DCT is equivalent to extend the original data to $2N$-point by mirror-extension and performing a $2N$-point DFT on the extended data followed by constant magnitude and phase compensation. Obviously, mirror-extension can solve the discontinuity problem introduced by periodic extension. Therefore, DCT indeed has better power concentration at low frequency. This benefits interpolation process.

The DCT-based channel estimator has the same restriction on pilot placement as DFT-based channel estimator. Let's assume the same pilot deployment as in section 4.1.4.5. First, LS estimate is used to obtain the channel frequency response at pilot subcarriers

$$\hat{H}_p(k) = \frac{Y_p(k)}{P(k)} \tag{4.22}$$

Given an extended symmetric mirror-duplicated data, then its DFT will be less distorted by high frequency and less affected by aliasing effect. Due to the symmetry property of input data, the DFT/IDFT operations in the interpolation process reduce to DCT-related ones. In the following demonstration, DFT-based interpolation on mirror-extended data and its reduction to DCT-based interpolator are introduced.

First, let's consider frequency response of a signal as a kind of time-domain signal. Then interpolation of this time-domain signal can be done based on the concept of ideal interpolation operation. For better low-pass interpolation, we can extend this "time-domain" as

$$\hat{H}_{2M}(k) = \begin{cases} \hat{H}_p(k) & 0 \le k \le M-1 \\ \hat{H}_p(2M-k-1) & M \le k \le 2M-1 \end{cases} \tag{4.23}$$

The second step is to transform the data by DFT and obtain its "spectrum coefficients" as

$$\hat{h}_{2M}(m) = \sum_{k=0}^{2M-1} \hat{H}_{2M}(k) \cdot e^{\frac{j2\pi mk}{2M}} \qquad k = 0,1,\cdots,2M-1 \tag{4.24}$$

Since $\hat{H}_{2M}(k)$ is symmetric, $\hat{h}_{2M}(m)$ has the following property

$$\hat{h}_{2M}(m) = \begin{cases} 0 & m = M \\ \hat{h}_{2M}(2M-m) \cdot e^{j\frac{2\pi m}{2M}} & M+1 \le m \le 2M-1 \end{cases} \tag{4.25}$$

This shows that the magnitudes of $\left\{\hat{h}_{2M}(m)\right\}$ are symmetric with respect to $m = M$. Then from the concept of interpolation, the ideal upsampled spectrum should be scaled down to a narrow bandwidth by a factor of M/N. This effect can be carried out by first doing zero-padding in the middle of $\left\{\hat{h}_{2M}(m)\right\}$ and multiplying $\left\{\hat{h}_{2M}(m)\right\}$ by a weighting gain 2N/2M to get the spectrum after upsampling.

$$\hat{h}_{2N}(m) = \begin{cases} \dfrac{2N}{2M}\hat{h}_{2M}(m) & 0 \le m \le M-1 \\ 0 & otherwise \\ \dfrac{2N}{2M}\hat{h}_{2M}(m-2N+2M) & 2N-M \le m \le 2N-1 \end{cases} \qquad (4.26)$$

Finally, the interpolation process is completed by performing 2N-point IDFT on the new spectrum coefficient $\hat{h}_{2N}(m)$. The estimated channel response is obtained by extracting the first N-point data after IDFT.

$$\hat{H}_{2N}(k) = IDFT_m\{\hat{h}_{2N}(m)\} = \frac{1}{2N}\sum_{m=0}^{2N-1}\hat{h}_{2N}(m)e^{j\frac{2\pi mk}{2N}} \qquad k = 0,1,2,\cdots 2N-1$$
$$\hat{H}(k) = \hat{H}_{2N}(k) \qquad k = 0,1,2,\cdots N-1 \qquad (4.27)$$

In this interpolation process, the original data is translated to a symmetric form, which definitely reduces the "high frequency" components for the desired signal $H_{2N}(k)$. Therefore, the aliasing effect would be reduced in the interpolation process and the estimated channel frequency response would be more accurate.

Next the following shows how the whole process is reduced to DCT-based computations. First let's examine the DFT operation in (4.24) and rewrites it as

$$\hat{h}_{2M}(m) = \sum_{k=0}^{2M-1}\hat{H}_{2M}(k)\cdot e^{-\frac{j2\pi mk}{2M}} = \sum_{k=0}^{M-1}\hat{H}_p(k)\cdot[e^{-\frac{j2\pi mk}{2M}} + e^{-\frac{j2\pi m(2M-k-1)}{2M}}]$$
$$= \sum_{k=0}^{M-1}\hat{H}_p(k)\cdot[e^{-\frac{j2\pi mk}{2M}} + e^{\frac{j2\pi m(k+1)}{2M}}] = e^{\frac{j\pi m}{2M}}\sum_{k=0}^{M-1}\hat{H}_p(k)\cdot\cos(\frac{(2k+1)m\pi}{2M}) \qquad (4.28)$$

On the other hand, the DCT transform of $\hat{H}_p(k)$ can be expressed as

$$\hat{h}_c(m) = w(m)\sum_{k=0}^{M-1}\hat{H}_p(k)\cos\frac{\pi(2k+1)m}{2M} \qquad m = 0,\cdots,M-1$$
$$w(m) = \frac{1}{\sqrt{M}},\ m = 0; \quad w(m) = \sqrt{\frac{2}{M}},\ m \ne 0 \qquad (4.29)$$

Then by (4.25), (4.28) and (4.29), the relationship between $\hat{h}_{2M}(m)$ and $\hat{h}_c(m)$ can be described by

$$\hat{h}_{2M}(m) = \begin{cases} \dfrac{2}{w(m)}\hat{h}_c(m) \cdot e^{\frac{j\pi m}{2M}} & 0 \le m \le M-1 \\ 0 & m = M \\ \dfrac{2}{w(2M-m)}\hat{h}_c(2M-m) \cdot e^{\frac{j\pi m}{2M}} & M+1 \le m \le 2M-1 \end{cases} \qquad (4.30)$$

Furthermore, $\hat{h}_{2N}(m)$ which is extended from $\hat{h}_{2M}(m)$ can be also expressed in terms of $\hat{h}_c(m)$:

$$\hat{h}_{2N}(m) = \begin{cases} \dfrac{2N}{Mw(m)}\hat{h}_c(m) \cdot e^{\frac{j\pi m}{2M}} & 0 \le m \le M-1 \\ 0 & otherwise \\ \dfrac{2N}{Mw(2N-m)}\hat{h}_c(2N-m) \cdot e^{\frac{j\pi(m-2N+2M)}{2M}} & 2N-M+1 \le m \le 2N-1 \end{cases} \qquad (4.31)$$

Finally, one can replace $\hat{h}_{2N}(m)$ with $\hat{h}_c(m)$ in the IDFT operation (4.27), and modify the equation to a DCT-related operation.

$$\begin{aligned}
\hat{H}(k) &= \frac{1}{2N}\sum_{m=0}^{2N-1}\hat{h}_{2N}(m)e^{j\frac{2\pi mk}{2N}} \\
&= \frac{1}{2N}\left[\sum_{m=0}^{M-1}\frac{2N}{2M}\hat{h}_{2M}(m)\cdot e^{\frac{j2\pi mk}{2N}} + \sum_{m=2N-M+1}^{2N-1}\frac{2N}{2M}\hat{h}_{2M}(m-2N+2M)\cdot e^{\frac{j2\pi mk}{2N}}\right] \\
&= \frac{1}{2M}\hat{h}_{2M}(0) + \frac{1}{2M}\sum_{m=1}^{M-1}\left[\hat{h}_{2M}(m)\cdot e^{\frac{j2\pi mk}{2N}} + \hat{h}_{2M}(2M-m)\cdot e^{\frac{j2\pi(2N-m)k}{2N}}\right] \\
&= \frac{1}{2M}\frac{2}{w(0)}\hat{h}_c(0) + \frac{1}{2M}\sum_{m=1}^{M-1}\left[\frac{2}{w(m)}\hat{h}_c(m)\cdot e^{\frac{j\pi m}{2M}}\cdot e^{\frac{j2\pi mk}{2N}} + \frac{2}{w(m)}\hat{h}_c(m)\cdot e^{-\frac{j\pi m}{2M}}\cdot e^{\frac{j2\pi m(-k)}{2N}}\right] \\
&= \frac{1}{\sqrt{M}}\hat{h}_c(0) + \sum_{m=1}^{M-1}\left[\frac{1}{Mw(m)}\hat{h}_c(m)\cdot\left(e^{\frac{j\pi m}{2M}}\cdot e^{\frac{j2\pi mk}{2N}} + e^{-\frac{j\pi m}{2M}}\cdot e^{\frac{j2\pi m(-k)}{2N}}\right)\right] \\
&= \frac{1}{\sqrt{M}}\hat{h}_c(0) + \sum_{m=1}^{M-1}\sqrt{\frac{2}{M}}\hat{h}_c(m)\cdot\cos\left(\left(\frac{k}{N}+\frac{1}{2M}\right)\pi m\right) \\
&= \sum_{m=0}^{M-1}w(m)\hat{h}_c(m)\cdot\cos\left(\left(\frac{k}{N}+\frac{1}{2M}\right)\pi m\right) \qquad k = 0,1,2\cdots,N-1
\end{aligned}$$

$$(4.32)$$

This equation is known as Extendible Inverse Discrete Cosine Transform (EIDCT) [25]. Therefore, the IDFT operation with input $\hat{h}_{2N}(m)$ can be replaced by the EIDCT operations on $\hat{h}_c(m)$. The whole process of DCT/EIDCT-based channel estimator is shown in Figure 4.8. The equivalent DFT-based and DCT/EIDCT-based channel

estimations are shown in Figure 4.9. Although these two methods are equivalent, the computation complexity of using DFT-based channel estimator is higher than DCT-based estimator. When using DFT-based estimator, the amount of input data is double, in addition that it needs complex multiplications. On the contrary, the computations of both DCT and EIDCT only need real multiplications. Furthermore, DCT and EIDCT can be realized by fast algorithms. Therefore, using DCT/EIDCT-based channel estimator has the advantage of low computation complexity.
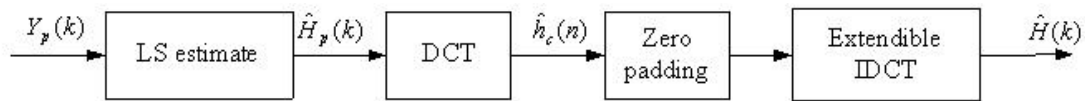
Figure 4.8 DCT/EIDCT-based channel estimator
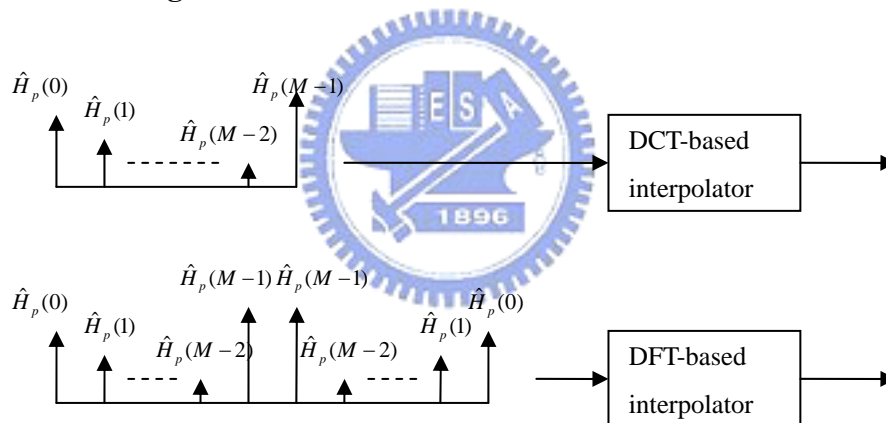
Figure 4.9 Equivalent DCT-based and DFT-based channel estimators

4.2 Channel Estimations for 802.16a and DVB Systems

4.2.1 Channel Estimations for 802.16a Uplink

Pilot arrangement in 802.16a Uplink is "Block type". Its channel estimation can be done by decision-directed scheme, as follows.

First, one can use preamble signal to estimate the entire channel frequency response by LS estimate.

$$\hat{H}_{LS}(m) = \frac{Y_p(m)}{X_p(m)} \quad m = 0, 1, \cdots, N-1 \qquad (4.34)$$

Then, the estimated channel frequency response based on $\hat{H}_{LS}(m)$ is used to recover the transmitted data $\hat{X}(m)$. From the noise reduced constellation mapped $\hat{X}(m)$, one can then get a better estimate of channel frequency response for next symbol.

If channel varies slowly, channel conditions of contiguous symbols can be assumed the same. Under such condition, the method is efficient. However, under fast fading channels, it is inappropriate that will lead to an error floor.

4.2.2 Channel Estimations for 802.16a DL

Before showing the performance comparisons of different channel interpolation schemes, two important characteristics in the spec of 802.16a DL must be addressed. One is the arrangement of pilot subcarriers which is different symbol by symbol but follows some rhythm. The other is the specified guard band which sends nothing at frequency band edges.

4.2.2.1 Pilot Arrangement and Guard Band Effect

The pilot arrangement has been already mentioned in section 3.1.2. Here we focus on its periodic property. One can see that the variable-location pilots have a period of twelve subcarriers in one symbol, six subcarriers in two combined successive symbols, and three subcarriers in four combined successive symbols. This implies that pilot subcarriers can be shared by different symbols for one-dimensional

interpolation or two-dimensional interpolations utilizing both time-domain and frequency-domain information can be applied to the channel estimation. Obviously, combined one-dimensional interpolations with shorter periods will produce better results than those of longer cases. But there is a tradeoff between channel variation and number of combined symbols to be utilized. When a channel is fast varying, it is not a good policy to generate a signal channel estimate across successive continuous symbols. On the other hand, two-dimensional interpolations can use linear interpolation using time-domain pilot subcarriers to trace the channel variation every four symbols.

In the discussion of DFT and DCT based interpolations, the pilot arrangement is assumed equi-spaced in the entire bandwidth. But in reality, 802.16a system deploys dc carrier and guard bands in order to avoid the interference between different communication systems. Since channel responses in these regions are unknown, performances of DFT and DCT based interpolations are susceptible. The miss of high frequency response leads to an error floor in signal detection. We try to (linearly) extrapolate those unknown channel responses by using the nearby pilot data for DFT and DCT based interpolations. But for the other polynomial-based interpolation schemes such as linear interpolation, Lagrange interpolation, the lost channel responses in guard band have nothing to do with those channel estimation algorithms.

4.2.2.2 Simulations and Performance Evaluation

Simulation parameters follow the 820.16a spec. An 802.16a OFDMA symbol consists of 2048 subcarriers. We pick a bandwidth of $6.857\,MHz$. Quadrature phase shift keying (QPSK) is used as the signal mapping scheme and the pilots are deployed as the discussion in section 3.2.1. Here we consider the cases that pilot subcarriers are formed by one symbol, two symbols, and four symbols, respectively. Transmission

environment is assumed "Vehicular A" channel defined by ETSI for the evaluation of UMTS radio interference proposals [26]. The multipath time delay and the average power of the multipath gains of the "Vehicle A" channel are shown in Table 4.1. The Doppler frequencies are set to 40 Hz and 120 Hz, corresponding to $f_d T = 0.0119$ and 0.0476, respectively.

In the simulation, perfect synchronization is assumed at the receiver. The bit error rate (BER) and the computation complexity are investigated to show the performance. BER's of the estimation algorithms in the "Vehicle A" channel with $f_d = 40Hz$ are depicted in Figure 4.10 ~ 12, corresponding to the cases of one-symbol, combined two-symbol and combined four-symbol pilot data, respectively. It is noted that performances of linear and cubic Bspline are almost the same and better than the other interpolation schemes. DFT and DCT based interpolations show the poorer performances than the others because of the inaccurate channel estimations in the guard bands. The linear interpolation rather than cubic Bspline interpolation is considered to be a suitable choice for 802.16a system if computational complexity is also taken into consideration. Figure 4.13 shows performances of linear interpolation versus pilot data composed by one symbol, two symbols, and four symbols assuming $f_d = 40Hz$. It is obvious that the performance of one-symbol pilot case is the best one of all cases. It is because that the duration of an OFDMA symbol is so long that the $f_d T = 0.012$ is relatively a large number. When $f_d T > 0.01$, the channel is considered as fast varying during a symbol period [27]. The result is that channel conditions are difficult to track from symbol to symbol. As such, estimation performances are poor when using pilot data composed of more than one symbol. For this problem, we can use two-dimension interpolation to trace the variation and the performance is showed in Figure 4.14. Although the performance is better than that in four symbols case, it is worse than that in one symbol case. As a result, it is not a good

**Table 4.1** Characteristics of ETSI "Vehicle A" channel environment

Tap	Time delays (μ sec)	Time delay (T_c)	Average Power (dB)
1	0	0	0
2	0.31	1.55	-1
3	0.71	3.55	-9
4	1.09	5.45	-10
5	1.73	8.65	-15
6	2.51	12.55	-20

policy to use two-dimensional interpolation, because higher complexities and lower performances than those of the one-dimensional interpolations are obtained.

Figure 4.15 17 shows BER performances of different interpolation schemes with $f_d = 120Hz$, corresponding to pilot data composed of one, two, and four symbols, respectively. The linear and cubic Bspline also holds better performances than the other interpolation schemes, while they are poorer than they are under the $f_d = 40Hz$ condition, because of faster channel variation. Figure 4.18 shows the performances of linear interpolation with $f_d = 120Hz$ versus pilot data composed by one symbol, two symbols, and four symbols. It shows that the one-symbol case shows the best BER than the others. In Figure 4.19, the performance of two-dimensional interpolation is poorer than the one-symbol case and better than the four symbols case. Hence, linear interpolation using one-symbol pilot data is a suitable choice for 802.16a DL channel estimation. In Figure 4.20, BER performances of linear interpolation versus Doppler frequencies are shown for the one-symbol case. It is obvious that the higher Doppler frequency is, the poorer performance is.
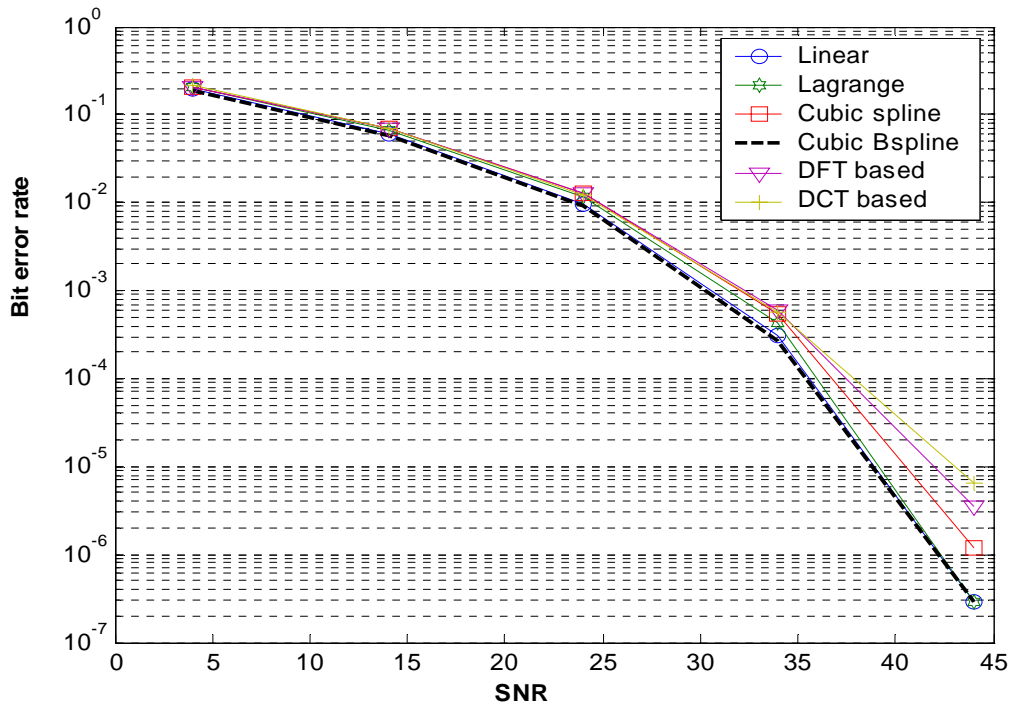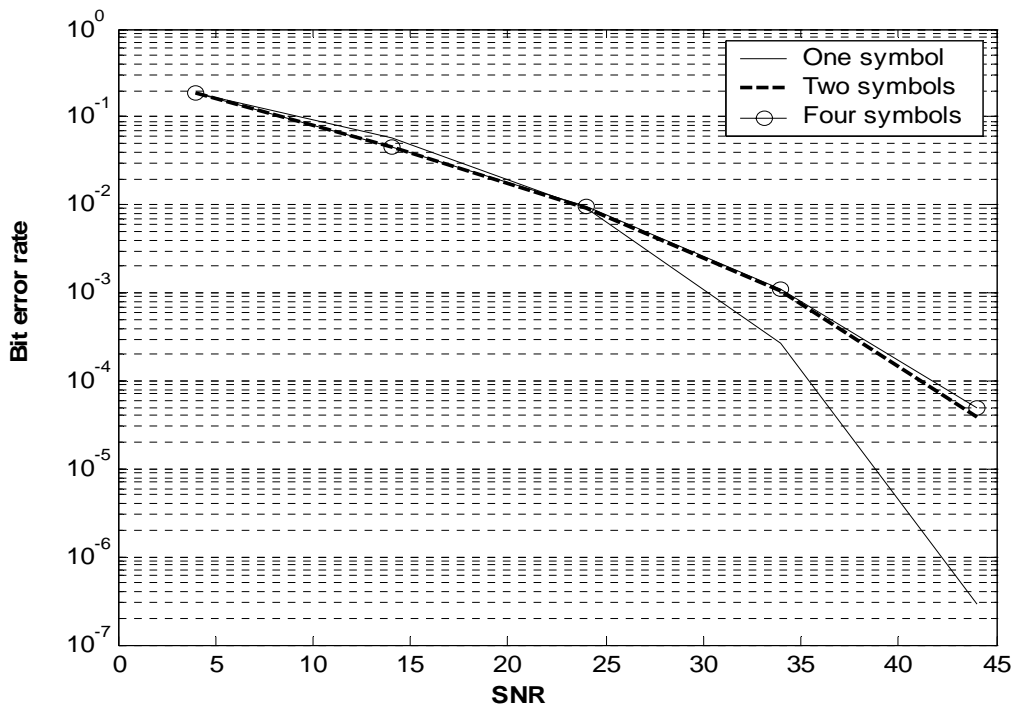
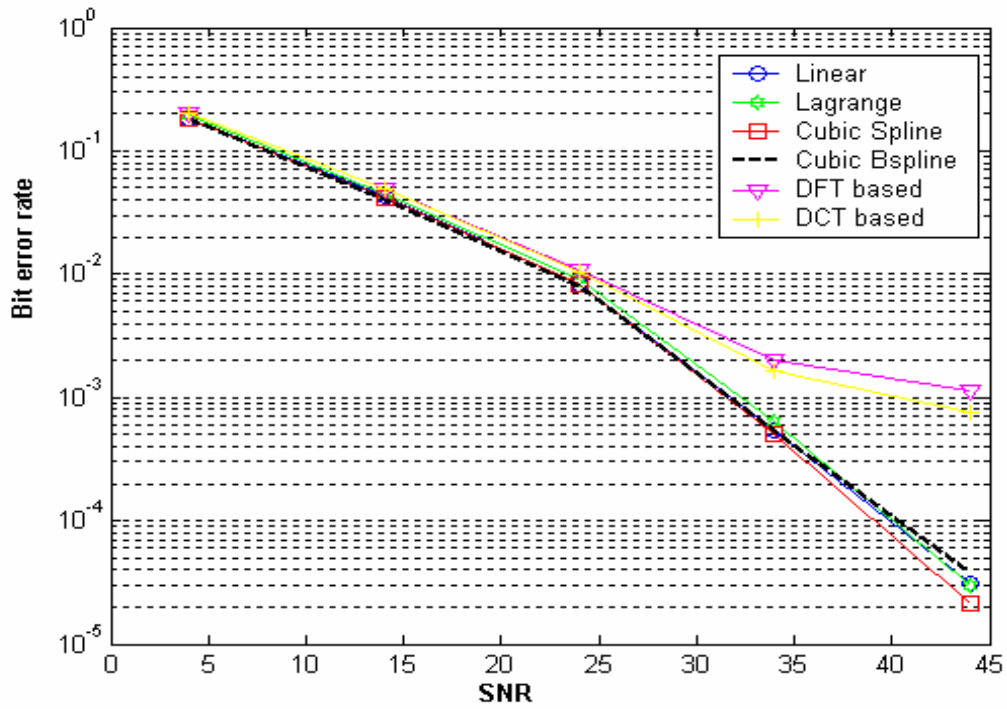**Figure 4.10** BER performance of various interpolation schemes with $f_d = 40Hz$, one-symbol pilot case
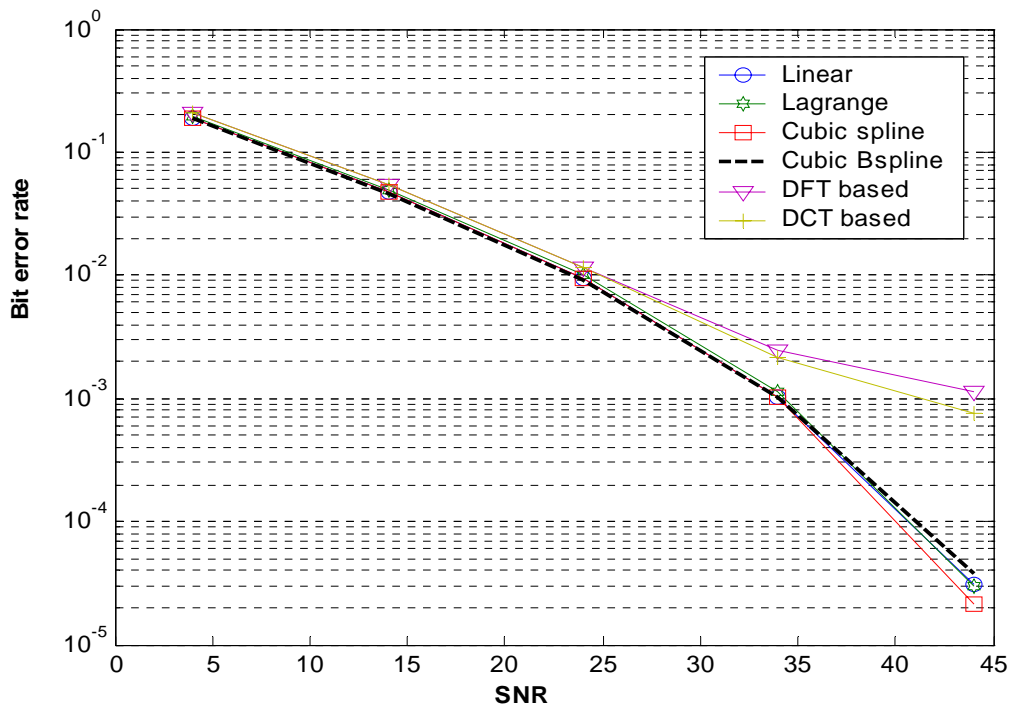
Figure 4.11 BER performance of various interpolation schemes with $f_d = 40Hz$,
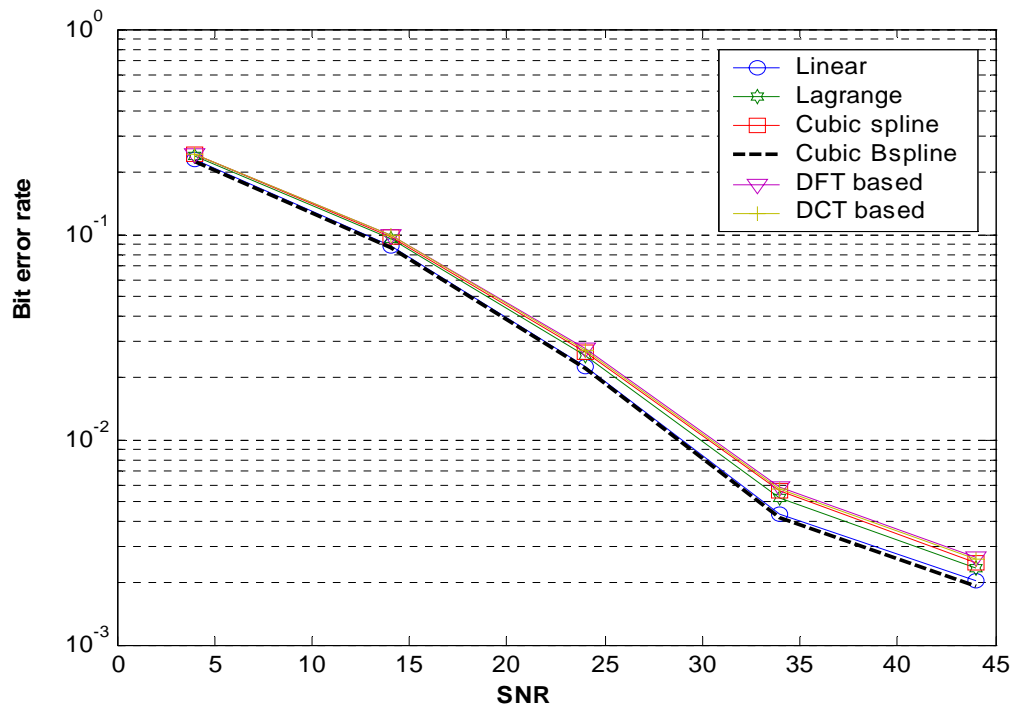
two-symbols pilot case
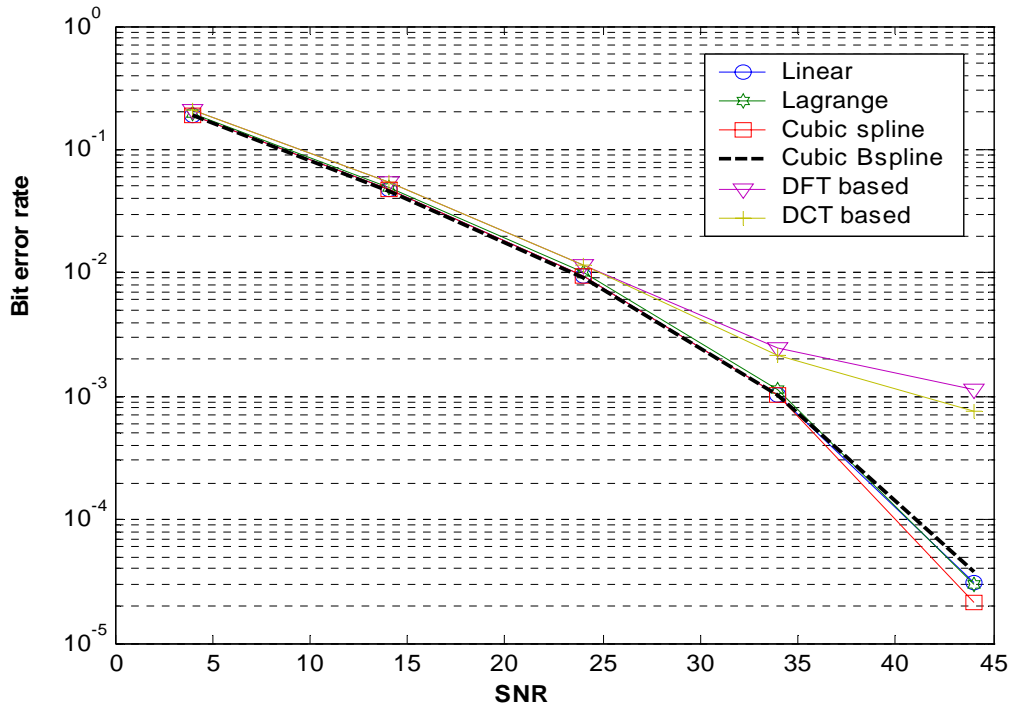
Figure 4.12 BER performance of various interpolation schemes with $f_d = 40Hz$,

four-symbols pilot case

Figure 4.13 BER performance of linear interpolation versus pilot symbol
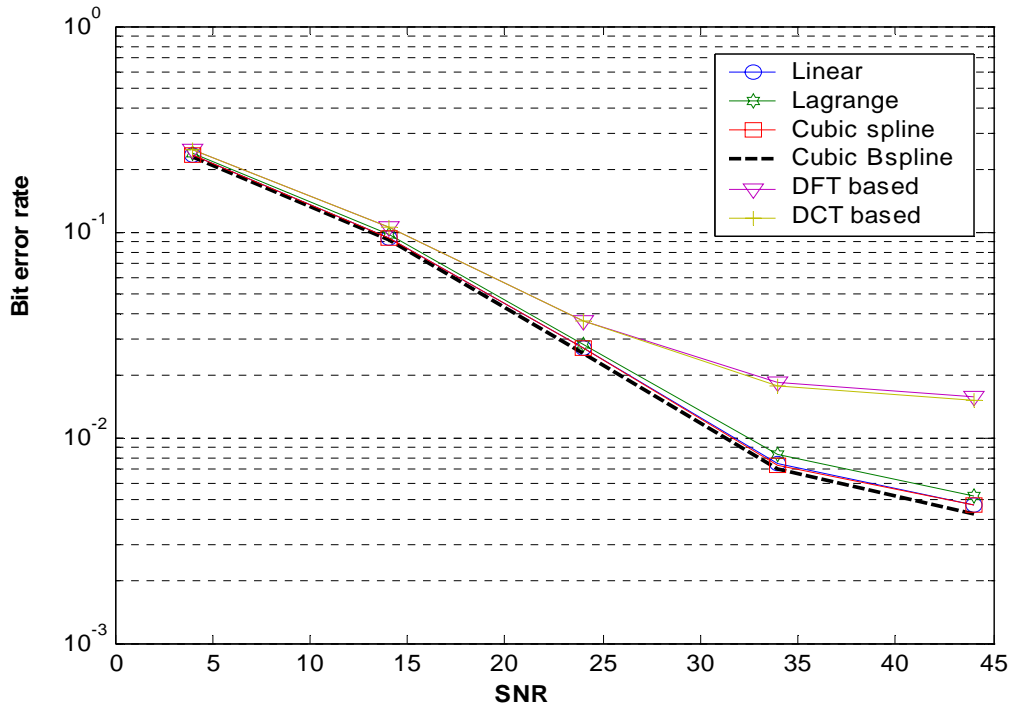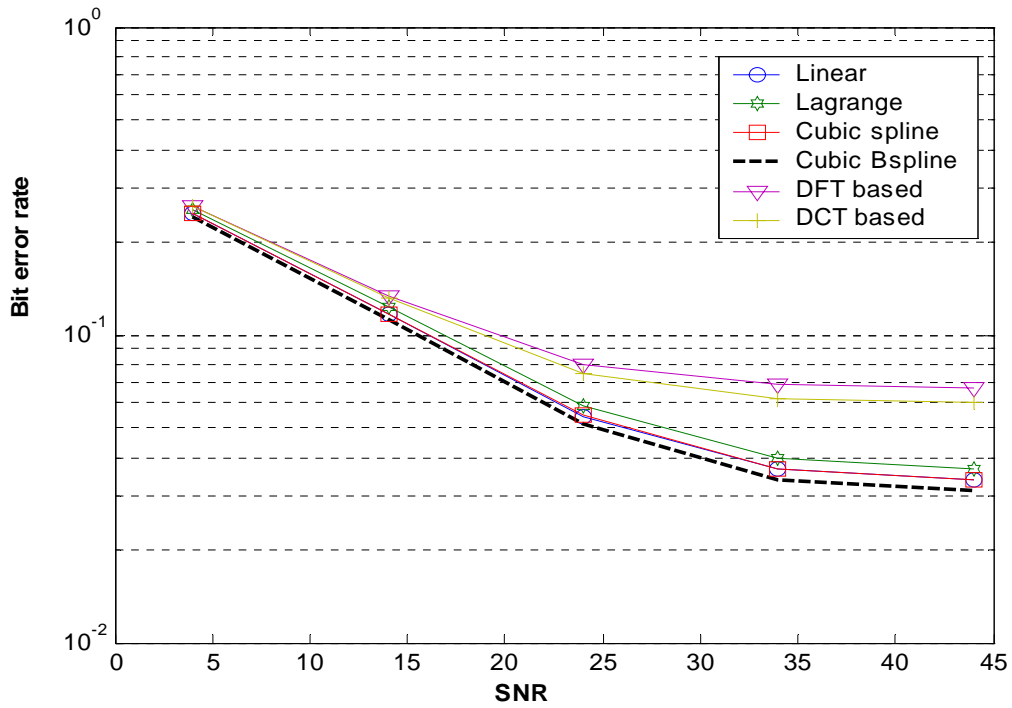
number with $f_d = 40Hz$

Figure 4.14 BER performance of various interpolation schemes with $f_d = 40Hz$,

two-dimensional interpolation

Figure 4.15 BER performance of various interpolation schemes with $f_d = 120Hz$,
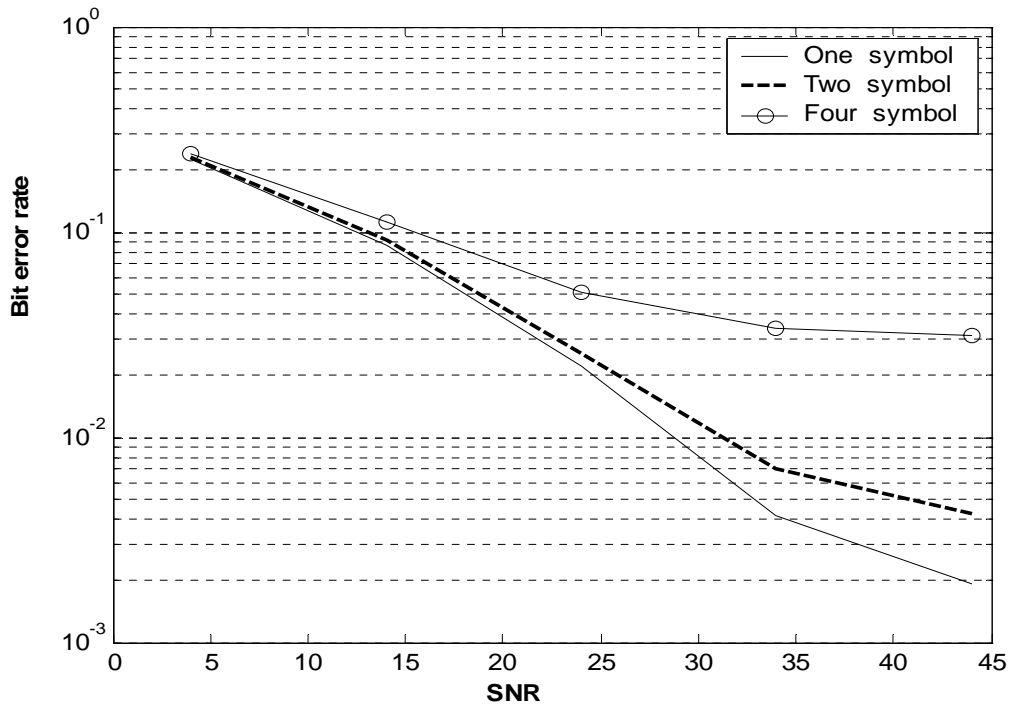
one-symbol pilot case
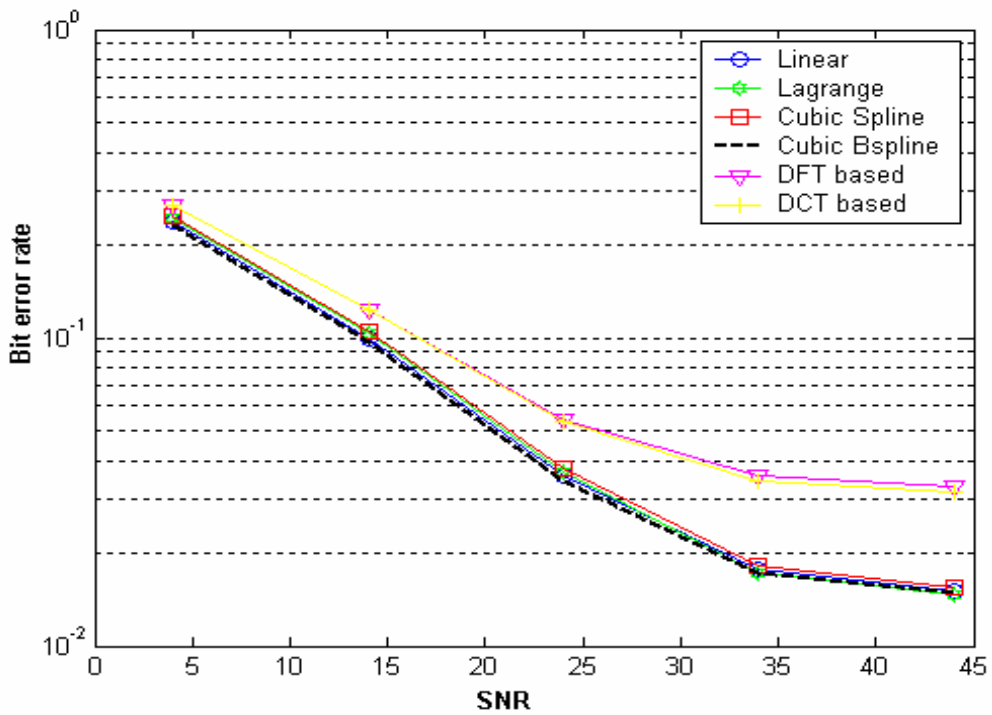
Figure 4.16 BER performance of various interpolation schemes with $f_d = 120Hz$,

two-symbols pilot case

Figure 4.17 BER performance of various interpolation schemes with $f_d = 120Hz$,

four-symbols pilot case

Figure 4.18 BER performance of linear interpolation versus pilot symbol number

with $f_d = 120Hz$

Figure 4.19 BER performance of various interpolation schemes with $f_d = 120Hz$,
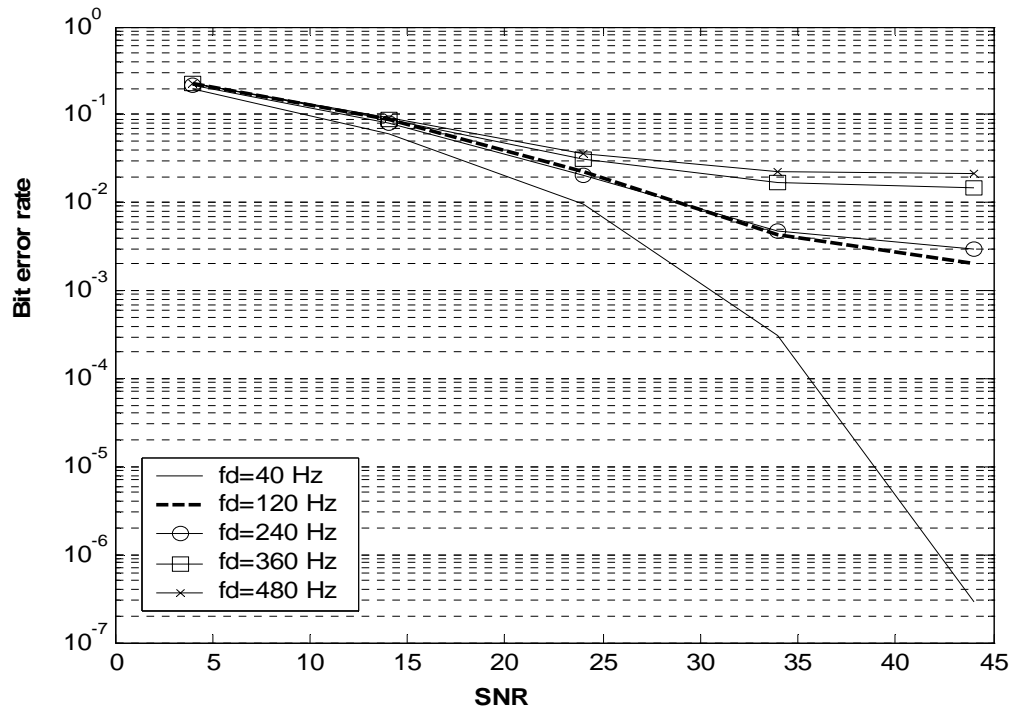
two-dimensional interpolation

Figure 4.20 BER performance of linear interpolation versus Doppler frequencies

4.2.3 Channel Estimations for DVB-T System

There are two modes of operation in DVB-T system: 2k mode and 8k mode. Here we only consider the 2k mode because its symbol arrangement is similar to 802.16 OFDMA. As in section 4.2.2, DVB-T system also has similar pilots and guard band structure to that of 802.16a system.

4.2.3.1 Pilot Arrangement and Guard Band Effect

Similar to the situation in 802.16a DL, one can see that the DVB-T variable-location pilots have periods of twelve subcarriers in one symbol, and three subcarriers in four combined successive symbols. Similarly, pilot subcarriers composed by successive symbols and two-dimensional interpolation schemes can be applied to the channel estimations. Likewise, we have to tradeoff between channel variation and pilot symbol numbers.

DVB-T system deploys guard bands which send nothing in order to avoid the interference between different communication systems. Since channel responses in these regions are unknown, performances of DFT and DCT based interpolations are susceptible. Those unknown guard band frequency responses lead to an error floor in signal detection. We try to do linear extrapolation of the unknown channel responses by using the nearby pilot data for DFT and DCT-based interpolation. But for the other polynomial-based interpolation schemes, the lost channel responses in guard band are not important as discussed in section 4.2.2.1 for 802.16a DL.

4.2.3.2 Simulations and Performance Evaluation

Simulation parameters are based on 2k-mode of DVB-T system. A 2k-mode OFDM symbol consists of 2048 subcarriers with a bandwidth of 7.611607 MHz. Quadrature phase shift keying (QPSK) is used as the signal mapping and the pilots are

described as in section 3.2.2. Here we consider 1-D interpolations based on one-symbol and combined four-symbol, and two-dimensional interpolations with linear interpolation in time-domain and the methods mentioned of section 4.1.4 in frequency-domain. Multipath channels defined by Annex B of DVB-T spec [15] is assumed. There are two channel models for our simulations, one is fixed-reception mode F_1 and the other is portable-reception mode P_1. The channel modes have been generated from (4.35), where $x(t)$ and $y(t)$ are input and output signals respectively.

$$y(t) = \frac{\rho_0 x(t) + \sum_{i=1}^{N} \rho_i e^{-j\theta_i} x(t-\tau_i)}{\sqrt{\sum_{i=0}^{N} \rho_i^2}} \quad \rho_0 = \sqrt{10 \sum_{i=1}^{N} \rho_i^2} \qquad (4.35)$$

where ρ_0 is the line-of-slight ray amplitude, N is the number of echoes equals to 20, and θ_i, ρ_i, τ_i are the phase, attenuation, relative delay of the i-th path listed in Table 4.2, respectively. The difference of channel conditions between mode F_1 and mode P_1 is that F_1 has the line-of-slight ray, ρ_0, while P_1 doesn't have. Here we consider F_1 case with multipath Rayleigh-fading channels. The Doppler frequencies are set to 40 Hz and 120 Hz, which correspond to $f_d T = 0.0108$ and 0.0324, respectively.

In the simulation, perfect synchronization is assumed at the receiver. The BER and the computational complexity are investigated to show the performance. BER's of the estimation algorithms with $f_d = 40 Hz$ and $f_d = 120 Hz$ are depicted in Figure 4.21～22 and Figure 4.25～26, where the pilot data are composed by one and four symbols, respectively. In both cases, the performances of linear and cubic Bspline interpolations are also better than those of the other schemes. The linear interpolation rather than cubic Bspline interpolation is considered to be a suitable choice for DVB-T system if the computational complexity is also taken into consideration.

Table 4.2 Relative power, phase and delay values for portable channel P_1

i	ρ_i	τ_i [μs]	θ_i [rad]
1	0,057 662	1,003 019	4,855 121
2	0,176 809	5,422 091	3,419 109
3	0,407 163	0,518 650	5,864 470
4	0,303 585	2,751 772	2,215 894
5	0,258 782	0,602 895	3,758 058
6	0,061 831	1,016 585	5,430 202
7	0,150 340	0,143 556	3,952 093
8	0,051 534	0,153 832	1,093 586
9	0,185 074	3,324 866	5,775 198
10	0,400 967	1,935 570	0,154 459
11	0,295 723	0,429 948	5,928 383
12	0,350 825	3,228 872	3,053 023
13	0,262 909	0,848 831	0,628 578
14	0,225 894	0,073 883	2,128 544
15	0,170 996	0,203 952	1,099 463
16	0,149 723	0,194 207	3,462 951
17	0,240 140	0,924 450	3,664 773
18	0,116 587	1,381 320	2,833 799
19	0,221 155	0,640 512	3,334 290
20	0,259 730	1,368 671	0,393 889

Figure 4.23 and Figure 4.27 show the performances of linear interpolation based on one-symbol and four-symbols pilot data, respectively, with $f_d = 40Hz$ and $f_d = 120Hz$. It is obvious that the performance of one-symbol estimation is better than the other in both fading conditions. It is because the channels are fast-fading in those channel conditions, i.e., $f_dT = 0.0119$ and 0.0357. The result is that the channel conditions are hard to track from symbol to symbol. As such, estimation performances are poor when using pilot data composed of more than one symbol. For two-dimensional interpolation, the simulation results for $f_d = 40Hz$ and $f_d = 120Hz$ are shown in Figure 4.24 and 4.28. Although BER of the two-dimensional interpolation is better than the four-symbol case, it is poorer than the one-symbol case. Hence, linear interpolation using one-symbol pilot data is a suitable choice for DVB-T system. In Figure 4.29, BER performances of linear interpolation versus Doppler frequencies are shown for the one-symbol case. It is obvious that the higher Doppler frequency is, the poorer performance is.
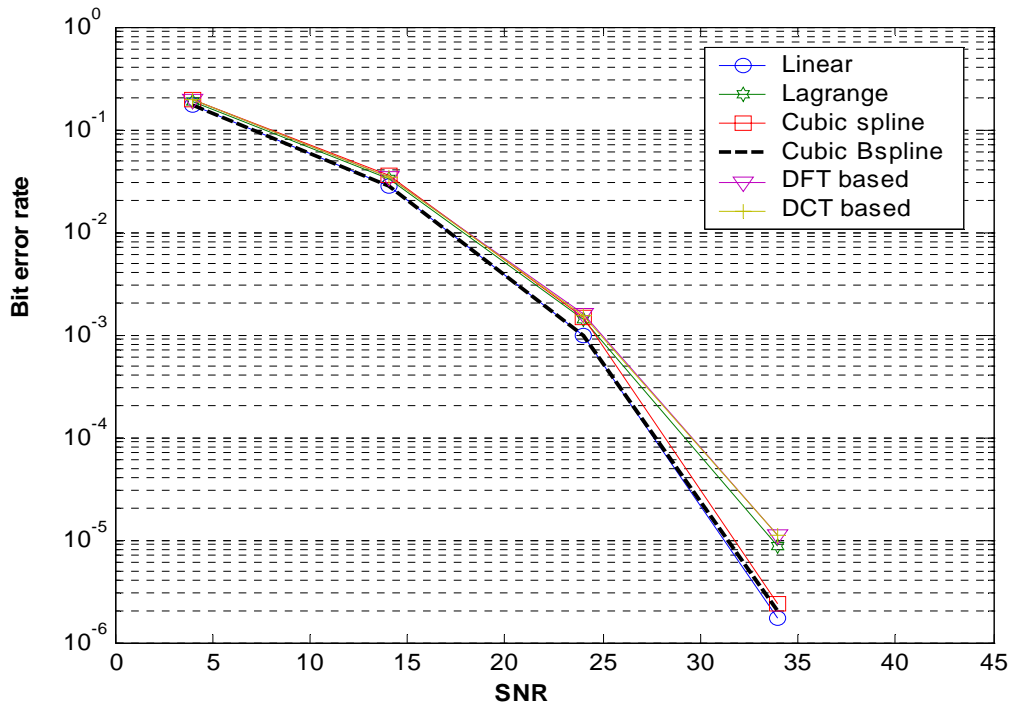
Figure 4.21 BER performance of various interpolation schemes with $f_d = 40Hz$, one-symbol pilot case
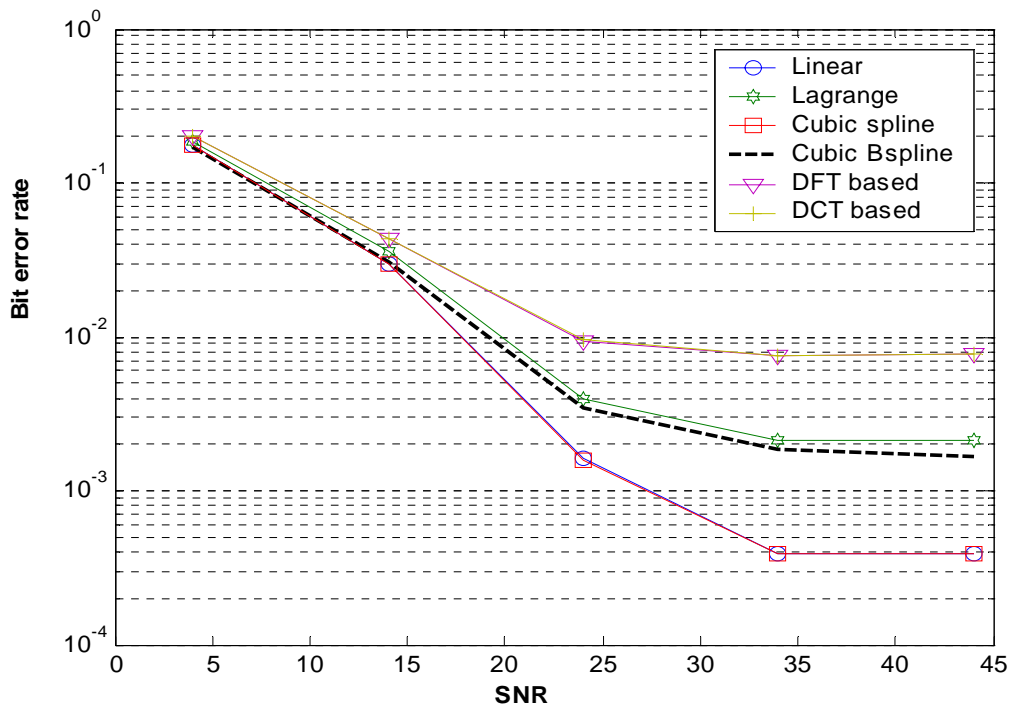
Figure 4.22 BER performance of various interpolation schemes with $f_d = 40Hz$,
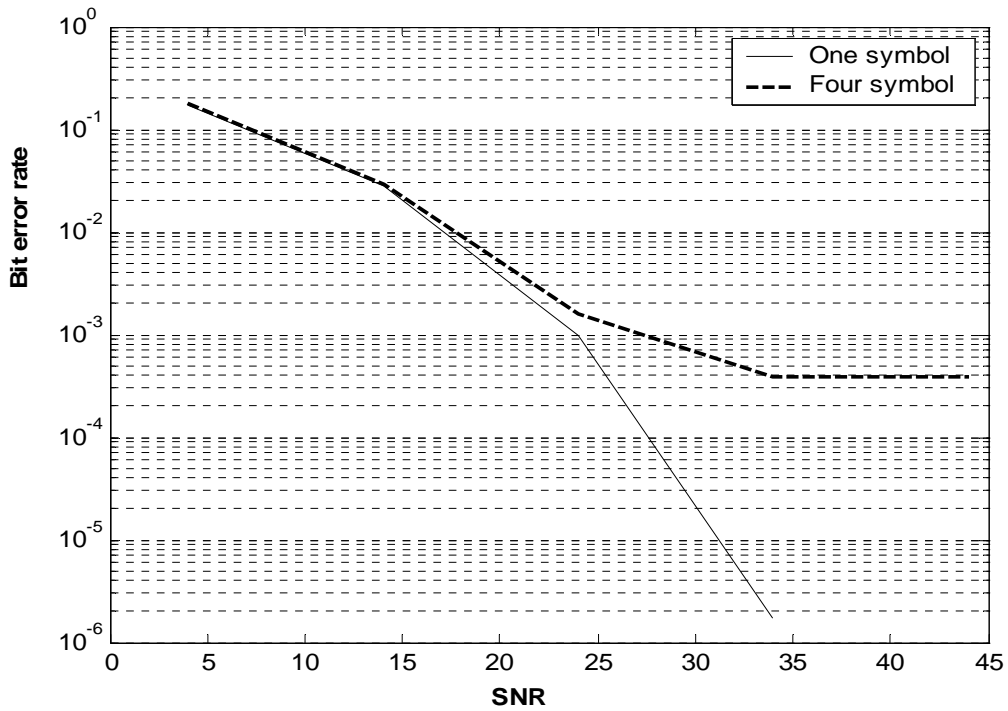
four-symbols pilot case

Figure 4.23 BER performances of linear interpolation versus pilot symbol number
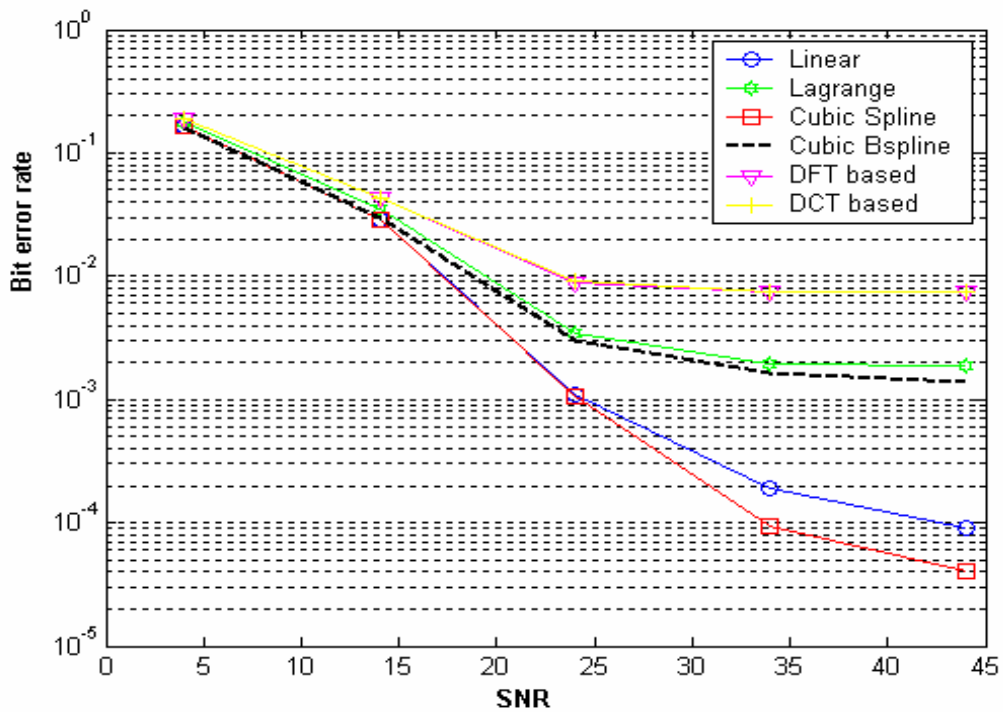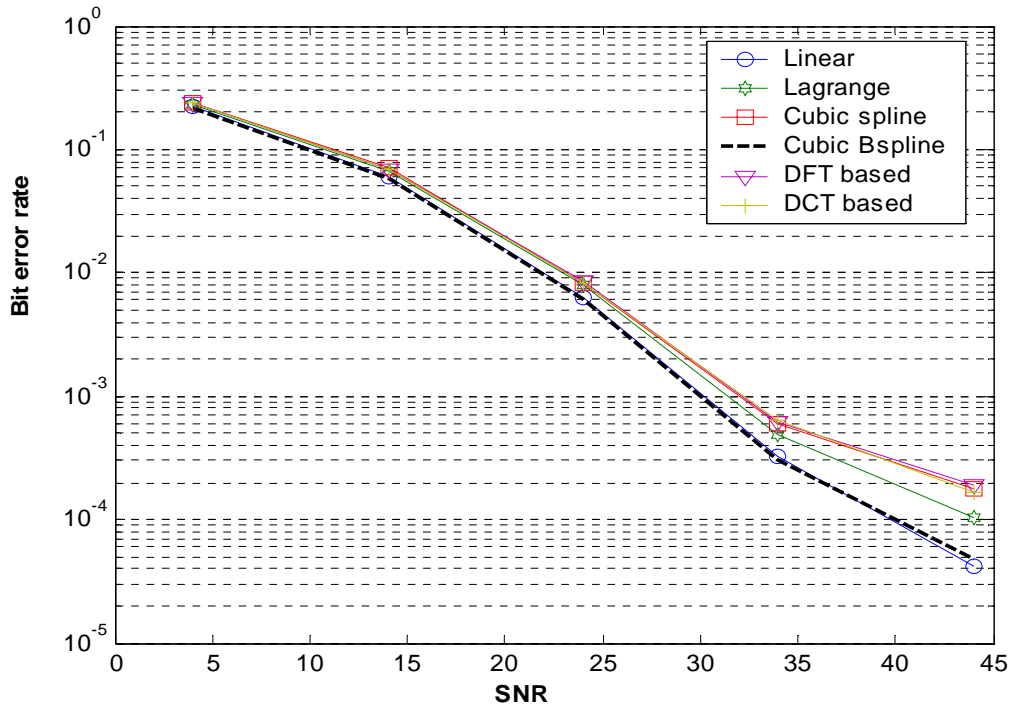
with $f_d = 40Hz$

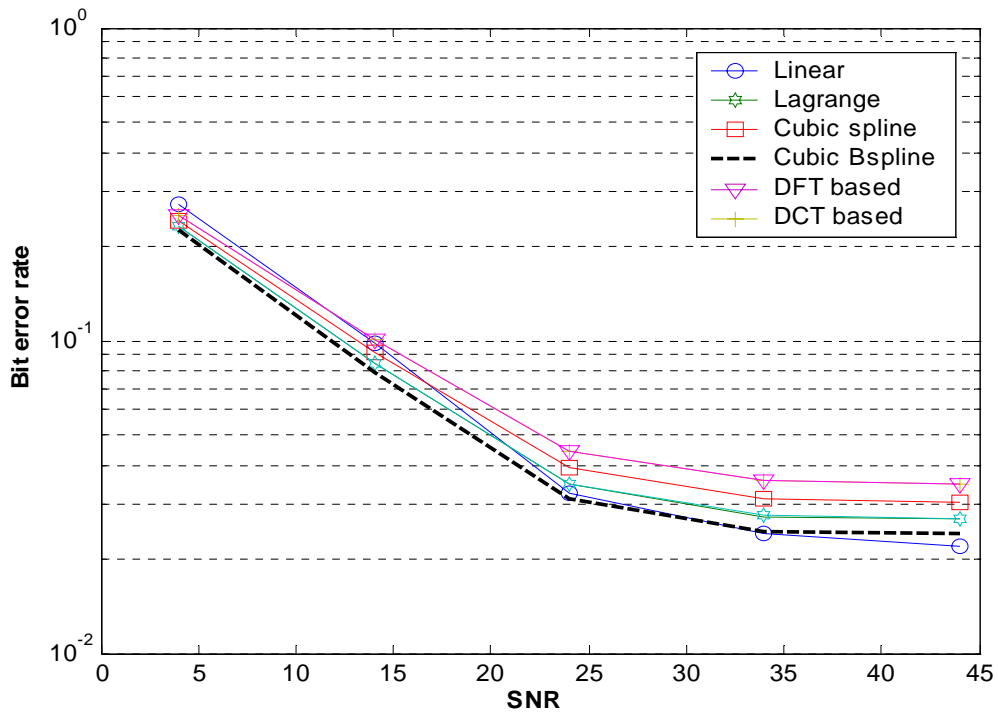**Figure 4.24** BER performance of various interpolation schemes with $f_d = 40Hz$,

two-dimensional interpolation

Figure 4.25 BER performance of various interpolation schemes with $f_d = 120Hz$,

one-symbol pilot case

Figure 4.26 BER performance of various interpolation schemes with $f_d = 120Hz$,
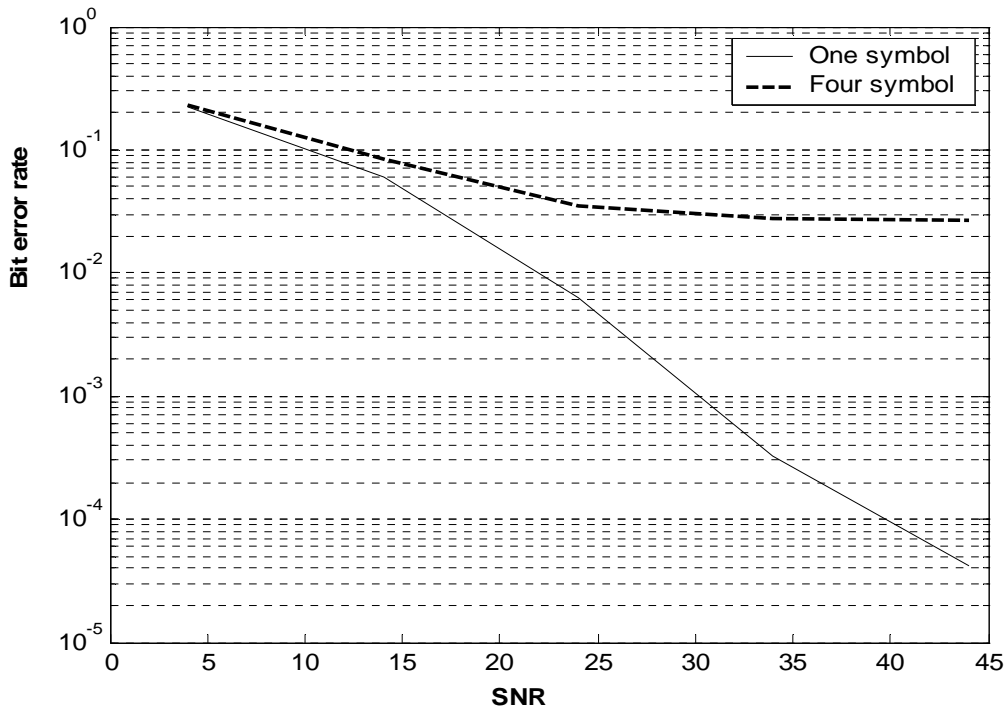
four-symbols pilot case

Figure 4.27 BER performances of linear interpolation versus pilot symbol number
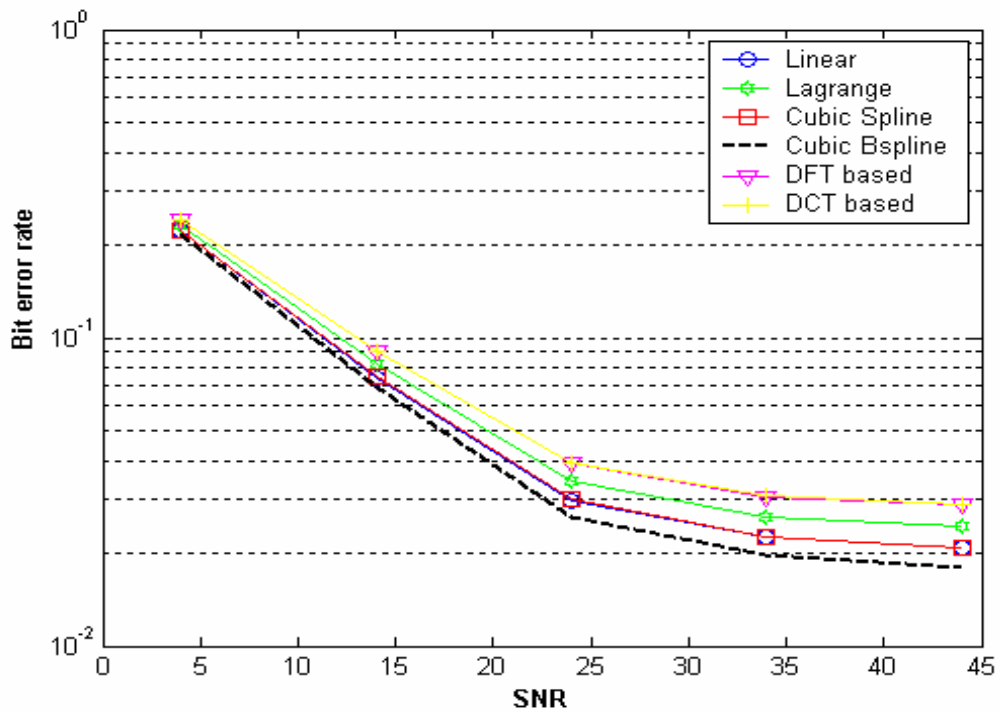
with $f_d = 120Hz$

Figure 4.28 BER performance of various interpolation schemes with $f_d = 120Hz$,
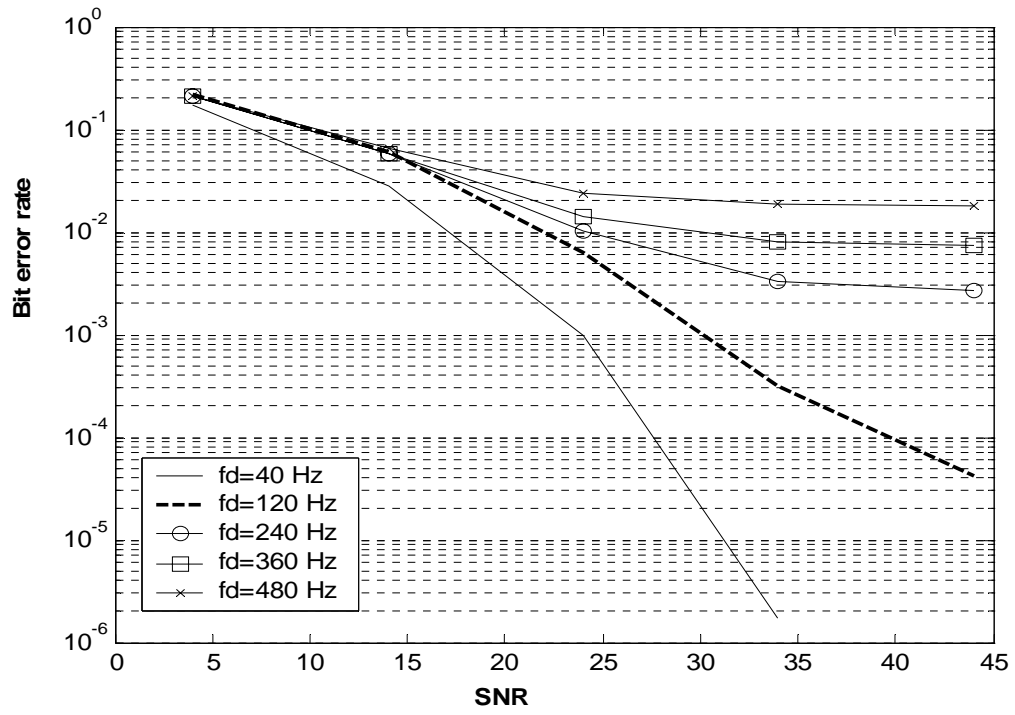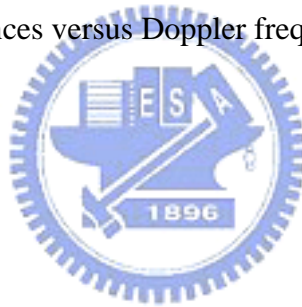
two-dimensional interpolation

Figure 4.29 BER performances versus Doppler frequencies of linear interpolation

4.2.4 Computational Complexities

The computational complexity is defined as the numbers of multiplications and additions required to find the channel estimate of each subcarrier. It is noted that one addition and one multiplication are needed in the piecewise linear interpolation. While three multiplications and two additions are necessary in the cubic Bspline interpolation. That is, the latter has a slightly higher complexity than the former one. The DFT-based interpolation adopts the radix-4 butterfly structure and N is the length of FFT function block. The computational complexities are compared and listed in Table 4.3, where N_M and N_A are the number of multiplications and additions, respectively.

Table 4.3 Computational complexity of various key interpolation schemes

Algorrithm	N_M	N_A
Piecewise linear	1	1
Lagrange	3	2
Cubic spline	6	4.8
Cubic Bspline	3	2
DFT based	$\frac{3}{4}*\log_4 N$	$2*\log_4 N$
DCT based	$\frac{3}{4}*\log_4 N$	$2*\log_4 N$

Chapter 5

Channel Estimations and Equalization with Fast Fading Channels and Carrier Frequency Offsets

In OFDM systems, the main advantage is that the adopted Fourier basis functions form an eigenbasis set for efficient orthogonal multicarrier transmission in time-invariant channels. It also simplifies channel equalization in the receiver, where the equalizer can be realized by a single-tap filter per subchannel in the frequency domain. However, the advantage fails when there is a high Doppler frequency shift and there are impairments such as the synchronization errors (e.g., frequency offset). In such situations, the orthogonality between subcarriers is lost at the receiver, resulting in inter-carrier interference (ICI). The performance degradation due to the inter-carrier interference becomes significant as the carrier frequency, symbol duration, and vehicle speed increase.

In OFDM systems, pervious studies have quantified the effects of ICI on the system performance: [28] uses central limit theorem arguments to model ICI as a Gaussian random process and quantified its impact on BER. [29] focuses on the

WSSUS (Wide-Sense Stationary and Uncorrelated Scattering) channels and shows that if the OFDM block duration is greater than 8% of the channel coherent time, then the signal-to-noise ratio (due to ICI) is less than 20dB. In [30] and [31], time domain and frequency domain compensation techniques are proposed to reduce the distortion caused by time-varying channel respectively. However, these two approaches are based on the assumption that channel is flat Rayleigh fading. For the multipath channels (frequency selective fading), [32] proposes a frequency-domain equalization technique to reduce the Doppler-induced ICI based on the assumption that the channel impulse response (CIR) varies in a linear fashion during an OFDM block period. [33] concludes that if fdT is less than 0.001, the channel can be assumed as constant during the symbol interval. When the OFDM block duration is less than 10 of the channel coherent time, [32] argues that the channel can be assumed varying in a linear fashion. In this chapter, the proposal and discussion will focus on the CIR with linear variation during a symbol block.

The papers mentioned above focus on the reduction of ICI caused by the time-varying channels but carrier frequency offset is also an important contributing factor of ICI. Conventional methods for carrier frequency offset estimations mostly apply autocorrelation operations to cyclic prefix and track phase shifts caused by the mismatch of carrier frequencies between the transmitter and the receiver [34]. The mismatch of carrier frequencies causes a linear phase rotation of each subcarrier in time domain and destroys the orthogonality between subcarriers in frequency domain. In this chapter, a method is proposed to combat the impact of ICI due to the time-varying channels and the mismatch of carrier frequencies.

5.1 Introduction of System Model

Before introducing the system model, the impact of inter carrier interference (ICI) caused by fast-fading channels and mismatch of carrier frequencies in OFDM systems is illustrated first.

5.1.1 Effect of Inter Carrier Interferences in OFDM Systems

One should realize that inter carrier interference appears when channels change during an OFDM symbol or frequencies are mismatch between the transmitter and the receiver oscillators. When channels change during an OFDM symbol, the convolution theorem no longer holds and results in the loss of orthogonality between subcarriers. On the other hand, the carrier frequency offsets can be divided into two parts, first part is the integer carrier frequency offset and second part is the fractional carrier frequency offset. The integer carrier frequency offset doesn't cause ICI but dislocates all subcarriers by some multiples of subcarrier spacing in frequency domain. This can be restored by detecting the shift number in pilot location using a matched filter. The fractional carrier frequency causes ICI and linear-phase shift in time domain of an OFDM signal. Here, we only consider the effect of fractional carrier frequency offsets and time-varying multipath channels which cause ICI.

5.1.2 System Model of Fast-Fading Channels with Carrier Frequency Offsets

To see how ICI is introduced by time-varying channels and fractional carrier frequency offsets, in this section we will derive the effect based on OFDM system

model. First the sampled received signal in time domain can be written as

$$r(n) = \frac{1}{N} e^{j2\pi\Delta fn} \sum_{k=0}^{N-1} H(n,k) \times d(k) \times e^{j\frac{2\pi nk}{N}} + \tilde{n}(n) \qquad n = 0,1,\cdots,N-1$$

$$H(n,k) = \sum_{l=0}^{L-1} h(n,l) \times e^{-j\frac{2\pi lk}{N}}$$

(5.1)

where $r(n)$ is the n-th received data, Δf is the carrier frequency offset between transmitter and receiver, $h(n,l)$ is the sampled time-varying channel impulse response, $d(k)$ is the transmitted data at the k-th subcarrier, $H(n,k)$ is the time-varying channel frequency response and L is the length of channels. The received signal is processed and demodulated by DFT to get signals in frequency domain as follows:

$$Y(m) = DFT_n\{r(n)\} = \frac{1}{N} \sum_{k=0}^{N-1} d(k) \times DFT_n\left\{e^{j2\pi\Delta fn} H(n,k)\right\} * \delta(m-k) + DFT_n\{\tilde{n}(n)\}$$

$$= \frac{1}{N} \sum_{k=0}^{N-1} d(k) \times \tilde{H}(m,k) * \delta(m-k) + \tilde{N}(m)$$

(5.2)

$$= \frac{1}{N} \sum_{k=0}^{N-1} d(k) \times \tilde{H}(m-k,k) + \tilde{N}(m) \qquad m = 0,1,\cdots,N-1$$

$$\tilde{H}(m,k) = DFT_n\left\{e^{j2\pi\Delta fn} H(n,k)\right\} = \sum_{l=0}^{L-1} DFT_n\left\{e^{j2\pi\Delta fn} h(n,l)\right\} \times e^{-j\frac{2\pi lk}{N}}$$

$$= \sum_{l=0}^{L-1} \tilde{h}(m,l) \times e^{-j\frac{2\pi lk}{N}}$$

(5.3)

By equation (5.2), the impact of carrier frequency offsets can be viewed as that the phases of time-domain channels are linearly rotated. In addition, the received signal at each subcarrier contains the ICI components from other subcarriers. The overall system can be expressed in matrix notation as

$$\mathbf{Y} = \mathbf{QAHQ}^H \mathbf{D} + \mathbf{N}$$

(5.4)

where $\mathbf{D} = [d(0),d(1)\ldots\ldots,d(N-1)]^T$ and $\mathbf{Y} = [Y(0),Y(1)\ldots\ldots,Y(N-1)]^T$ are transmitted and received data vectors in frequency domain, respectively, $\mathbf{N} \in C^N$ is the Gaussian noise vector, $\mathbf{Q} \in C^{NXN}$ is the standard N-dimensional DFT matrix defined by $Q_{p,q} = 1/\sqrt{N} e^{-j(2\pi/N)(p-1)(q-1)}$, $\mathbf{A} \in C^{NXN}$ is a diagonal matrix for modeling the effect of carrier frequency offsets, and $\mathbf{H} \in C^{NXN}$ is the time-varying

channel matrix. The matrix standing for frequency offsets and time-varying channels can be defined by

$$\tilde{\mathbf{H}} = \begin{bmatrix} e^{j2\pi\Delta f 0} & \cdots & & & 0 \\ & e^{j2\pi\Delta f 1} & & & \\ & & e^{j2\pi\Delta f 2} & & \\ & & & \ddots & \\ & & & & \ddots & \\ 0 & & & & e^{j2\pi\Delta f(N-1)} \end{bmatrix} \begin{bmatrix} h_{(0,0)} & 0 & \cdots & \cdots & h_{(0,L-1)} & \cdots & h_{(0,1)} \\ h_{(1,1)} & h_{(1,0)} & 0 & \cdots & 0 & h_{(1,L-1)} & \cdots & h_{(1,2)} \\ \vdots & & & & & \\ h_{(L-1,L-1)} & \cdots\cdots & h_{(L-1,0)} & \cdots & 0 & \cdots & 0 \\ \vdots & & & & \\ & & \cdots & & \\ 0 & \cdots & 0 & & h_{(N-1,L-1)} & \cdots & h_{(N-1,0)} \end{bmatrix}$$

$$\tilde{\mathbf{H}} = \mathbf{A}\mathbf{H} \tag{5.5}$$

The first matrix $\mathbf{A}$ accounts for the impact of carrier frequency offsets, and the second matrix $\mathbf{H}$ accounts for time-varying channels. Then $\mathbf{Y}$ can be rewritten as

$$\mathbf{Y} = \mathbf{G}\mathbf{D} + \mathbf{N} \tag{5.6}$$

where $\mathbf{G} = \mathbf{Q}\mathbf{A}\mathbf{H}\mathbf{Q}^H = \mathbf{Q}\tilde{\mathbf{H}}\mathbf{Q}^H \in C^{N \times N}$ is the system matrix where $\mathbf{Q}^H$ is the complex conjugate transpose of $\mathbf{Q}$.

$$G_{m,k} = \frac{1}{N}\sum_{n=0}^{N-1}\sum_{l=0}^{L-1} e^{j2\pi\Delta fn} h(n,l) D_{m,k}(n,l) \tag{5.7}$$

where $D_{m,k}(n,l) = e^{j(2\pi/N)(n(m-k)+l(1-k))}$. Moreover,

$$Y(m) = G_{m,m}d(m) + \sum_{k=1,k\neq m}^{N} G_{k,m}d(k) + \tilde{N}(m) \tag{5.8}$$

and the ICI component for the m-th subcarrier is

$$ICI(m) = \sum_{k=1,k\neq m}^{N} G_{k,m}d(k) = \frac{1}{N}\sum_{k=0 \, k\neq m}^{N-1} d(k) \times \tilde{H}(m-k,k) \tag{5.9}$$

We can see that the ICI component will vanish if

$$\tilde{H}(m-k,k) = G(k)\delta(m-k) \tag{5.10}$$

That is, this result happens when $\tilde{H}(n,k)$ is independent of time index n.

5.2 The Proposed Estimation Method for Fast-Fading Channels

To cope with ICI effect due to time-varying channels, one must accurately estimate the channel condition and carrier frequency offsets. If we can get matrix $\tilde{\mathbf{H}}$, then the transmitted data $\mathbf{D}$ can be obtained either by LS estimate or MMSE estimate. Song and Lim proposed an estimation method with the aid of frequency-domain pilots and a pilot tone placement scheme [35]. In this section, we mainly refer to their method and consider reducing carrier frequency offsets at the same time. After that, a simplified method is proposed for the purpose of low computational complexity.

5.2.1 Proposed Estimation Scheme

By (5.5), the estimates of $\tilde{\mathbf{H}}$ contain the combined time-varying channel impulse response and phase distortion due to carrier frequency offsets. A channel vector with phase shift is defined by

$$\tilde{\mathbf{h}}_n = e^{j2\pi\Delta fn}[h(n,0)\ h(n,1)\ h(n,2)\ \cdots\ h(n,L-1)]^T \qquad 0 \le n \le N-1$$
$$\tilde{\mathbf{h}} = [\tilde{\mathbf{h}}_0^T\ \tilde{\mathbf{h}}_1^T\ \cdots\ \tilde{\mathbf{h}}_{N-1}^T]^T \tag{5.11}$$

Where $\tilde{\mathbf{h}}_n$ is the modified multipath channels vector for the n-th subcarrier in time domain. If no assumption is made on the channel variation, there will be $NL+1$ parameters to be estimated. As a result, even when full N training subcarriers are used, it is far from enough for the estimation. To make the problem solvable, the number of parameters needed for channel estimation must be reasonably reduced. Therefore, [32] proposes that if the multipath fading channels are slowly time-varying, the time variation of the channel impulse response $h(n,l)$, for all the L paths, can be approximated by straight lines with small slopes during an OFDM symbol period. The

relative Doppler frequency change ($f_d T$) indicates the degree of time variation of CIR. For channels with $f_d T > 0.1$, the assumption that the CIR varies in a linear fashion during a block period no longer holds and gives rise to an error floor in signal estimation. When the multipath fading channels are slowly time-varying, the matrix equation in (5.5) can be greatly simplified.

The carrier frequency offsets matrix **A** causes the phase of CIR to rotate linearly with the subcarrier index so that we could combine the effect of matrix **A** with time-varying channels matrix **H** without loss of linear assumption. That means that the variation of $\tilde{\mathbf{H}}$ is also linear. Figure 5.1 shows the time variation of CIR in a symbol duration and the corresponding magnitude response (absolute value of the Fourier transform of the signal in Fig. 5.1(a)), for three different Doppler frequencies. From Fig. 5.1, one can see that the time variation of the CIR can be modeled as a straight line, and most energies of those CIR's are concentrated in the neighborhood of the dc component.
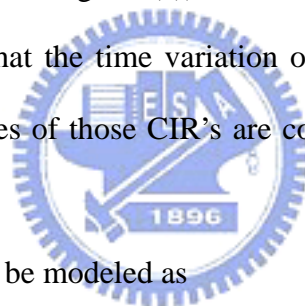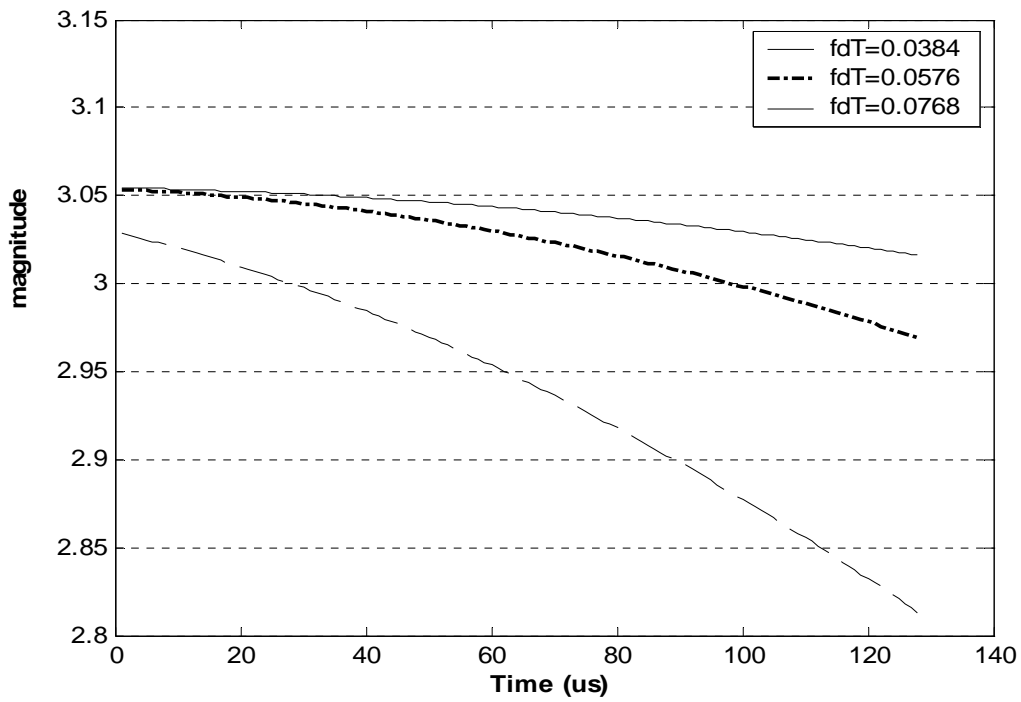
Then equation (5.11) can be modeled as

$$\tilde{h}(n,l) = s_l n + a_l \tag{5.12}$$

and

$$
\begin{aligned}
\tilde{\mathbf{h}} &= (\tilde{\mathbf{h}}_0^T, \tilde{\mathbf{h}}_1^T, \cdots \tilde{\mathbf{h}}_{N-1}^T)^T \\
&= (h(0,0)\ h(0,1) \cdots h(0,L-1)\quad \cdots \quad h(N-1,0)\ h(N-1,1) \cdots h(N-1,L-1))^T \\
&= (a_0, a_1,\ \cdots, a_{L-1}\quad \cdots\quad ,(s_0(N-1)+a_0), \cdots, (s_{L-1}(N-1)+a_{L-1}))^T \\
&= \mathbf{C}(a_0\ a_1 \cdots a_{L-1}\ s_0\ s_1 \cdots s_{L-1})^T \\
&= \mathbf{C}\hat{\mathbf{h}}
\end{aligned}
$$

$$\tag{5.13}$$

where s_l and a_l define the slope and the initial value of the l-th path, and matrix **C** defines the transform matrix for $\hat{\mathbf{h}}$ which includes the initial values and slopes of the multipath channels.

75

Figure 5.1(a) Time variation of the CIR for different relative Doppler frequency

changes within a block symbol.
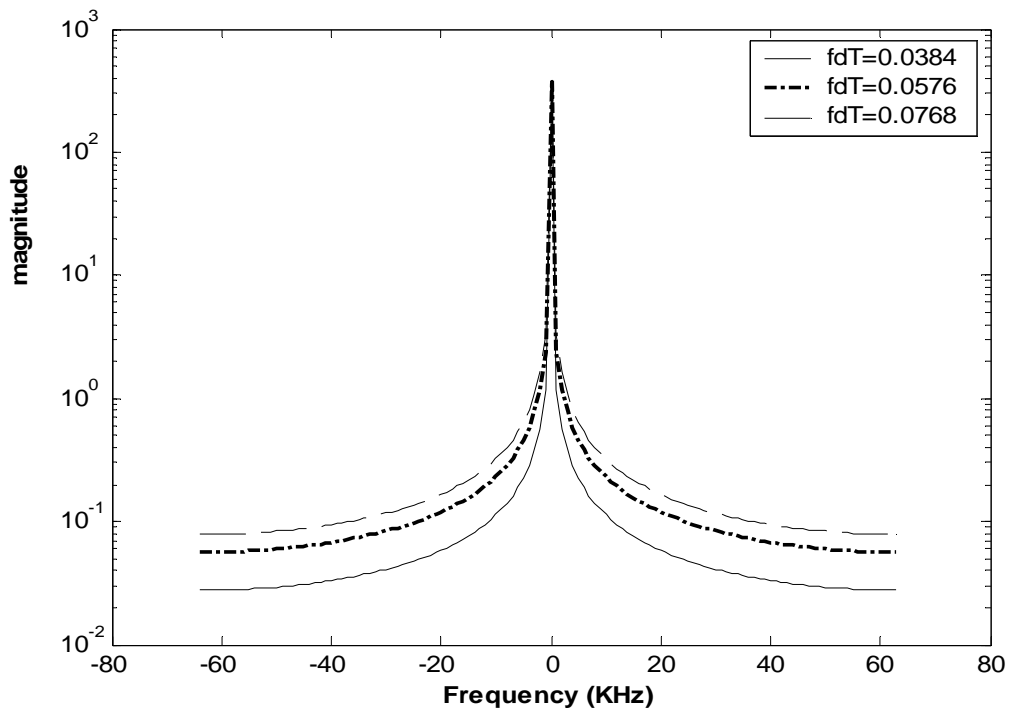
Figure 5.1(b) Magnitude responses for CIR versus Doppler frequencies

Under linear variation assumption, let's consider the channel estimation method [35] for fast-fading channels. To facilitate channel estimations on frequency-offset channels, equation (5.6) is changed to the form of $\mathbf{Y} = \mathbf{WAH} + \mathbf{N} = \mathbf{W\tilde{H}} + \mathbf{N}$. Then the m-th received subcarrier $Y(m)$ can be expressed as:

$$
\begin{aligned}
Y(m) &= \sum_{k=1}^{N} G_{m,k} d(k) + N(m) \\
&= \frac{1}{N} \sum_{k=1}^{N} \sum_{n=0}^{N-1} \sum_{l=0}^{L-1} \tilde{h}(n,l) D_{m,k}(n,l) d(k) + N(m) \\
&= \frac{1}{N} \sum_{n=0}^{N-1} \sum_{l=0}^{L-1} \tilde{h}(n,l) (\sum_{k=1}^{N} D_{m,k}(n,l) d(k)) + N(m) \\
&= \sum_{n=0}^{N-1} \sum_{l=0}^{L-1} \tilde{h}(n,l) W_{m,q} + N(m)
\end{aligned}
\tag{5.14}
$$

where matrix $\mathbf{W}$ is defined as

$$
W_{m,q} = \frac{1}{N} \sum_{k=1}^{N} D_{m,k}(n,l) d(k), \quad n = (q-1-l)/L, \; l = (q-1) \bmod L \tag{5.15}
$$

As shown in the equations, if $W_{m,q}$ is known, then the modified channel can be obtained by the LS estimation based on equation (5.14). However, $\mathbf{W}$ are only known at pilot locations, $d(p(1)), d(p(2)) \cdots\cdots, d(p(P))$, which are placed at subcarrier locations, $p(1), p(2), \cdots\cdots, p(P)$. Thus, we can divide estimates of $\mathbf{W}$ into unknown data part and known pilot data part:

$$
\begin{aligned}
W_{m,q} &= \frac{1}{N} \sum_{k \in pilot} D_{m,k}(n,l) d(k) + \frac{1}{N} \sum_{k \notin pilot} D_{m,k}(n,l) d(k) \\
&= W_{m,q}^{(p)} + W_{m,q}^{(n)}
\end{aligned}
\tag{5.16}
$$

where $W_{m,q}^{(p)}$ is decided by the pilot data, and $W_{m,q}^{(n)}$ is decided by the estimate of transmitted data. Thus, $Y(m)$ can be expressed by

$$
Y(m) = W_{m,q}^{(p)} \tilde{h} + W_{m,q}^{(n)} \tilde{h} + n(m) \tag{5.17}
$$

As long as $\mathbf{W}$ is solved, the modified channel impulse response $\mathbf{\tilde{h}}$ can be calculated by equation (5.16).

The proposed method consists of two steps. The first step is to estimate $W_{m,q}^{(n)}$ and the second step is to estimate $\tilde{\mathbf{h}}$ and recover the transmitted data. First, we use the existing channel estimation scheme [36] to estimate $W_{m,q}^{(n)}$ as detailed below. It begins with the estimate of the channel frequency responses at pilot subcarriers based on the LS algorithm given by

$$H(m) = \frac{Y(m)}{d(p(m))} \quad m = p(1), p(2), \cdots\cdots p(P) \tag{5.18}$$

For $H(m)'s$ at data subcarriers, they are obtained by linear interpolation scheme. Then data subcarriers are estimated from the interpolated channel response. After that, $W_{m,q}$ is obtained by equation (5.15). Let $\hat{\mathbf{W}}$ be the estimate of $\mathbf{W}$. Then using equation (5.14), one can form the system of $N \, X \, NL$ matrix equation.

$$\begin{pmatrix} Y_1 \\ \vdots \\ Y_N \end{pmatrix} = \begin{pmatrix} \hat{W}_{1,1} & \cdots & \hat{W}_{1,NL} \\ \vdots & \vdots & \vdots \\ \hat{W}_{N,1} & \cdots & \hat{W}_{N,NL} \end{pmatrix} \tilde{h} + \begin{pmatrix} N_1 \\ \vdots \\ N_N \end{pmatrix} \tag{5.19}$$

$$\mathbf{Y} = \hat{\mathbf{W}}\tilde{h} + \mathbf{N} \tag{5.20}$$

In the equation, the number of variables is larger than the dimension of the matrix equation. However, due to the linear variation condition described by equation (5.13), equation (5.20) can be rewritten as

$$\mathbf{Y} = \hat{\mathbf{W}}\mathbf{C}\hat{\mathbf{h}} + \mathbf{N} = \mathbf{T}\hat{\mathbf{h}} + \mathbf{N} \tag{5.21}$$

Since the matrix $\mathbf{C}$ is known *a priori*, matrix $\mathbf{T} \in C^{N \, X \, 2L}$ can be obtained from the estimate of $\mathbf{W}$. Then all the unknown parameters left to be estimated are the initial values and slopes of multipath channels affected by the carrier frequency offsets. The variables of the system equations are reduced to $2L$ from $NL+1$. As a result, $\hat{\mathbf{h}}$ can be obtained by the least-square solution:

$$\hat{\mathbf{h}} = \mathbf{T}^\perp \mathbf{Y} \qquad \mathbf{T}^\perp \equiv pseudoinverse \; of \; \mathbf{T} \tag{5.22}$$

With this result, $\tilde{\mathbf{H}}$ can be calculated by equation (5.13) and the transmitted data can be obtained by (5.6)

$$\mathbf{D} = \mathbf{G}^{-1}\mathbf{Y} \qquad (5.23)$$

where $\mathbf{G}$ can be calculated by (5.7) after getting $\tilde{\mathbf{H}}$.

5.2.2 Proposed Simplified Estimation Scheme

Since the proposed estimation scheme has two estimation steps that include a large matrix inversion, it is very complicated. Thus, a simplified estimation scheme is proposed to reduce the complexity. However, the simplified scheme results in performance loss as detailed below.

First, let's see ICI component described by (5.9)

$$ICI(m) = \sum_{k=1,k\neq m}^{N} G_{k,m} d(k) = \frac{1}{N} \sum_{k=0 \atop k\neq m}^{N-1} d(k) \times \tilde{H}(m-k,k) \qquad (5.24)$$

It is obvious that ICI is due to sidelobes of the other subcarriers, caused by time-varying channels and carrier frequency offsets. From matrix $\mathbf{G}$, we can see the effect of ICI and the idea of simplified estimation scheme, based on the observation of $\mathbf{G}_m$, where $\mathbf{G}_m$ is the m-th row vector of matrix $\mathbf{G}$. Figure 5.2 and Figure 5.3 show $\mathbf{G}_1$ and $\mathbf{G}_3$ with N=64, respectively.

Under the assumption that the multipath fading channel is slowly time-varying during an OFDM symbol, one can see that most ICI components are concentrated in the neighborhood of the desired subcarrier in the frequency domain so that the matrix $\mathbf{G}$ can be greatly simplified by ignoring the ICI terms due to far-away subcarriers which do not significantly affect $\mathbf{Y}$ in (5.6). Consequently, matrix $\mathbf{G}$ can be reduced to

$$\tilde{\mathbf{G}}_7 = \begin{bmatrix} 0 & G_{0,1} & G_{0,2} & G_{0,3} & 0\cdots\cdots & \cdots\cdots & G_{0,N-2} & G_{0,N-1} & G_{0,N} \\ G_{1,0} & 0 & G_{1,2} & G_{1,3} & G_{1,4} & 0\cdots\cdots & \cdots\cdots & G_{1,N-1} & G_{1,N} \\ G_{3,0} & G_{3,1} & 0 & G_{3,4} & G_{3,5} & G_{3,6} & 0 & \cdots\cdots & \cdots\cdots & G_{3,N} \\ & & \cdots\cdots & \cdots\cdots & & & \cdots\cdots & \cdots\cdots \\ & & & \cdots\cdots\cdots\cdots & & & & \cdots\cdots & \cdots\cdots \\ & & \cdots\cdots & \cdots\cdots & \cdots\cdots & 0\cdots\cdots G_{N,N-1} & 0 \end{bmatrix} \qquad (5.25)$$

where $\tilde{\mathbf{G}}_7$ is an example of the simplified ICI matrix only considering the ICI components from the six most nearby subcarriers. Then the simplified estimation scheme can be expressed as

$$\tilde{\mathbf{Y}} = \mathbf{Y} - \tilde{\mathbf{G}}_p \tilde{\mathbf{X}}$$
$$x(m) = \tilde{y}(m) / G(m,m) \qquad (5.26)$$

where $\tilde{\mathbf{G}}_P$ is the reduced ICI matrix.
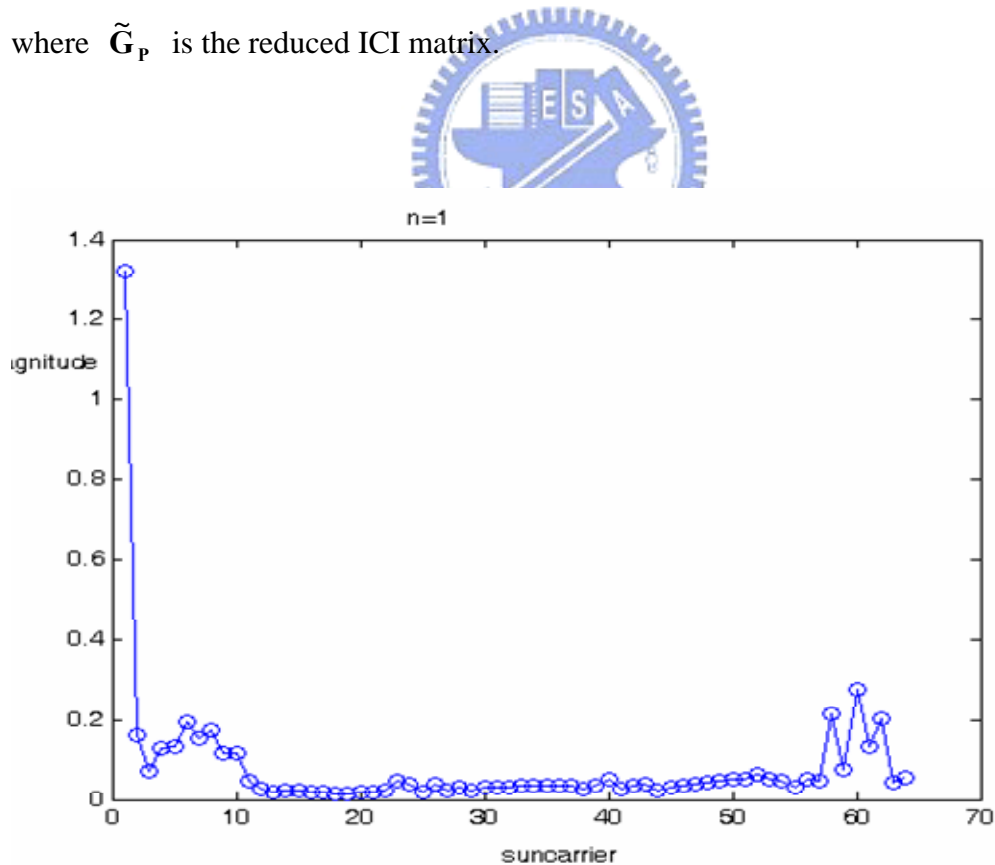
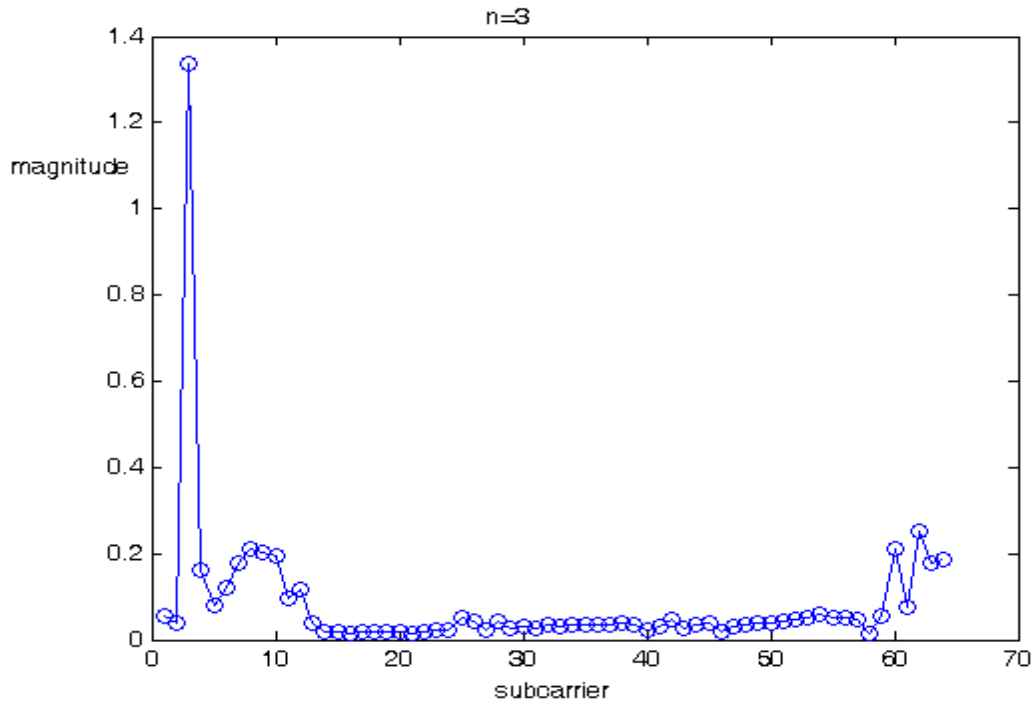**Figure 5.2** The shape of $\mathbf{G}_1$ (ICI effect for 1-th subcarrier)

Figure 5.3 The shape of G_3 (ICI effect for 3-th subcarrier)

5.3 Simulation Results

In this section, we demonstrate performances of the proposed estimation scheme to combat the impact of fast-fading channels and carrier frequency offsets. To construct an OFDM signal, assume that the entire channel bandwidth, 500 kHz, is divided into 128 subcarriers, and the sampling period $T = 1us$ [24]. The length of cyclic prefix is $T/4$ to prevent the inter symbol interference due to multipath channel delay spread. 16-QAM modulation is used and pilot subcarriers are equispaced in the system and is 12.5% of all subcarriers. Moreover, the multipath channel delays are assumed sample-spaced with $L = 3$ and the path gains follow the exponential-decay power profile as described by (2.4). The delay time constant is chosen such that the last path power is 10dB below the first path and the relative time delay and power of the i-th path are listed in Table 5.1.

Table 5.1 Relative power and delay values for multipath channels

Tap	Time delays (μ sec)	Average Power (dB)
1	0	0
2	0.83	-1
3	2.61	-9

In the simulation environment, the channels under three different Doppler frequencies $f_d = 120Hz \, (f_d T = 0.0384)$, $f_d = 180Hz \, (f_d T = 0.0576)$, $f_d = 240Hz$ $(f_d T = 0.0768)$ and the carrier frequency offset, $f_o = 0.5/T$, are taken into consideration. Here we compare the proposed method with the original Won and Lim's method [35], Yeh's method [24], and conventional LMMSE channel estimator mentioned in section 4.1.3. The three compared channel estimation methods are assumed to use the conventional method (by performing the autocorrelation functions during the period of cyclic prefix) to estimate the frequency offsets and compensate the phase rotation in time domain [27]. In contrast, the proposal algorithm does not need the compensation. The proposed algorithm solves the phase rotation due to frequency offsets along with time-varying channel ICI effect all together in one shot. Figure 5.4 shows the BER performances of those estimation schemes for $f_d T = 0.0384$ and $f_o = 0.5/T$. It is obvious that the LMMSE equalizer has an error floor due to the non-negligible ICI and Yeh's method is a little bit better than the LMMSE method in high SNR but worse than the proposed method. The proposed method achieves better performance in high SNR because the ICI effect dominants the impairment. Won and Lim's method has the worst performance for all SNR values, mainly due to carrier frequency offsets. Although the three compared methods use the conventional method to combat carrier frequency offsets, the estimate is not accurate due to ISI and ICI. ISI is due to the multipath channels delay and ICI is due to the variation of channel impulse response during an OFDM symbol which produced a

poor autocorrelation power gain. Figure 5.5 and 5.6 shows the case for $f_d T = 0.0576$ and $f_d T = 0.0768$ with $f_o = 0.5/T$, respectively. In these two cases, the performances follow the discussion for the case of $f_d T = 0.0384$. However, the larger $f_d T$ is, the worse the performance is. In the proposed method, the assumption of linear-varying channels during an OFDM symbol is increasingly incorrect, which results in an error floor when $f_d T > 0.0768$.

For the simplified estimation scheme, the ICI matrix $\mathbf{G}$ is simplified to $\tilde{\mathbf{G}}_{15}$ which means that it only considers the most nearby fifteen subcarriers for ICI components. The simulation results are shown in Figures 5.7 9 for $f_d T$ = 0.0384, 0.0576, 0.0768, respectively, with f_o = 0.5 carrier spacing. One can see that although the proposed method has better BER performance, the simplified method is just a little bit worse than the proposed method which verified that the dominant ICI components are due to adjacent subcarriers, while the other ICI components can be ignored.
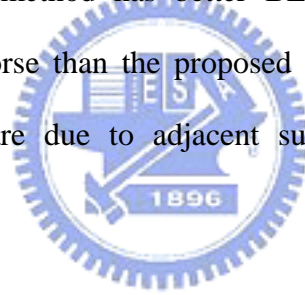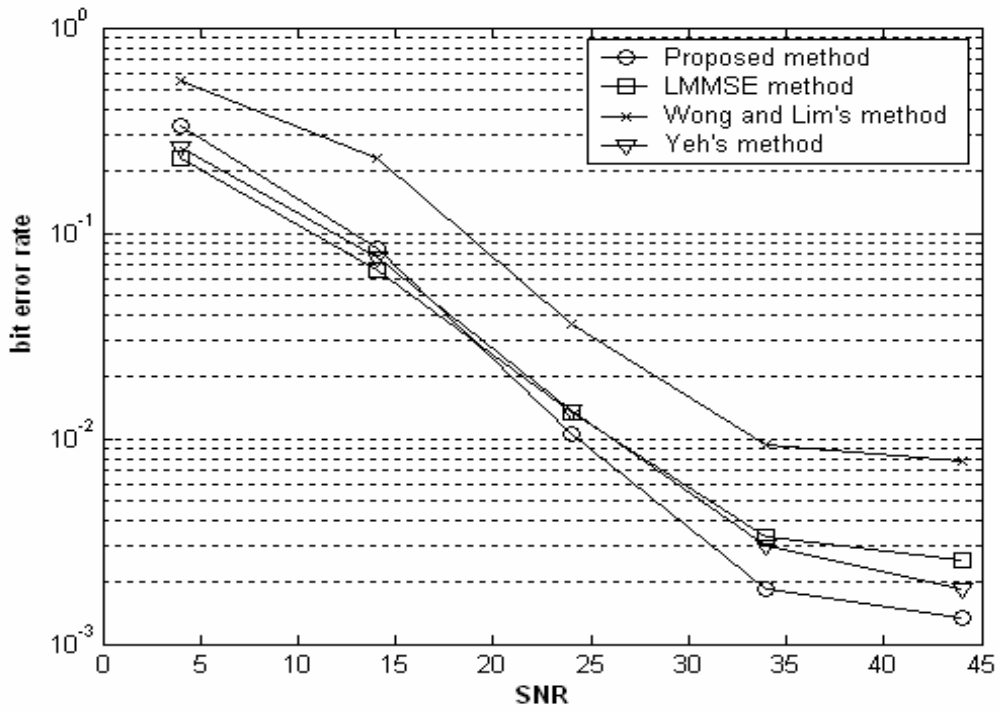
Figure 5.4 BER comparison with $f_d T = 0.0384$ and $f_o = 0.5$ carrier spacing
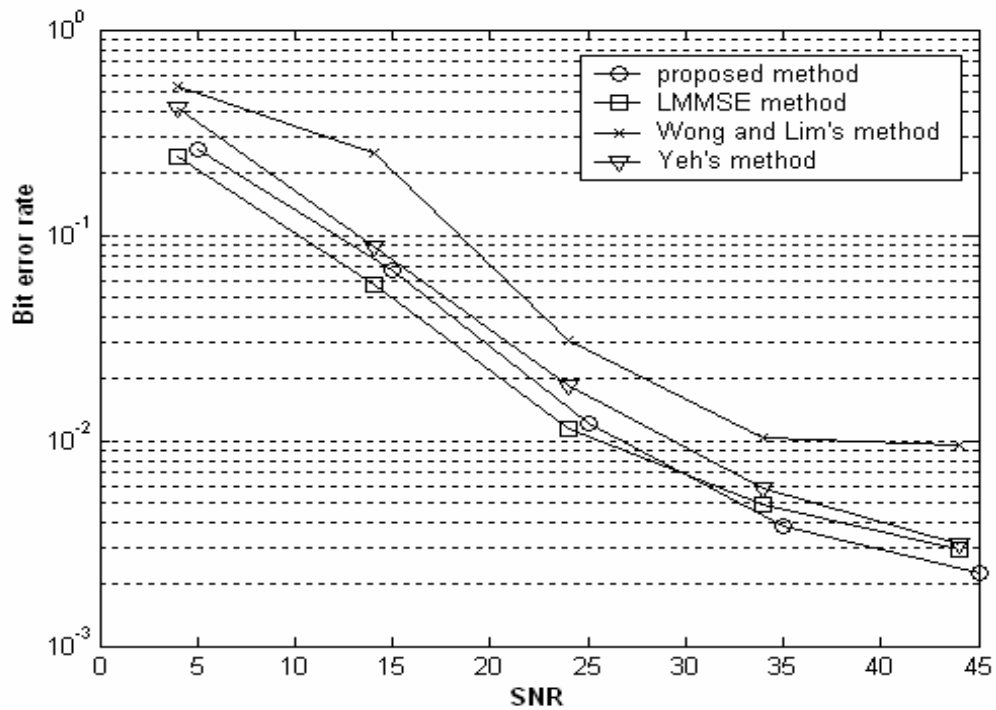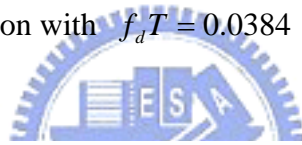

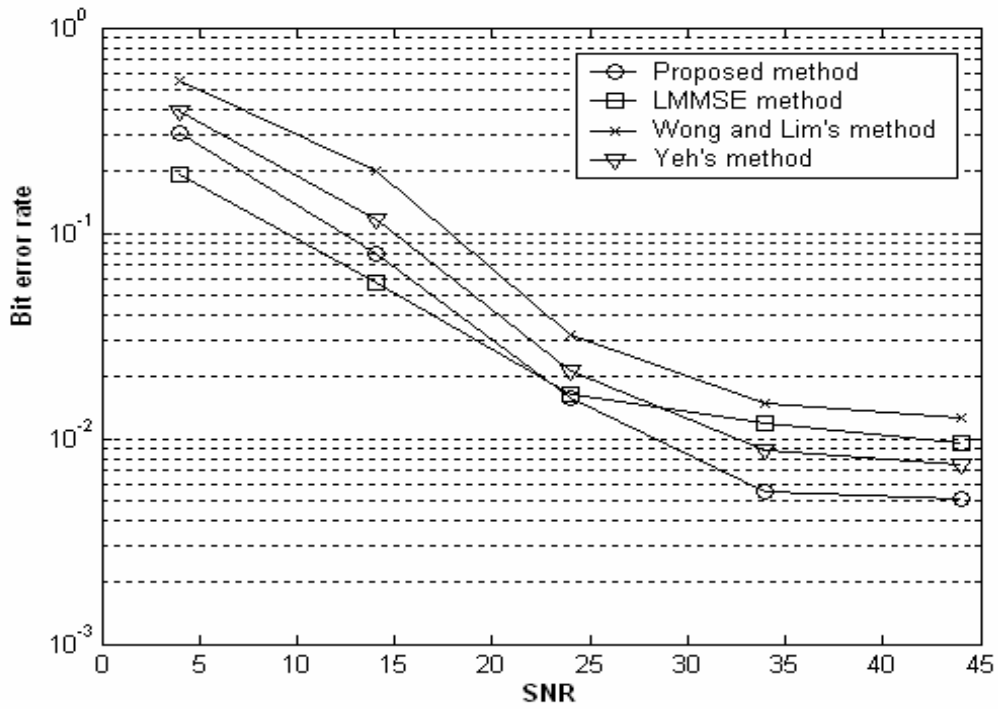**Figure 5.5** BER comparison with $f_d T = 0.0576$ and $f_o = 0.5$ carrier spacing

Figure 5.6 BER comparison with $f_d T = 0.0786$ and $f_o = 0.5$ carrier spacing
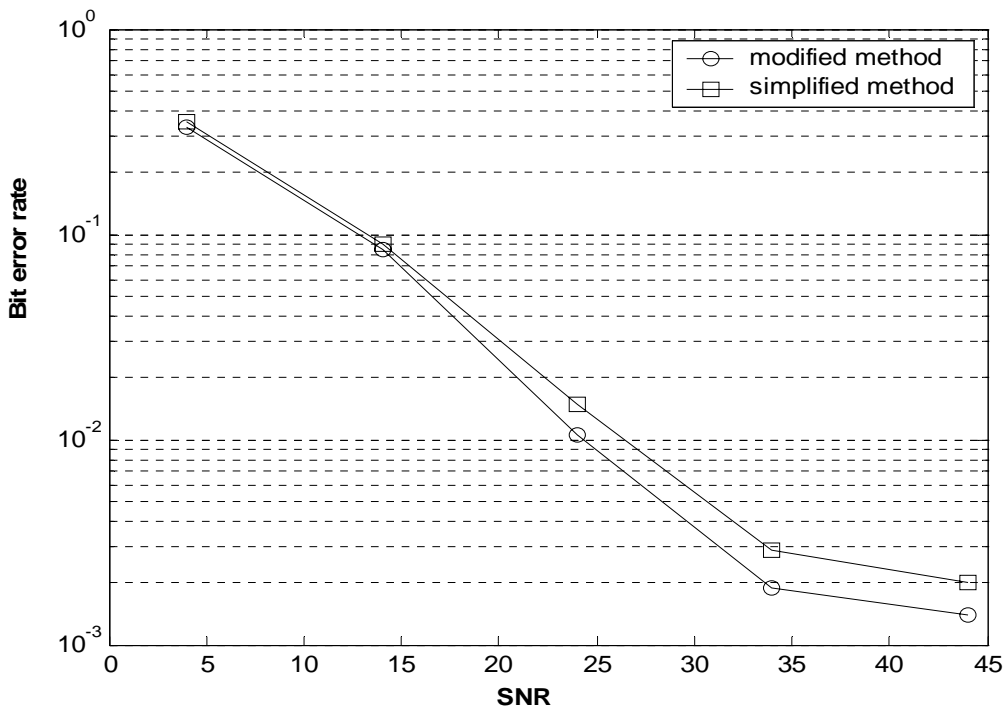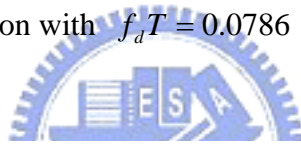

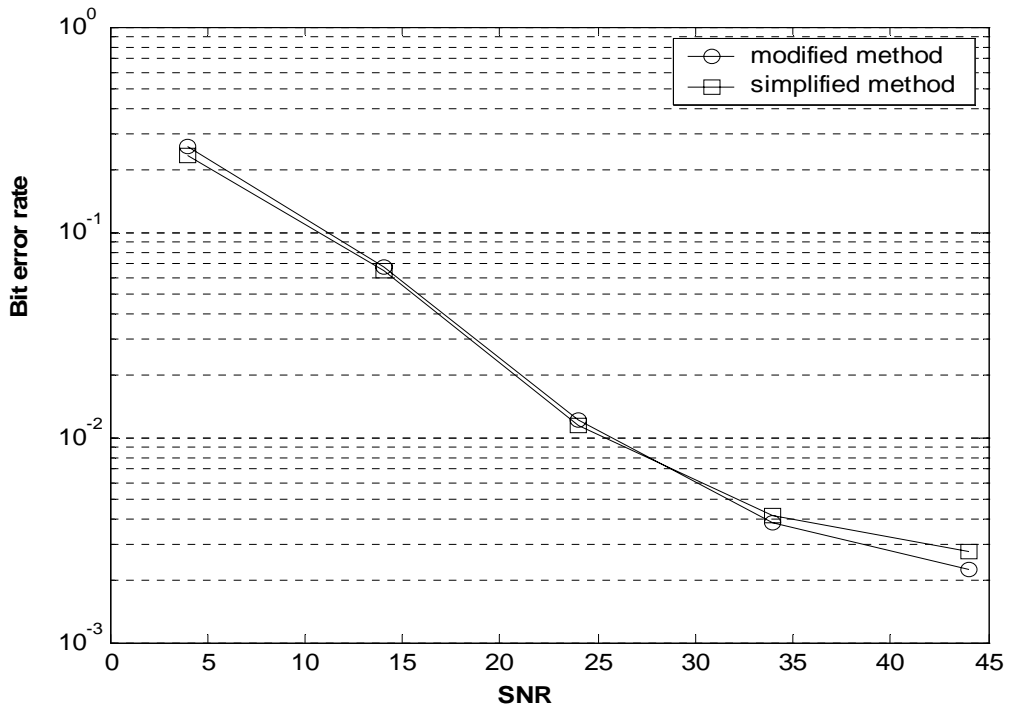**Figure 5.7** BER comparison with $f_d T = 0.0384$ and $f_o = 0.5$ carrier spacing

Figure 5.8 BER comparison with $f_d T = 0.0576$ and $f_o = 0.5$ carrier spacing
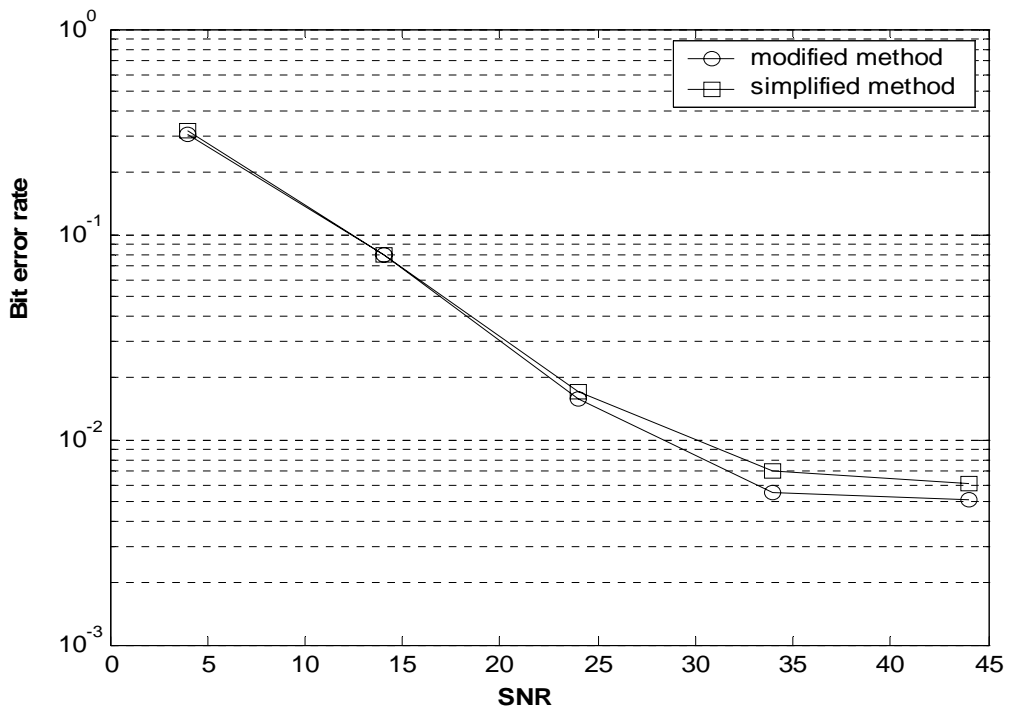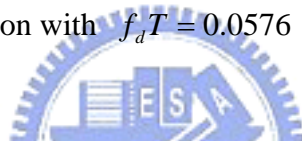

Figure 5.9 BER comparison with $f_d T = 0.0768$ and $f_o = 0.5$ carrier spacing

Chapter 6

Conclusion

In this thesis, a comparative investigation on various channel estimation algorithms for IEEE 802.16a and DVB-T systems in the mobile communication environment is presented and analyzed in terms of bit error rate and computational complexity. As a result, piecewise linear interpolation and cubic Bspline interpolation show the best error performance than the others. Concerning the computational complexity as well as the performance, however, the piecewise linear interpolation is considered as a proper choice for both systems.

For OFDM systems with ICI effect caused by time-varying channels and carrier frequency offsets, we propose an estimation scheme to equalize the received data by assuming a linear-variation model for channel impulse response. But, due to its high computational complexity, a simplified estimation method with small performance loss is proposed. Simulations show that ICI effect can be effectively reduced by the proposed methods.

Channel estimation and equalization for OFDM systems with the ICI effect are quite challenging tasks especially when the channel is fast fading. Although, we have

presented methods to solve the ICI effect, the computational complexity is still too high. Therefore, how to achieve the same performance with low computational complexity is an even bigger challenge to consider in the future work, including more general channel conditions.

Bibliography

[1]   L. J. Cimini Jr., "Analysis and simulation of a digital mobile channel using orthogonal frequency-division multiplexing," *IEEE Trans. Commun.*,vol. 33, pp. 665–675, July 1985.

[2]   M. Alard and R. Lassalle, "Principles of modulation and channel coding for digital broadcasting for mobile receivers," *EBU Tech. Rev.*, no. 224, pp. 3–25, Aug. 1987.

[3]   M. K. Tsatsanis and Z. Xu, "Pilot symbol assisted modulation in frequency selective fading wireless channels," *IEEE Trans. Signal Processing*, vol. 48, no. 8, pp. 2353–2365, 2000.

[4]   S. Y. Park and C. G. Kang, "Performance of pilot-assisted channel estimation for OFDM system under time-varying multi-path Rayleigh fading with frequency offset compensation," in *VTC2000*, pp. 1245–1248.

[5]   K. Y. Han, K. Ha, K. M. Sung, and C. W. Lee, "Time domain equalization using linear phase interpolation for OFDM in time variant multipath channels with frequency offset," in *VTC2000*, pp. 1255–1258.

[6]   M. de Courville, P. Duhamel, P. Madec, and J. Palicot, "A least mean squares blind equalization techniques for OFDM systems," *Ann. Telecommun.*, vol. 52, nos. 1–2, pp. 12–20, Jan.–Feb. 1997.

[7]   J.K. Cavers. "An analysis of pilot symbol assisted modulation for Rayleigh fading channels (mobile radio)," *IEEE Transactions on Vehicular Technology*, 40:686–693, November 1991.

[8]   Won-Gyu Song; Jong-Tae Lim, "Pilot-symbol aided channel estimation for OFDM with fast fading channels," Broadcasting, *IEEE Transactions on*, Volume: 49 , Issue: 4 , Dec. 2003, Pages:398 – 402.

[9] R. W. Chang, "Synthesis of Band Limited Orthogonal Signals for Multichannel Data Transmission," *Bell Syst. Tech. J.*, vol. 45, pp. 1775-1796, Dec. 1966.

[10] S. Rappeaport, "Wireless Communications Principles and Practice", 1996.

[11] S. B. Weinstein and P. M. Ebert, "Data transmission by frequency-division multiplexing using the discrete Fourier transform," *IEEE Trans. Comm.*, vol. COM-19, pp. 628-634, Oct. 1971.

[12] A. Peled and A. Ruiz, "Frequency domain data transmission using reduced computational complexity algorithms," *Proc. IEEE ICASSP*, pp. 964-967, April 1980.

[13] W. C. Jakes and John Wiley & Sons , "Microwave Mobile communications," *Inc.*, 1994.

[14] IEEE Std 802.16a™-2003 IEEE Standard for Local and metropolitan area networks Part 16: Air Interface for Fixed Broadband Wireless Access Systems— Amendment 2: Medium Access Control Modifications and Additional Physical Layer Specifications for 2–11 GHz. Published by The Institute of Electrical and Electronics Engineers, Inc. 3 Park Avenue, New York, NY 10016-5997, USA. 1 April 2003.

[15] Digital Video Broadcasting (DVB); Framing structure, channel coding and modulation for digital terrestrial television, European Telecommunications Standards Institute 2001. European Broadcasting Union 2001.

[16] J. G. Proakis, "Digital Communications," 3rd ed. Englewood Cliffs, NJ: Prentice-Hall, 1995.

[17] Radio Broadcasting Systems; Digital Audio Broadcasting (DAB) to Mobile, Portable and Fixed Receivers, *ETSI Standard ETS* 300 401, Feb. 1995.

[18] Y. Li, L. J. Cimini, Jr., and N. R. Sollenberger, "Robust channel estimation for OFDM systems with rapid dispersive fading channels," *IEEE Trans. Comm.*, vol.

46, no. 7, pp. 902-915, July 1998.

[19] O. Edfors, M. Sandell, J. J. van der Beek, S. K. Wilson, and P. O. Borgesson, "OFDM channel estimation by singular value decomposition," *IEEE Trans. Comm.*, vol. 46, no. 7, pp. 931-939, July 1998.

[20] G. S. Liu and C. H. Wei, "Programmable fractional sample delay filter with Lagrange interpolation", Electronics Letters, vol: 26, Issue: 19, pp. 1608 - 1610, 13th Sept. 1990.

[21] R. D. Harding and D. A. Quinney, "A Simple Introduction to Numerical Analysis Volume 2: Interpolation and Approximation," Adam Hilger, 1949.

[22] S. A. Dyer and J.S. Dyer, "Cubic-spline interpolation; Instrumentation & Measurement Magazine," *IEEE* , Volume: 4 , Issue: 1 , March 2001.

[23] Y. Zhao and A. Huang, "A Novel Channel Estimation Method for OFDM Mobile Communication Systems Based on Pilot Signals and Transform-Domain Processing," *Proc. VTC'97*, pp. 2089-2094.

[24] Y.H. Yeh and S.G. Chen, "Design of Pilot-Symbol-Aided Channel Estimation and Equalization for OFDM Systems," NCTU, June 2003.

[25] Y. F. Hsu and Y. C. Chen, "Rational interpolation by extendible inverse discrete cosine transform," *Electronics Letters*, vol. 33, no. 21, pp. 1774-1775, 9 Oct. 1997.

[26] ETSI TR 101 112 V3.2.0, "Universal mobile telecommunications system (UMTS); selection procedures for the choice of radio transmission technologies of the UMTS (UMTS 30.03 version 3.2.0)," *ETSI*, Apr. 1998.

[27] P. Chen and H. Kobayashi, "Maximum Likelihood Channel Estimation and Signal Detection for OFDM Systems," *IEEE ICC*, vol. 3, pp.1640-1645, 2002.

[28] M. Russell and G. L. Stuber, "Interchannel Interference Analysis of OFDM in a Mobile Environment," *Proc. IEEE VTC*, pp. 820-824, July, 1995.

[29] J. Li and M. Kavehrad, "Effect of Time Selective Multipath Fading on OFDM Systems for Broadband Mobile Application," *IEEE Comm. Letters*, vol. 3, no. 12, pp. 332-334, Dec. 1999.

[30] L. J. Cimini, Jr., "Analysis and simulation of a digital mobile channel using orthogonal frequency-division multiplexing," *IEEE Tran. Comm.*, vol. 33, pp. 665-675, July 1985.

[31] J. Ahn and H. S. Lee, "Frequency domain equalization of OFDM signals over frequency nonselective Rayleigh fading channels," *Electronics Letters*, vol. 29, no. 16, pp. 1476-1477, Aug. 1993.

[32] W. G. Jeon, K. H. Chang, and Y. S. Cho, "An Equalization Technique for Orthogonal Frequency-Division Multiplexing Systems in Time-Variant Multipath Channels," *IEEE Trans. Comm.*, vol. 47, no. 1, Jan. 1999.

[33] P. Chen and H. Kobayashi, "Maximum Likelihood Channel Estimation and Signal Detection for OFDM Systems," *IEEE ICC*, vol. 3, pp.1640-1645, 2002.

[34] Beek, J.J.; Sandell, M.; Borjesson, P.O.; "ML estimation of time and frequency offset in OFDM systems," Signal Processing, *IEEE Transactions* on [see also Acoustics, Speech, and Signal Processing, *IEEE Transactions* on] , Volume: 45 , Issue: 7 , July 1997.

[35] W.G. Song; J.T. Lim*;"* Pilot-symbol aided channel estimation for OFDM with fast fading channels," Broadcasting, *IEEE Transactions on* , Volume: 49 , Issue: 4 , Dec. 2003, Pages:398 – 402.

[36] Y. Li, "Pilot-symbol-aided channel estimation for OFDM in wireless systems," *IEEE Trans. Veh. Technol.*, vol. 49, no. 4, pp. 1207–1215,2000.

Autobiography

吳清泉，1980 年 2 月 29 日出生於彰化縣。2002 年自國立清華大學電機工程系畢業，隨即進入國立交通大學電子工程研究所攻讀碩士學位，致力於無線通訊系統研究。論文題目是先導訊號輔助式之正交分頻多工通信系統通道估測設計